Abstract

Abl2 Regulates Microtubule Dynamics through Interaction with both the

Microtubule Lattice and Tubulin Dimers

Wanqing Lyu

2022

Abl family kinases are believed to serve as central signaling nodes to transduce signals from upstream receptors to downstream signaling and cytoskeletal-associated proteins. Genetic studies in Drosophila indicate that Abl2 interacts functionally with microtubules (MTs), but the underlying mechanism(s) is (are) completely unclear. Here, I report that Abl2 directly binds MTs and tubulin to regulate MT dynamics. Abl2 binds with MTs via the C-terminal half, which is also mediated by the phosphorylation level of the N-terminus. Abl2 recognizes different MT lattice states, with a higher preference for GMPCPP-MTs than GDP-MTs. Abl2 also binds tightly to tubulin dimers, which is mediated by amino acids 688-924 in the C-terminus. As a naturally existing isoform, Abl2Δ688-790 loses its binding ability to tubulin dimers. I found that Abl2 promotes MT assembly and nucleation, as measured by the turbidity change. Interestingly, Abl2-eGFP formed spherical condensates in a concentration- and salt-dependent manner, which can recruit tubulin into Abl2:tubulin co-condensates. Co-condensation of Abl2 and tubulin further facilitates MT nucleation. Single-MT filament TIRF microscopy revealed that Abl2 increases MT elongation rate, which is consistent with the cellular observation that MTs have slower growth rates in Abl2 knockout cells. Lastly, the loss of the Abl2 in cells leads to an abnormally high cell migration speed, which

can be partially rescued by the C-terminal half that mediates the MT binding. Collectively, my data suggest the molecular mechanism that Abl2 acts as a MT nucleator and regulator to modulate MT dynamics and coordinate cellular behaviors.

Abl2 Regulates Microtubule Dynamics through Interaction with both

the Microtubule Lattice and Tubulin Dimers

A Dissertation

Presented to the Faculty of the Graduate School

Of

Yale University

In Candidacy for the Degree of

Doctor of Philosophy

By

Wanqing Lyu

Dissertation Director: Anthony J. Koleske, Ph.D.

December, 2022

Table of Contents

Acknowledgments

First and foremost, I would like to express my gratitude for Dr. Anthony Koleske. Tony has been, and will always be, not only my mentor, my friend, also my family. I am always inspired by the hardworking of Tony and his passion for pursuing scientific questions. Tony is not only my role model in science, but also in life. He is always there for me whenever I am stuck in life or in research. I will benefit from all the lessons from him for many years to come, and I cannot thank him enough for that.

I would also like to thank my thesis committee, Dr. Thomas Pollard and Dr. Yong Xiong, and my previous committee Dr. Charles Sindelar, for generously offering their time, guidance, and support over the last several years. My committee meetings have always been a hallmark for me to reflect on what I have been doing and thinking, and I have benefited a lot from all the constructive advices from my committee. I would also thank Dr. Chunxiang Wu in the Xiong Lab and Dr. Amy Wyler in the Boggon lab for generously shared their laboratory resources and help me conduct the experiments.

I have never seen more supportive colleagues than all my friends in the Koleske Lab. I would like to thank all of the former lab members, Brian Rosenberg, Aaron Levy, Sara Katrancha, Alex Scherer, Mitch Omar, Juliana Shaw, Shufang Feng, and Xiao Xiao. They established the friendly and supportive lab environment by organizing all the common lab materials and always helping each other in discussing project directions and proofreading the writing materials. I would like to thank Yuhan Hu for not only mentoring me and also being a supportive friend both

1

in life and in career development, and also Ke Zhang for inviting me to be a collaborator of his project and teaching me all the cell-based experiments. To all the current lab members, Yevheniia Ishchenko, and Robert Niecier, Melissa Carrizales, Alyssa Blaise, Amanda Jeng, Ellen Corcoran, Josie Bircher, and Daisy Duan. I feel so lucky and happy to work with you guys. I remember all the food/snacks that you guys send to me with love. As an innate person not liking to talk with people, I really enjoy my conversations with you guys, all the time. I would like to specifically thank my collaborator Daisy Duan, without whom this work would have been impossible. The endless brainstorming between Daisy and me has been the major pushing force for me to dig into the project and think a lot more in the big picture. I enjoyed having her as a sister, a friend, and a collaborator, and wish her the best in the future adventure in science. Last but not least, as the OGs of the lab, Liz Vellali and Xianyun Ye has always been my powerful backing. Liz can always help me figure out any lab- or department-related problems in the most efficient way. And Xianyun not only supports me by providing all the reagents, but also takes care of me in life.

I would like to thank my friends for all their time with me that encourages me to endure the difficult and disappointing moments in graduate school. Bichen Zhang and Kanthy Peng, Jun Zhao and Chao Zhang (now with my goddaughter Irene) were the two other cutest couples in New Haven besides Kuanlin and me. I enjoyed all the time hanging out with them, and learned a lot about how to live my life from them. I couldn't survive the seventh year in graduate school without Yinyu Wu, my study mate and ally for many long-night writing. It is also my privilege to

be in the Laji family: Xiangyu Shi (the big sister takes care of three of us), Jinyu Li (my favorite chef and little sister who always makes us laugh), and Yuyao Lin (the other me in the world). I am also thankful for my life-long friends starting from childhood, Xiaoxi Zhang, Nan Zhou and Dehua Zhang, who has been supporting me and also taking care of my parents when I am not home. I would also like to thank Andang Dai, Peiqi Li, Sisi Yang, Runfeng Miao, Xiruo Li, Mengyuan Sun, and Tengfei Li for all the support and care they gave me.

Most importantly, I would like to thank my family for their unconditional love. My dad always showed extreme passion and creativity for his career in education, which is one of the reasons lead me to exploring scientific research in graduate school. My mom, Fang Zhang, used to have separation anxiety even when I went to Beijing for college. I cannot imagine how she spent the last several Spring Festivals when I was only be able to go back home only once during my graduate school. The long distance does not shed shades on our love for each other. She is always there, listening to my confusions and help me releasing my negative energy. Thanks to my cutie cats Sleepy and Boss, for always providing the mental support. And my dearest husband Kuanlin Wu, he was the one pulling me back from repetitive deathly desperate situations. Literally without him, I wouldn't be able to still sit here and finish this project. I cannot count how much energy and sunshine he has brought to my life. I was always wondering, how can there be such a person with so many positive energies and never ever give up on me no matter how many terrible things I have done. I have never said this out loud, thank you for loving me, I love you more than you can imagine.

Chapter 1 – An overview of microtubule structure and dynamics

Introduction

Microtubules (MTs), together with actin filaments and intermediate filaments, comprise the three major components of the eukaryotic cytoskeleton. The diverse cellular MT morphology and precise regulation of MT dynamics underly many crucial cellular processes, including cell morphogenesis, motility, mitosis, neuronal development, and intracellular transport. Higher order complexes of MTs, microtubule-associated proteins (MAPs), and accessory proteins constitute a diverse array of sub-cellular structures that mediate key functions, e.g., the mitotic spindle that provides forces for chromosome separation during mitosis (Mitchison, 1988), cilia and flagella for motility of many organisms (Ginger et al., 2008), and axons and dendrites in neuron morphogenesis (Conde & Caceres, 2009). MTs also serve as tracks for molecular motors to transport cargoes inside cells for efficient delivery (Goodson et al., 1997). To regulate these essential cellular processes, MTs undergo dynamic instability, a phenomenon by which individual MTs switch stochastically between growth and shortening. Dynamic instability enables MTs to provide mechanical forces to explore the cytoplasm, alter membrane shapes, and support transport and positioning of organelles and other structures. An overview of current research on the MT structures and mechanisms underlying its regulation is critical for understanding how they support these fundamental cellular processes.

Physical attributes of microtubule and tubulin structure

Microtubules (MTs) are ~25 nm wide hollow cylindrical structures consisting of α/β-tubulin heterodimers. These subunits are arranged in a head-to-tail fashion to build polarized protofilaments, which then interact laterally to form cylindrical MTs (Amos & Schlieper, 2005) (**Figure 1.1A**).

α-tubulin and β-tubulin are similar in both protein structure and amino acid sequence, with 40% amino acid sequence identity (Li et al., 2002). The mammalian genome encoded 7 α-tubulins and 9 β-tubulins, with conserved structure but distinct cellular expression patterns and associated dynamics (Cleary & Hancock, 2021). Each tubulin monomer is formed by a core of two β-sheets surrounded by *α*-helices and contains three domains (Downing & Nogales, 1998): 1) the amino-terminal N-domain containing the nucleotide-binding site; 2) an intermediate I-domain as the primary globular base; and 3) the unstructured carboxyl-terminal C-domain, also known as E-hook, which bears post-translational modification (PTM) sites (Song & Brady, 2015) and is enriched in negatively charged residues that mediate electrostatic interactions with MT-binding proteins (MTBPs) (Wang & Sheetz, 2000). Whereas the I-domain of α-tubulin is exposed at minus ends trapping a nonhydrolyzable GTP inside the intradimer interface, the N-domain of β-tubulin is exposed at the plus ends of MTs, which contains the exchangeable GTP.

Microtubules assembled in vitro, using brain-derived bovine or porcine tubulin (Gell et al., 2011), contains mixtures of heterogeneous tubulin isotypes with various PTMs. This tubulin mix gives rise to heterogeneous MT structures, which can be comprised of 9 to 16 protofilaments (Amos & Schlieper, 2005). MTs with

13 protofilaments and the left-handed three-start helix set (13_3) are primarily observed in vivo (Chaaban & Brouhard, 2017). Differences in lateral interactions give rise to two distinct microtubule lattice structures: lattice type A and type B. In the A-lattice, α-tubulin from one protofilament interacts with β-tubulin from the adjacent one. In the B-lattice, lateral interactions are mediated between α-/α-, and β-/β-tubulin (**Figure 1.1B**) (Chretien & Wade, 1991). Modeling based on the lateral interactions between protofilaments showed that the electrostatic interactions formed in the B-lattice make it the most favorable configuration (Sept et al., 2003). Microtubules usually adopt B-lattice configuration, but the A-lattice configuration is preferred when microtubules are polymerized in the presence of an allele of EB1 (McIntosh et al., 2009). The subunit organization in the B-lattice leads to the formation of a seam, where adjacent protofilaments interact with α- and β-tubulin. MTs accommodate the increase and decrease in the number of protofilaments through a skew mechanism. In structures with more than 13 protofilaments, the lattice rotates to maintain the local lattice geometry in the 13_3 MTs (Amos & Schlieper, 2005). Together, the multiple axial and lateral contacts make microtubules rigid with ~5000 µm persistence length, a basic mechanical property indicating the bending stiffness (Gittes et al., 1993).
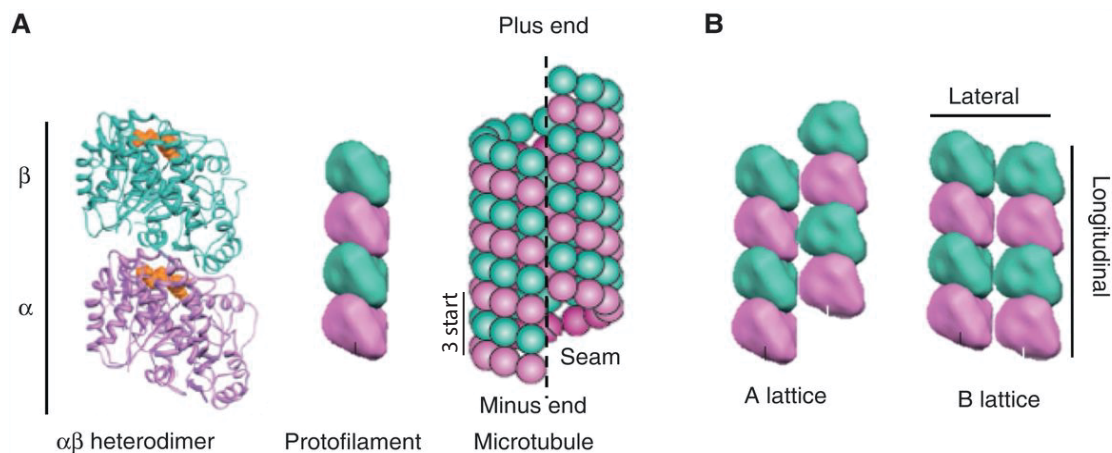
Figure 1.1 Microtubules are polar tubulin polymers with specific structure. A) α/β tubulin heterodimers are the building blocks of MTs (Left). Heterodimers are arranged longitudinally in a head-to-tail fashion into linear protofilaments (Middle). The protofilaments interact laterally with each other forming a hollow tubular structure (Right). The scheme here depicts a microtubule consisting of 13 protofilaments with a seam. **B)** In the A-lattice configuration, two adjacent protofilaments contain two tubulin heterodimers with α subunits interacting with β subunits. In the B-lattice configuration, α subunits interact with α subunits, and β subunits interact with β subunits. Figure adapted from (Goodson & Jonasson, 2018).

Mechanisms underlying MT nucleation

Purified porcine tubulin in solution spontaneously self-assembles into MTs in the presence of GTP and appropriate buffer systems (Voter & Erickson, 1984). The assembly process is characterized as having three phases: nucleation, elongation, and steady-state (Gaskin et al., 1974). The addition of new tubulin dimers to

existing MT ends is an energetically favorable process (Kuchnir Fygenson et al., 1995). However, the formation of the "critical nucleus" – where a few oligomers first come together to create stable polymers – has to overcome a large energy barrier to serve as the ends for elongation (Voter & Erickson, 1984) (**Figure 1.2**). The concentration of tubulin at which the system reaches a steady state whereby subunit loss and addition are balanced is termed the critical concentration, which is ~20 µM for mammalian tubulin (Voter & Erickson, 1984). Below the critical concentration, the critical nucleus cannot be formed – which is essential for subsequent MT assembly. Turbidity assays in which MT polymerization are monitored through absorbance provides a simple way to evaluate how different reagents or proteins regulate nucleation. The size of the critical nucleus can be estimated under simplified assumptions based on the nucleation lag phase in turbidity assays. Previous work suggested the nucleus to be in the range of 5 to 20 tubulin dimers (Voter & Erickson, 1984). The energy barrier of *in vitro* nucleation can be dramatically lowered by the addition of non-hydrolysable GTP-analogue guanosine-5'-[(α,β)-methyleno]triphosphate (GMPCPP) (Hyman et al., 1992), glycerol (Shelanski et al., 1973), DMSO (Robinson & Engelborghs, 1982), and other microtubule stabilizing reagents like taxol (Kumar, 1981), albeit through different mechanisms. The turbidity assays serve as a tool in my project to analyze the potential mechanism of Abl2 regulation on microtubule nucleation, as shown in **Chapter 5**.

The most common in vivo MT nucleation is templated by the γ-tubulin ring complex (γ-TuRC), mainly localized in the centrosome microtubule organization

center (MTOC), which overcomes the high energy barrier (Teixido-Travesa et al., 2012). γ-tubulin arranges itself in a helical manner at the edge of the ring complex cap, mimicking existing MT ends to promote nucleation. The observation of non-centrosome-dependent MT nucleation has uncovered a host of regulatory proteins and the underlying mechanisms, which I will discuss in the later sections. Given the inherent complexity associated with MT nucleation and formation of various potential intermediate structures, the mechanism or mechanisms of microtubule nucleation are not uniformly understood. A better understanding of nucleation will require the elucidation of these heterogeneous structural intermediates.
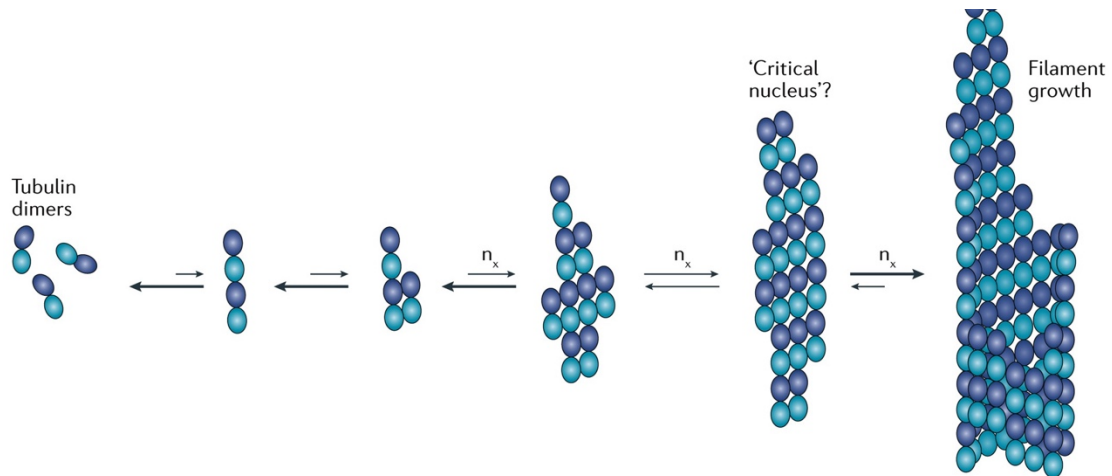
Figure 1.2 Simplified hypothetic model of microtubule nucleation. Spontaneous tubulin assembly into microtubules starts from the formation of tubulin oligomers. The first several steps are rate-limiting until the formation of so-called "critical nucleus", from which the addition of new tubulin is energetically favorable. The exact structure of the tubulin critical nucleus is not known yet, but the bulk assays estimate that the nucleus contains 5 to 20 tubulins. The size of the arrowheads indicates the likelihood of the reaction direction. Figure adapted from (Roostalu & Surrey, 2017).

Microtubule dynamic instability

In cells, MT minus-ends are stabilized by proteins in the MTOC or other structures like the Golgi apparatus (Akhmanova & Steinmetz, 2015), whereas the plus ends undergo rapid dynamics to sample the cytoplasmic environment. After localizing to the subcellular regions, *e.g.*, the kinetochore of chromosomes, Golgi, ER, and plasma membrane, MT plus-end dynamics are spatiotemporally regulated by

MTBPs in the local environment to generate pushing or pulling forces or to be stabilized as a transportation track (Yue & Wu, 2014).

MT dynamic instability is driven by GTP hydrolysis of the nucleotide at the β-tubulin N-domain, rendered by the addition of new tubulin at growing plus ends. With distinct structures, the MT plus-ends, as compared to the minus-ends, have exposed β-tubulin subunits and have faster kinetic rate constants for GTP-subunit association and GDP-subunit dissociation, therefore are relatively more dynamically unstable (Strothman et al., 2019). MT plus-ends are more extensively studied due to their critical role underlying a variety of cellular processes.

In vitro MT instability is usually measured by Total Internal Reflection Fluorescence (TIRF) Microscopy. This technique visualizes single MT filament dynamics in the presence of short GMPCPP-stabilized microtubule segments, which bypasses the rate-limiting nucleation phase. Dynamic instability is determined by 4 distinct parameters: catastrophe frequency, rescue frequency, elongation rate, and shortening rate (**Figure 1.3**) (Mitchison & Kirschner, 1984). Growing MTs oscillate between phases of growth and shrinkage. The short delay between inorganic phosphate release and hydrolysis event results in a GTP/GDP-Pi-rich region, as known as the GTP cap (Voter et al., 1991), while the older MT lattice is mainly composed of GDP-tubulin. Loss of the GTP cap exposes GDP-bound β-tubulin dimers to solution, causing the plus ends of MT to rapidly disassemble into oligomers – an event termed catastrophe. The catastrophe is observed as the switch from growth to shrinkage in vitro, and the switch from shrinkage to growth is termed as "rescue". Direct observation of single MTs in vitro

via TIRF is commonly used to determine the effect of the MTBPs on MT dynamics.

In **Chapter 4**, I show how the addition of Abl2 impacts single MT dynamics.
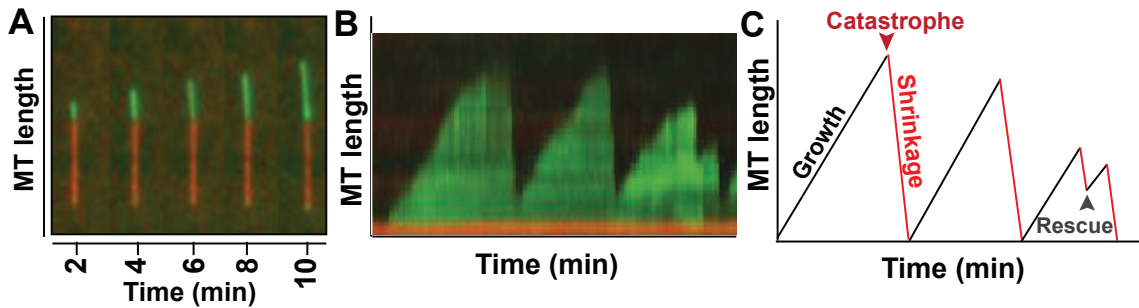
Figure 1.3 MT dynamics measurement in TIRF single filament assays. (A) A representative single MT growth under TIRF Microscopy. The red segment represents tetra-rhodamine-labeled GMPCPP-stabilized MT seeds, the green dynamic segment represents Alexa Fluor 488-labeled tubulin addition onto the seeds. **(B)** Kymograph (length/time plot derived from a movie) of single MT undergoing dynamic instability in vitro revealing dynamic behaviors at the plus ends. **(C)** Diagram of a single MT kymograph undergoing dynamic instability. The key processes, growth, shrinkage, catastrophe, and rescue, of MT dynamics are indicated. The growth and shrinkage rate can be quantified by the slope of the phase, and the catastrophe frequency and rescue frequency can be quantified by counting the events over time. **Figure 1.3B** is adapted from (Fees & Moore, 2018).

Structural basis of microtubule instability

How GTP hydrolysis regulates dynamic instability has been subject to considerable debate. Two models, 1) the allosteric model and 2) lattice model,

have been proposed (Gudimchuk & McIntosh, 2021). In the allosteric model, GTP-tubulin dimers exist in the straight conformation (Mandelkow et al., 1991), while the GDP-tubulin dimers are more bent in solution (Marantz & Shelanski, 1970). The hydrolysis of tubulin-bound GTP in MT lattice causes more bending strain, making it less stable (Muller-Reichert et al., 1998). The lattice model suggests that both GTP- and GDP-tubulin dimers are both bent in solution. GTP-tubulin might be more flexible and/or make stronger bonds with longitudinal tubulins or tubulins in neighboring protofilaments, which stabilizes the GTP-MT lattice. Elucidation of the high-resolution intermediate structures will be the key to distinguish these models.

Recent biophysical and computational studies provide more evidence favoring the lattice model (Brouhard & Rice, 2014). Small-angle X-ray scattering (SAXS) results indicate that GTP- and GDP-tubulin dimers have very similar structures in solution (Rice et al., 2008). All-atom molecular dynamics studies also predict curved structures for both GTP- and GDP-tubulin (Gebremichael et al., 2008; Grafmuller & Voth, 2011; Igaev & Grubmuller, 2018; Tong & Voth, 2020). Additionally, high-resolution cryo-EM structures reveal two major differences between the GMPCPP-MTs and GDP-MTs: 1) The MT lattice compacts longitudinally by ~2 Å per dimer following GTP hydrolysis (**Figure 1.4A**)(Alushin et al., 2014; Zhang et al., 2015); 2) The GDP-MT lattice contains ~1-3 Å separation of protofilaments at the seam, deviating from the cylindrical symmetry, making the seam a weaker point in the structure (**Figure 1.4B**)(R. Zhang et al., 2018). Additionally, the GDP•Pi-MTs, although decorated with the MTBP Doublecortin,

exhibited uneven compression of α-tubulin in the short-lived intermediate structure (Manka & Moores, 2018b), rendering further weakening of the lateral contacts.

Despite all these exciting results, the physiological relevance and mechanisms relating lattice compaction and dynamic instability are challenged by two arguments. Lattice compaction has not yet observed in yeast MTs (Howes et al., 2017; von Loeffelholz et al., 2017), indicating that other biochemical means might underlie MT dynamic properties. Additionally, the GMPCPP-MT may not be a perfect mimic of GTP-MT, thus the lattice compaction from GMPCPP- to GDP-MT may not recapitulate the transition of GTP-MT to GDP-MT lattice (Estevez-Gallego et al., 2020). High-resolution structures of GTP-tubulin dimers in solution and the GTP-MT lattice would represent a fundamental advance to elucidate the mechanisms.
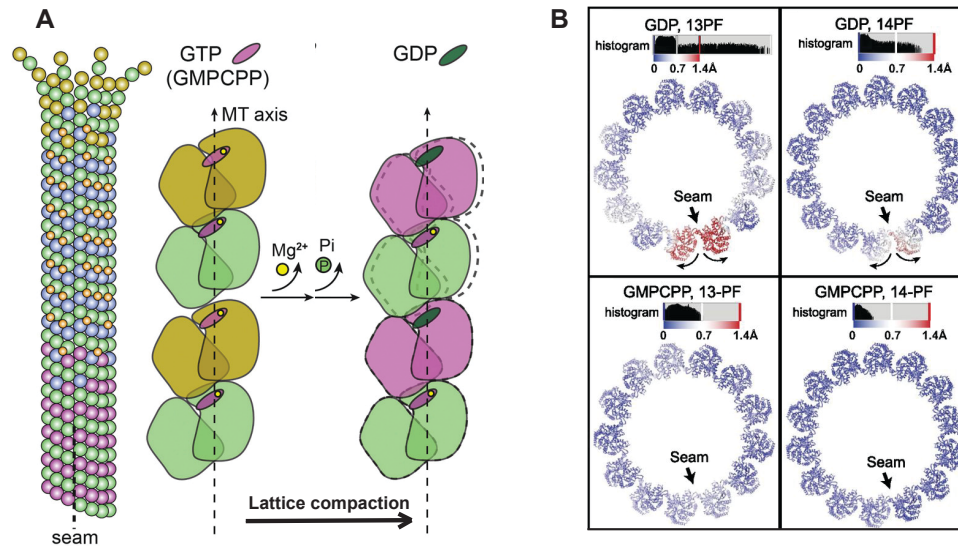
Figure 1.4 High resolution of microtubule structure reveals differences in GMPCPP (GTP-like) state and GDP state. A) As compared to GMPCPP state, GDP-MTs showed ~2 Å compaction in the longitudinal direction. **B)** These panels are the top view of MTs in A). The comparisons of the perfect helical symmetry and the resolved microtubule structure in different states, with deviations colored from blue to red. The histograms of Cα-atoms displacements are also shown above the atomic models. The top two panels are GDP-MTs and the bottom two panels are GMPCPP-MTs. Figure 1.3A is adapted from (Zhang et al., 2015); **Figure 1.3B** is adapted from (R. Zhang et al., 2018).

Ultrastructure of the MT tips and lattice

In addition to the GTP-cap, MT plus-end ultrastructure is another key determinant of dynamic instability. Early electron microscopic visualization showed that growing MT ends were tapered (Simon & Salmon, 1990). However, the dissembling MT ends were viewed as curved, outward-facing protofilaments with

broken lateral contacts (Kirschner et al., 1974; Simon & Salmon, 1990). However, recent cryo-electron tomography (cryo-ET) studies revealed that the curved structures also exist amongst growing MT tips, with the presence of sheet-like structures (**Figure 1.5**) (Chretien et al., 1995; Guesdon et al., 2016). A central and ongoing challenge would be the structural resolution of the heterogeneous growing tips, and how these growing ends serve as structural platforms for control by the MTBPs.

Interestingly, the studies on the ultrastructure inside the MT shaft started by the observation of GTP-tubulin-rich islands surrounded on both sides by the aged GDP-MT lattice, suggesting the self-repair function of MTs both *in vitro* and in cells (Aumeier et al., 2016). MT bending (Schaedel et al., 2015), movement of motors on MT (Triclin et al., 2021), and MT severing by spastin/katanin (Srayko et al., 2006) can all potentially lead to lattice defects through loss of tubulin. The self-repair process requires new GTP-tubulin to replenish sites of lattice defect, which is expedited in the presence of GTP-MT binding proteins, mostly +TIPs (Reid et al., 2019). The resulting GTP-enriched islands function as potent rescue sites to increase the MT lifespan. Data not shown here, my collaborator Daisy found that Abl2 assists in the self-repair of MTs and further protects the MT lattice.
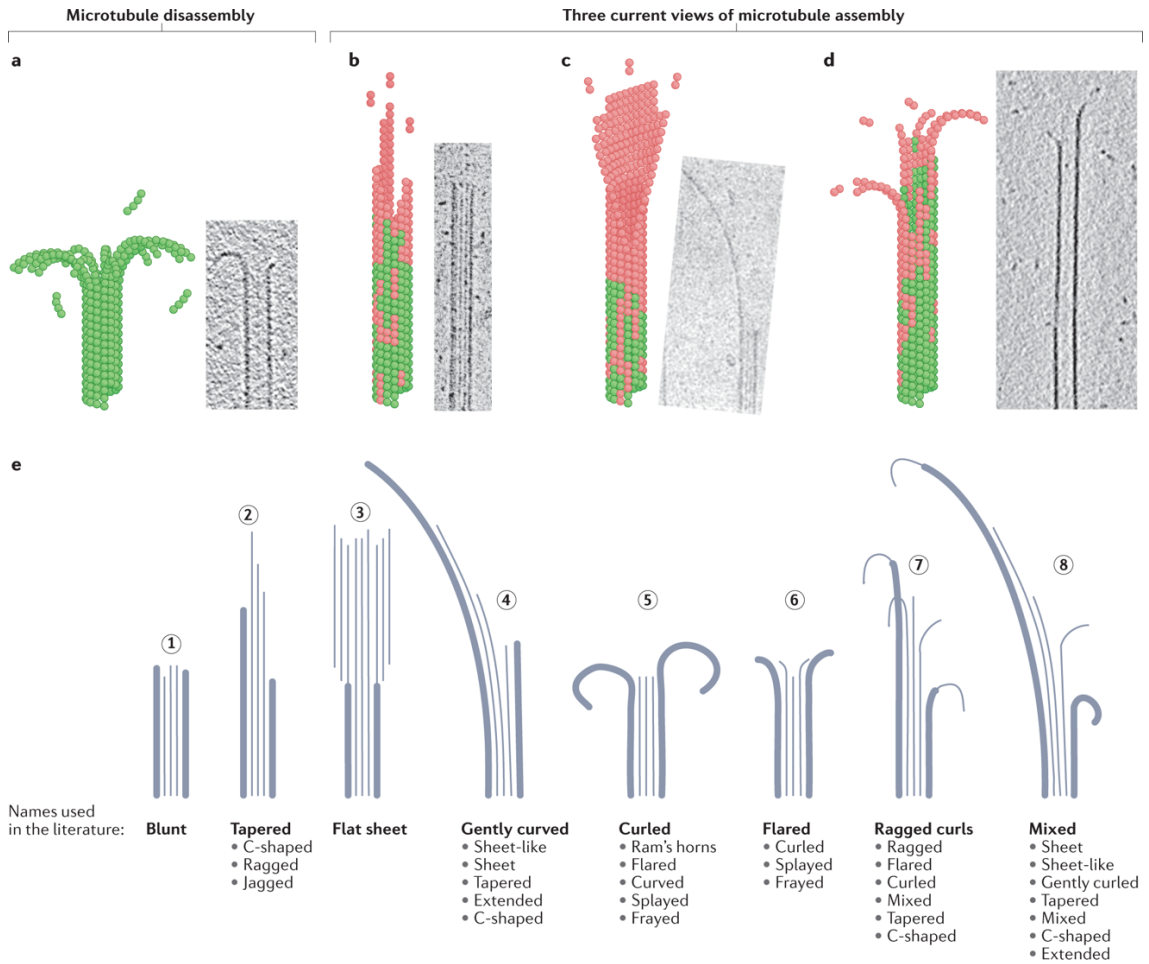
Figure 1.5 Summary of known microtubule plus ends ultrastructure. a) The left panel showed the diagram of microtubule plus ends with curled protofilaments. The right panel showed the cryo-EM image. **b)-d)** Diagram and cryo-EM images of current observed microtubule growing ends, including straight ends, curled multi-protofilaments sheet, and flared or ragged ends. **e)** Detailed collections of MT growing ends diagrams. Figure is adapted from (Gudimchuk & McIntosh, 2021).

Mechanism of MT stabilization by taxol

In the following sections, I will discuss how MT dynamics are regulated by small molecules and MTBPs. In recent years, high-resolution structures of MT stabilized by various drugs have been solved to shed light on their distinct structural impact (Manka & Moores, 2018a). Paclitaxel (taxol), the most well-known natural-source cancer chemotherapy drug, has been shown to stabilize MTs and is widely used in many in vitro MT experiments, including MT cosedimentation assays in my thesis project. However, the mechanism of its stabilization has been under debate over the years due to lack of high-resolution structures. Taxol binds to the luminal side of β-tubulin and induces a conformational change of the M-loop – the domain that mediates MT lateral contact (Nogales et al., 1998). The tubulin straight-to-bent conformation transition moves the M-loop away from the lateral contact (Li et al., 2002). The binding of taxol keeps the M-loop in the lattice-like/straight-like conformation (Elie-Caille et al., 2007). Interestingly, it was believed that taxol binding prevents the lattice compaction upon GTP hydrolysis, hence mimicking GTP-like structures (Alushin et al., 2014). Recent structural studies revealed that the taxol-MT structure harbors a minimal ~0.4 Å expansion in the longitudinal direction relative to the length of GDP-MTs, contradicting the hypothesis that taxol-stabilized MTs mimic GTP-MT structure (Kellogg et al., 2017). Distorted taxol-MTs with compacted lattices maintain lateral contact but harbor heterogeneous intermediate structures upon taxol binding (Ettinger et al., 2016; Manka & Moores, 2018b). It is for this reason that MTs may harbor structural lattice damage upon

taxol addition (Reid et al., 2017). Therefore, taxol is also applied to generate damaged MTs in the evaluation of MT lattice repair.

Regulation of MT dynamics via MTBPs

MT dynamic instability is tightly modulated via a broad spectrum of the associated proteins *in vivo*. MTBPs can be functionally categorized as stabilizers, destabilizers including severing enzymes, nucleators, end-binding proteins, bundlers/crosslinkers, and structural proteins (Goodson & Jonasson, 2018). Classic microtubule-associated proteins (MAPs) like tau, MAP2, and MAP6 stabilize MTs (Bodakuntla et al., 2019; Bosc et al., 2003; Dehmelt & Halpain, 2005). +TIPs, like EB1 (Komarova et al., 2009; Vitre et al., 2008) and XMAP215 (Brouhard et al., 2008), directly regulate MT growth by coordinating the tip GTP-tubulin incorporation. On the other hand, stathmin destabilizes MTs by binding tubulin dimers, sequestering them from the MT lattice, and decreasing the available free tubulin concentration (Howell et al., 1999). Severing enzymes spastin and katanin break inside of the MT lattice by extracting tubulin dimers out of the MT lattice (Srayko et al., 2006; Vemu et al., 2020). Here, I will briefly discuss how two known MTBPs, XMAP215 and TPX2, acting as MT nucleators and compare and constrast their different underlying mechanisms.

XMAP215/Dis1 family proteins were first identified for their abilities to regulate centrosome-dependent MT assembly (Tournebize et al., 2000) and proper chromosome disjunction (Rockmill & Fogel, 1988). It was later discovered that XMAP215 acts as a processive polymerase that interacts with both MTs plus ends

and tubulin dimers to catalyze subunit addition at the MT ends (Brouhard et al. 2008). *In vitro* experiments with purified XMAP15 additionally revealed its intrinsic capacity to promote spontaneous MT nucleation (Thawani et al., 2018). Together, these data suggested that binding of MTBPs to both tubulin and MTs not only stabilizes and promotes growth, but also facilitate MT nucleation potentially by stabilizing MT intermediate structures.

Similar to XMAP215, another protein TPX2/Xklp2 was also found to synergize with γ-TuRC in *Xenopus* eggs for templated nucleation (Kufer et al., 2002). Recent work from the Petry Lab revealed the striking mechanism underlying nucleation and branching formation by TPX2, that TPX2 phase separates into co-condensates with tubulin to enhance the nucleation efficiency (King & Petry, 2020). This discovery opens up a new field for the study of cytoskeletal related proteins and their regulation of MT dynamics. Liquid-liquid phase separation (LLPS) was discovered as a potential feature of the proteins, which are intrinsically disordered and contain multivalent binding domains, to drastically increase the local protein concentrations for function.

Regulation of MT dynamic via kinases

Phosphorylation by kinases was originally reported to regulate the binding affinity of MTBP:MT interactions. A classic example is tau, hyperphosphorylation of which abolishes its MT-binding ability and induces large aggregation formation – neurofibrillary tangles – that contribute to pathologies such as Alzheimer's Disease (Dehmelt & Halpain, 2005). Phosphorylation of MAPs also regulates the crosstalk

of microtubule and actin filaments. In vitro assays showed that phosphorylation of MAP6 by CaMKII (Calcium/calmodulin-dependent protein kinase II) prevents its binding to MTs, but does not affect binding to actin filaments, indicating phosphorylation may serve as a switch for MAP6 to translocate from MTs in dendritic branches to the pools of actin within spines (Baratier et al., 2006; Lefevre et al., 2013; McVicker et al., 2015). In most cases, phosphorylation plays an inhibitory role in MAPs binding to MTs, as the addition of negative charges from phosphate groups increases the overall negatively-charge electrostatics of the tubulin C-terminal tails. However, rare cases exist where phosphorylation enhances binding to MTs, like MAP2 (Brugg & Matus, 1991) and Eg5 (Cahu et al., 2008). Recent studies on MT-binding kinases revealed that kinases play more diverse roles in fine tuning MAPs and microtubule networks (Ramkumar et al., 2018). Phosphorylation of specific sites does not dissociate MAPs from MTs, but re-localizes them to different subcellular regions and alters the function of MAPs in the regulation of MT dynamics (Eot-Houllier et al., 2010; Lefevre et al., 2013; Tanaka et al., 2006).

Recent work identified an emerging number of kinases that directly interact with MTs. The first several kinases with direct interactions were identified by their ability to phosphorylate free tubulin subunits, e.g., CDK1 (Fourest-Lieuvin et al., 2006), DYRK1 (Ori-McKenney et al., 2016), Syk1 (Peters et al., 1996), and c-Fes (Laurent et al., 2004). Interestingly, several kinases bind to MTs, but do not appear to phosphorylate tubulin, including Abl2 (Y. Hu et al., 2019), TAOK2 (Nourbakhsh et al., 2021) and LRRK2 (Deniston et al., 2020) – mutations in all of which are

associated with defects in neuronal development. The structural resolution of LRRK2 decorating on MTs indicates that the kinase domain conformation, open or closed, regulates its MT binding (Deniston et al., 2020). Interestingly, in my project, Abl2 fragments lacking the kinase domain retain the high-affinity binding to MTs. However, we do find that the affinity is slightly reduced upon removal of the kinase domain, indicating a potential role of the kinase domain in regulating the binding function.

Summary

The MT cytoskeleton is one of the most remarkable components in eukaryotic cells. Recent advances in structural and functional analysis of MTs and MTBPs have elucidated many exciting mechanisms through which MTs adopt lattice rearrangements and presents altered dynamic instability. The inherent complexity underlying the multiple protofilaments structures have made a mechanistic understanding of its assembly and turnover a difficult undertaking, even after years of research. Much remains to be elucidated, such as determining the various structures that growing plus ends adopt and how would those structures hinder differences in dynamics. Fine control structural and dynamic changes is central to proper coordination of essential cellular processes. A better understanding of the specific roles for different MTBPs in specific cellular contexts will provide insights into how the MT network is perturbed to give rise to diseases, and how therapeutics, like taxol, can compensate for such alterations to thwart pathology.

Chapter 2 – Regulation of physiological and cellular processes by Abl

family kinases

Introduction

Abl family nonreceptor tyrosine kinases, including *Drosophila* D-Abl, *C. elegans* Abl, and the vertebrate Abl1 and Abl2 (also known as Abl-related gene, Arg) translate diverse extracellular cues, e.g., growth factors (Pendergast, 2006), DNA damage (Maiani et al., 2011; Meltser et al., 2011), and oxidative stress (Cao et al., 2003; Cao et al., 2005), into cellular responses, such as cell edge protrusion (Lapetina et al., 2009), migration (Bradley & Koleske, 2009; Kain & Klemke, 2001), proliferation and survival (Gil-Henn et al., 2013). ABL genes were first identified as an oncogene in the Abelson murine leukemia virus. Initial interest on ABL was focused on its oncogenic potential, due to the discovery of BCR-ABL1, which is a constitutively activated oncogenic kinase in human chronic myeloid leukemia (CML) (Abelson & Rabstein, 1970; Ben-Neriah et al., 1986; Goff et al., 1980). Recent studies on the unique C-terminal extensions of Abl family kinases revealed their multivalent functions in interacting with actin and MTs, which may underlie their novel roles in neuronal degeneration (Y. H. Hu et al., 2019; Miller et al., 2004; Moresco & Koleske, 2003; Omar et al., 2017). Studies on the evolution of Abl proteins, along with their structure and function, will be crucial to understand tissue-specific and context-dependent biological roles of Abl family kinases.

Developmental and physiological roles of Abl family kinases

Vertebrate genomes encode two paralogs, Abl1 and Abl2, while nonvertebrate metazoans, *Strongylocentrotus purpuratus*, *Caenorhabditis elegans*, and *Drosophila melanogaster*, have a single ABL gene (Colicelli, 2010). Abl family

kinases exhibit high conservation across these species (Colicelli, 2010; Kruh et al., 1990). After the alternatively spliced N-terminal domain, each protein contains tandem Src Homology 3 (SH3), SH2, and a tyrosine kinase domain, followed by a less-conserved C-terminal extension (**Figure 2.1**). A unicellular protist *Monosiga brevicollis* has two kinases that align well with ABL N-terminal sequence but terminate soon thereafter, suggesting the functional additions of the extended C-terminal regions occurred during evolution (Colicelli, 2010).

Genetic studies using *Drosophila* firstly revealed the potential interactions between Abl family kinases and the cytoskeleton. Drosophila Abl (D-abl) is abundant and localized at axons in the developing nervous system (Gertler et al., 1989). Mutations in *D-abl* leads to defects in the nervous system, including aberrant midline crossing of central nervous system axons and defects in motor neuron axon pathfinding (Wills, Bateman, et al., 1999; Wills, Marr, et al., 1999).

With ~40% sequence similarity to D-Abl, vertebrate Abl1 and Abl2 are extensively expressed in mammals and play especially critical roles in development of the immune and nervous systems. Abl1 is expressed in a wide range of mouse tissues, including the spleen, thymus and brain. Abl2 is mainly enriched in brains, with significant levels also in spleen, thymus, and muscle tissue (Koleske et al., 1998; Muller et al., 1982; Renshaw et al., 1988). Even with an overlap in tissue expression, protein levels and cellular localization of Abl1 and Abl2 vary. Abl2 is only found in the cytoplasm, with specific enrichment in the cell edge of fibroblasts and synapses of neurons (Y. Hu et al., 2019; Miller et al., 2004; K. Zhang et al., 2018). Abl1 also exists in the cytoplasm, but with the ability to

transport into nucleus (Colicelli, 2010; David-Cordonnier et al., 1998). Homozygous mutant mice expressing a null allele of *abl1* show low viability and increased susceptibility to infections (Schwartzberg et al., 1989; Tybulewicz et al., 1991). Interestingly, the loss of the C-terminal one-third of Abl1 in mice show a similar phenotype (Schwartzberg et al., 1991). *abl2*$^{-/-}$ mice survive to adulthood, but with neuronal defects (Koleske et al., 1998). Double deletion of *abl1* and *abl2* in mice causes early embryonic lethality, with abnormalities in neuroepithelial cells and defects in neurulation (Koleske et al., 1998), suggesting the distinct roles of Abl paralogs in mammalian development, while retaining substantial functional overlap.

Both *in vivo* and *in cellulo* analyses showed that loss of Abl family kinases leads to a significant decrease in neuronal dendritic arbor complexity and dendritic spine density, which is likely to explain the neuronal defects in knockout mice (Kerrisk & Koleske, 2013; Lin et al., 2013; Moresco et al., 2005). Studies of normal and cancer cells in culture showed that Abl family kinases increased cell motility and invasion of cancer cells potentially through its function in regulating adhesion, protrusion dynamics, and downstream cytoskeletal rearrangement (Gil-Henn et al., 2013; Mader et al., 2011; Srinivasan & Plattner, 2006). Recent work indicates that Abl family kinases are also important in cell cycle arrest (Wolanin et al., 2010), receptor endocytosis (Echarri et al., 2012), lysosome targeting, and autophagy (Yogalingam & Pendergast, 2008).
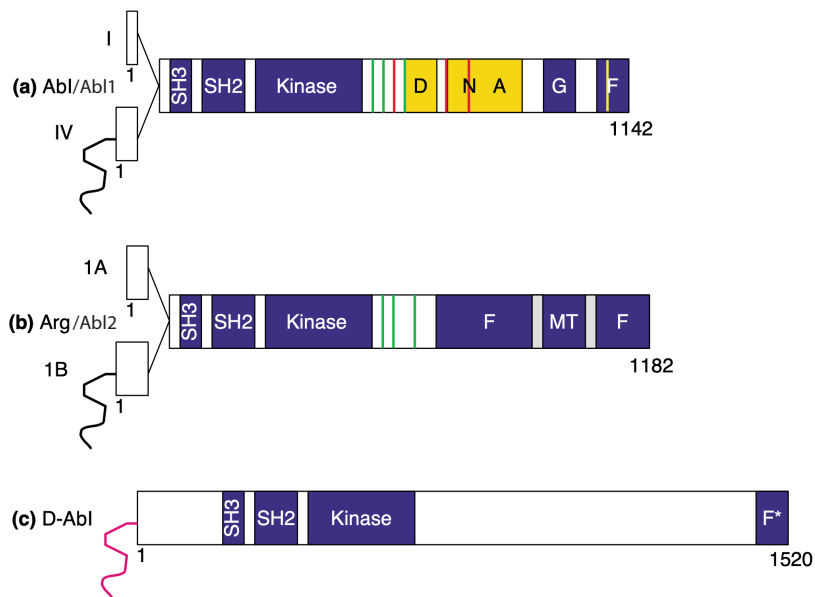
Figure 2.1 Domain structures of Abl1, Abl2/Arg, and D-Abl. (a) The domain architecture of murine Abl1. Starting at the N-terminus, the indicated features are: alternatively spliced first exon type I and IV (bound to a myristoyl fatty acid, undulated line), SH3, SH2, and kinase domains, proline-rich region (Pro-X-X-Pro, green), nuclear localization signals (red), DNA-binding domains (DNA), globular- (G) and filamentous- (F) actin-binding domains and a nuclear export sequence (yellow) **(b)** The domain architecture of murine Abl2/Arg. Abl2 also contains alternatively spliced exons type IA and IB (bound to a myristoyl fatty acid). Abl2 contains two F-actin binding domains (F) and a microtubule-binding domain (MT) in the C terminus. (c) The domain architecture of Drosophila Abl (D-Abl). D-Abl shares a consensus sequence for myristoylation, but has not been shown to be myristoylated. The C terminus domain organization is less defined. Figure adapted from (Hernandez, Krishnaswami, et al., 2004).

29

Domain functions and structural insights into Abl family kinases

The multivalent functions of Abl family kinases are embedded in the protein sequence and multi-domain organization. The N-terminal SH3-SH2-kinase cassettes of Abl1 and Abl2 share more than 90% sequence identity and 75% similarity to D-Abl (Colicelli, 2010; Hernandez, Krishnaswami, et al., 2004). The SH3 domain binds to proline-rich peptide with a Pro-X-X-Pro consensus motif to mediate both intermolecular and intramolecular interactions (Barila & Superti-Furga, 1998; Cicchetti et al., 1992; Pisabarro et al., 1998; Ren et al., 1993). The SH2 domain binds to phosphotyrosine-containing peptides with sequence specificity based on the three to six residues downstream from the phosphorylated tyrosine (Liu & Machida, 2017; Wagner et al., 2013). The Abl family kinase SH2 domain binds preferentially to the consensus sequence of pTyr-X-X-Pro/Leu (pYyr is phosphotyrosine) (Songyang et al., 1993; Tinti et al., 2013). The kinase domain specifically catalyzes the phosphorylation of the tyrosine residues in target substrates, which further modulates their localizations or functions (Boyle et al., 2007; Hernandez, Settleman, et al., 2004a; Simpson et al., 2015). Besides autophosphorylation (Brasher & Van Etten, 2000), Abl family kinases have been reported to phosphorylate many different substrates including cortactin (Boyle et al., 2007), Crk (Kain & Klemke, 2001), integrin β1 (Simpson et al., 2015) and p190RhoGAP (Bradley et al., 2006; Hernandez, Settleman, et al., 2004b) to coordinate the downstream signaling events and cellular behaviors. Even though Abl1 and Abl2 exhibit high sequence similarity, they can preferentially interact with some substrates, consistent with having unique cellular. For example, Abl2 has

significantly higher (over 10-fold) binding affinity for cortactin than Abl1, mediated through a two-residue difference in their SH2 domain sequence (Gifford et al., 2014).

The distinct subcellular localization and function of Abl1 and Abl2 result from their unique C-terminal domain composition which share 29% sequence identity. The Abl1 C-terminal domain contains a DNA binding domain; a proline-rich region (PRD) with the SH3 binding site and Pro-X-X-Pro motifs; 3 nuclear localization signals; a nuclear export signal; a G-actin binding domain; and a calponin homology (CH) F-actin binding domain (FABD). Abl2 has a PRD, an (I or L)WEQ F-actin binding domains, a microtubule binding region, and a conserved CH F-actin binding domain (**Figure 2.1**)(Bradley & Koleske, 2009).

Structural insights into Abl family kinases and their binding partners in atomic resolution provide details on the interaction mechanism. I will mainly focus on the structural advances in Abl2. The crystal structures of Abl2 SH3-SH2-kinase cassette in complex with different small molecules have been resolved (Nagar et al., 2003). A 17-residue peptide in Abl2 PRD encompassing a Pro-X-X-Pro-X-X-Pro-X-X-Pro motif adopts a type II-like SH3-PPII helix interaction in a co-crystal with cortactin (Liu et al., 2012). The structure of Abl2 C-terminal F-actin binding CH domain has been determined as a compact left-handed four-helix bundle in solution using Nuclear Magnetic Resonance (NMR) (Liu et al., 2010). Through structural alignment, this structure is found similar to the focal adhesion targeting domain (FAT) of focal adhesion kinase (FAK), indicating a potential function of Abl2 in competing with FAK for binding partners to regulate focal adhesion

dynamics. The intrinsic disorder sequence in the C terminus is the biggest obstacle of resolving the structure. However, recent advances in electron microscopy (EM) raises the possibility of obtaining the structure of the Abl2 C-terminal domain. Negative-stain EM has been applied to the investigation of the Abl2-F-actin interaction. Low-resolution structures of actin filaments decorated with Abl2 FABDs revealed that these two FABDs bind to different regions of actin filaments and induce distinct F-actin conformational changes, which is likely to explain their different roles in regulating actin filament rearrangements (Courtemanche et al., 2015; Galkin et al., 2005).

Activation mechanism of Abl family kinases

Abl family kinases relay signals from diverse upstream pathways and stimuli including growth factor receptors, integrin adhesion receptors, immune cell receptors, DNA damage, cytokines and microbial invasion, mainly through the N-terminal SH3-SH2-kinase cassette (Backert et al., 2008; Bradley et al., 2006; Plattner et al., 2003; Plattner et al., 1999; Plattner et al., 2004; Shaul & Ben-Yehoyada, 2005; Simpson et al., 2015; Wessler & Backert, 2011). The N-terminal half of Abl family kinases have similar domain organization to Src kinase, with 52% identity in the kinase domain, and 37% in the SH3-SH2 domains (Nagar et al., 2003). Similar to Src family kinases, Abl family kinases are regulated via the "latch-clamp-switch" mechanism (**Figure 2.2**)(Hantschel, 2012). In the natively inactive state, Abl kinase domains are held in a locked conformation through the intramolecular interaction, "clamp", with the SH3 and SH2 domain. This clamp is

held together with the aid of molecular "latch". In the case of Abl family kinases, the N-terminal myristoyl group binding to the hydrophobic cavity of the kinase C-lobe serves as a latch by inducing a conformational change in the C-terminal kinase domain helix which allows the docking of SH2 domain on to the kinase C-terminal lobe. Signaling through receptors or binding partners of SH3 and SH2 domains can release the clamp from the inhibitory state. Full kinase activation is then achieved by the "switch", phosphorylation of several key tyrosine residues in the kinase domain, which prevents the kinase from returning back to the inactive state (Hantschel, 2012; Harrison, 2003; Nagar et al., 2003; Tanis et al., 2003). Another critical activation mechanism is through the self-association of Abl kinases. Dimerization or tetramerization through the coiled-coil domain of BCR in BCR-ABL promotes the kinase activity, potentially due to the autophosphorylation of the oligomerized kinases (Beissert et al., 2008; Hantschel, 2012; Mcwhirter et al., 1993; Smith et al., 2003).
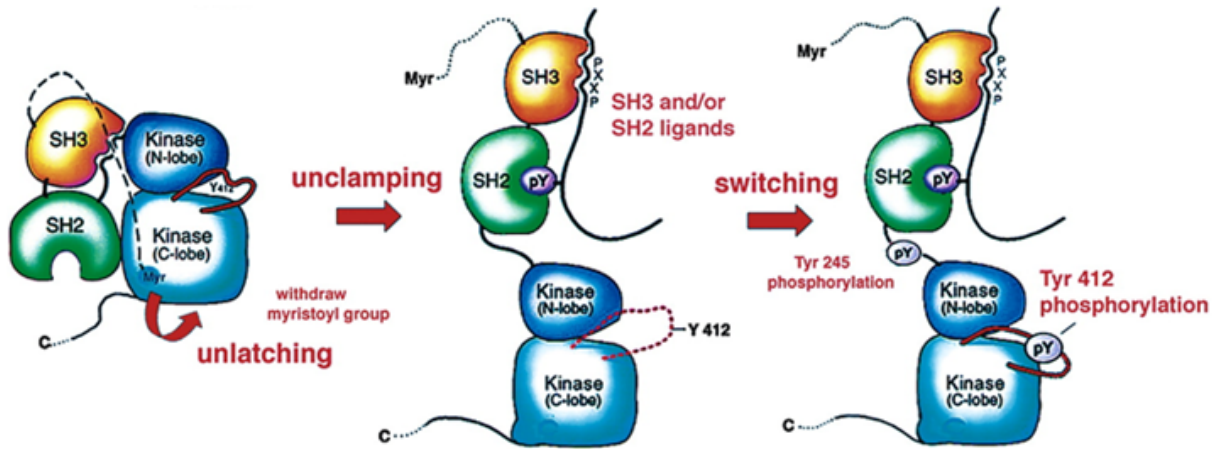
Figure 2.2 The "latch-clamp-switch" regulation mechanism of Abl2 kinase activity. Model of Abl family kinase activation propose that engagement of the SH3 and SH2 domains with cellular binding partners release the "clamp". Subsequent phosphorylation both at the Abl1/Abl2 SH2-kinase linker and Abl1/Abl2 activation loop act as a switch and promote the adoption of an active kinase state. Figure adapted from (Hantschel, 2012).

Indirect and direct interactions of Abl family kinases with F-actin

The striking findings that BCR-ABL phosphorylates focal adhesion proteins (Gotoh et al., 1995; Salgia et al., 1995) and promote dramatic changes in the actin cytoskeleton (McWhirter & Wang, 1993), which further lead to altered protrusion and migration attracted interests in how Abl family kinases might interact with actin filaments. Several Abl kinase substrates are implicated in the indirect regulation of the F-actin network (**Figure 2.3**), including Abi (Stradal et al., 2001), WAVE (Westphal et al., 2000), cortactin (Boyle et al., 2007), p190RhoGAP (Peacock et al., 2007), and N-WASp (Miller et al., 2010).

Integrin-mediated adhesion stimulates Abl2 to phosphorylate p190RhoGAP (GTPase-activating protein) on Tyrosine 1105. This phosphorylation event activates p190RhoGAP and allows it to bind to p120RasGAP, forming a complex (Bradley et al., 2006; Hernandez, Settleman, et al., 2004b; Peacock et al., 2007). The p190RhoGAP/p120RasGAP complex then translocates to the cell periphery (Bradley et al., 2006). Once localized to the membrane, the activated p190RhoGAP is positioned such that its GAP activity can act on nearby membrane-bound RhoA molecules and inactivate them. RhoA inactivation results in an inhibition of Rho-mediated contractility by decreasing signaling to Rho kinase (ROCK), thereby decreasing phosphorylation and activation of myosin light chain (MLC) (Chrzanowska-Wodnicka & Burridge, 1996). This ultimately results in a decrease in myosin-actin interaction and therefore, contractility. The decrease in contractility relaxes the cell in preparation for actin-based protrusion, thus facilitating the protrusive spreading of the cell on the extracellular matrix (Miller et al., 2004; Woodring et al., 2002).

Phosphorylation of the adapter proteins Abi1 and WAVE promote the formation of the WAVE regulatory complex (WRC) that activates the Arp2/3 complex (Mendoza, 2013), which is capable of stimulating actin branching and remodeling (Pollard, 2007). Abl2 also interacts with another activator of the Arp2/3 complex, cortactin (Boyle et al., 2007; Lapetina et al., 2009). The interaction between Abl2 and phosphorylated cortactin potently activated actin nucleation by the Arp2/3 complex (Courtemanche et al., 2015; Mader et al., 2011). Recent work showed that the disruption of Abl2:cortactin interactions eliminates stable actin

filaments in dendritic spines, significantly reducing spine density (Shaw et al., 2021). Abl family kinases coordinate cytoskeletal rearrangements via the kinase-dependent interactions with key actin-binding proteins. However, the defining characteristics of Abl family kinases are their direct interactions actin and MTs. The Abl2 C-terminal region contains two distinct F-actin-binding domains that cooperatively bind actin filaments and can bundle F-actin in vitro. Abl2 localizes to the periphery of mouse fibroblasts during adhesion and spreading where it colocalized with concentrations of F-actin (Wang et al., 2001). The C-terminal half, which lacked the kinase domain, was necessary and sufficient for this localization. Interestingly, in vitro single filament TIRF experiments showed that direct binding of Abl2 stabilizes actin filaments and can cooperate with cortactin and Arp2/3 complex to stimulate actin branching (Courtemanche et al., 2015). The decoration of Abl2 also greatly potentiates cofilin severing of actin filaments, which may be due to the actin filaments conformational change induced by the binding (Courtemanche et al., 2015). Together, these results suggest that Abl2 regulates actin structures through both direct and indirect interactions.
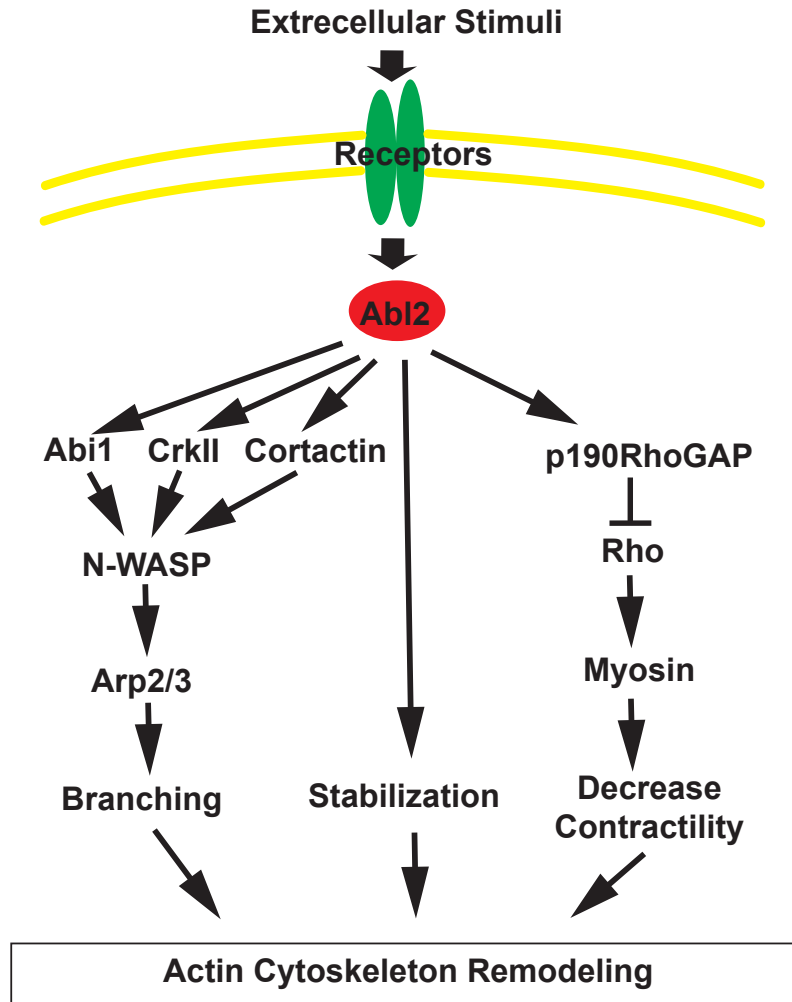
Figure 2.3 Abl2 control actin dynamics via direct binding or through other actin-binding proteins. Upon activation by extracellular cues, Abl2 interacts directly with actin filaments or through phosphorylation and cooperation of actin-binding proteins to achieve actin cytoskeleton remodeling. Figure adapted from (Tang & Gerlach, 2017).

Interaction of Abl family kinases with microtubules

The finding that Abl1 kinase activity could be activated by paclitaxel provided the first evidence of possible crosstalk between MTs and Abl family kinases (Nehme

et al., 2000). BCR-ABL-expressing cells were shown to escape the mitosis arrest under nocodazole treatment, potentially through the dysfunctional mitotic checkpoint (Wolanin et al., 2010). Recent results that Abl1 directly phosphorylates γ-tubulin, one of the key components of centrosome, also suggested a possible mechanism by which Abl family kinases might regulate MTs during mitosis (Wang et al., 2022).

Genetic studies in *Drosophila* first revealed that Abl family kinases interact functionally with MTs through the plus-end regulatory protein Orbit/CLASP to guide neuronal axon pathfinding (Lee et al., 2004). Flies carrying mutations of *D-abl* display abnormal CNS axon midline crossing and premature pathfinding of the neuromuscular junction motor ISNb axons. Mutations of *orbit*, the ortholog of vertebrate CLASP in *Drosophila*, phenocopy these *D-abl* deficiencies, which are enhanced in *D-abl*, *orbit* double mutants (Lee et al., 2004). Epistasis analysis suggests that *D-abl* acts upstream of *orbit* to mediate the growth cone targeting and axon guidance. Where and how Orbit functions were difficult to visualize in *Drosophila* growth cones, so the mechanism was further dissected in vertebrates using the orthologue protein, the cytoplasmic linker protein-Associated proteins (CLASPs). CLASPs are found localized to the growing tips of microtubules, through direct binding interactions with CLIPs and EBs (Lee et al., 2004; van de Willige et al., 2016), and act as a local stabilizer of MTs (Beffert et al., 2012; Lee et al., 2004). In vitro studies revealed that Abl1 directly phosphorylates CLASP, which then modulates its binding to MTs, but how the phosphorylation and interaction with Abl1 impacts MT network and cellular physiology are still unclear

(Engel et al., 2014). Through a yeast two hybrid screen, kinesin heavy chain (*Khc*), a member of the kinesin-1 subfamily of microtubule motors, was discovered as an interactor of *D-abl* downstream substrate *Drosophila* Enabled (*Ena*). Genetic analysis suggested that *D-abl* has a positive influence on the transport function of *Khc*, probably by inhibiting *Ena* (Martin et al., 2005). Interestingly, the orthologue of another microtubule regulator XMAP215, minispindle (*Msps*) in *Drosophila*, was shown to function during this axon guidance process by antagonizing the *D-abl* signaling through *orbit* (Lowery et al., 2010).

A milestone advance showed that Abl2 directly binds to MTs (Miller et al., 2004). Dr. Yinxiang Wang in the Koleske lab utilized the *in vitro* microtubule cosedimentation assays to show that Abl2 directly interacts with MTs. Together with its F-actin binding domains, Abl2 can act as a crosslinker of MTs and actin filaments *in vitro*. Abl2 localizes to and is required for the formation of dynamic actin-rich cell edge protrusions in 3T3 cells, which are also enriched for MTs. Inhibitors of either F-actin or MT polymerization disrupt Abl2 localization to the cell periphery and eliminate these dynamic cell edge protrusions (Miller et al., 2004). Despite these compelling data that Abl family kinases interact functionally with MTs (**Figure 2.4**), the physical and mechanistic basis by which Abl family kinases interact and regulate MTs is still unclear. My thesis aimed to understand how Abl family kinases interact with MTs and tubulin to regulate MT dynamics.
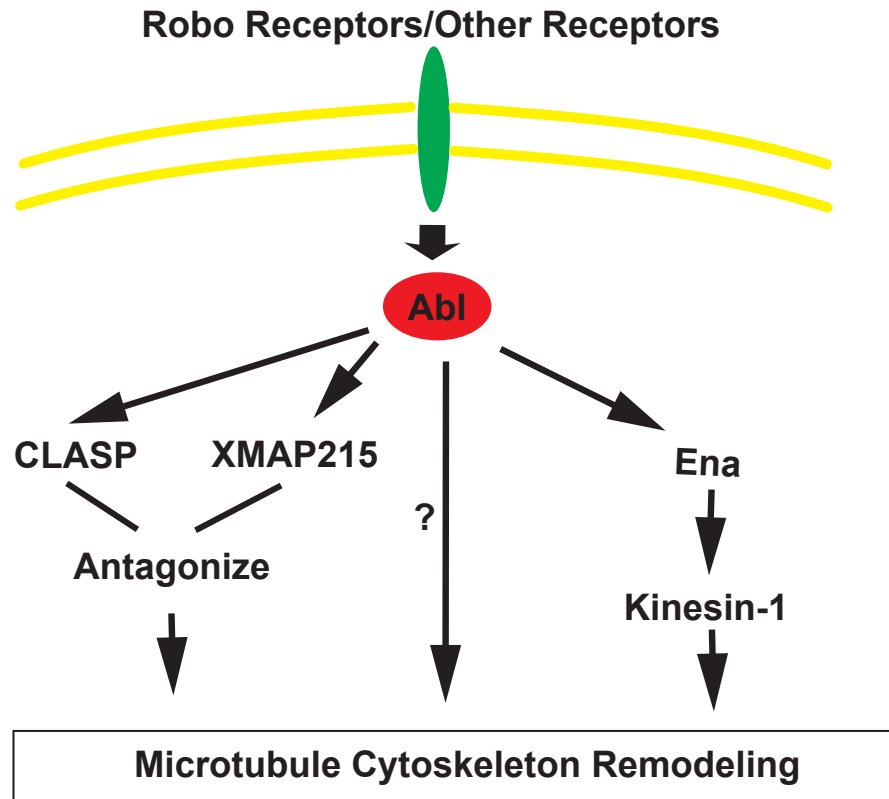
Figure 3.5. Abl Family Kinases Functionally Interact with Microtubules. Abl cooperates with multiple effectors, including kinesin, CLASP, and XMAP215 (Lee et al., 2004; Lowery et al., 2010; Martin et al., 2005). The direct interactions of Abl family kinases and the resulting regulation mechanism are still unknown.

Cell migration is mediated by the interaction of Abl2 and cytoskeleton

Cell migration is the process that requires delicate cooperation of signaling transduction and cytoskeletal remodeling with exquisite spatial and temporal precision (Seetharaman & Etienne-Manneville, 2020). In many polarized motile cells, actin polymerization provides the major force for cell migration, whereas MTs extension and capture in the periphery assist in cell mechanics, intracellular trafficking, and signaling (Kaverina et al., 1998; Seetharaman & Etienne-

Manneville, 2020). This allows the cell to sense the microenvironment and controls the focal adhesion dynamics and the polarity of migration (Gundersen, 2002a; Kirschner & Mitchison, 1986; Rodriguez et al., 2003; Waterman-Storer et al., 1999). Capture of MT ends occurs mainly through the interaction and stabilization by microtubule plus-end binding proteins (+TIPs), e.g. ACF7 (Kodama et al., 2003), IQGAP1, CLIP-170, and the associated CLASPs (Gundersen, 2002b).

The multivalent functions of Abl2 in its interaction with cytoskeleton and signaling transduction make it a potential hub in motile cells (Bradley & Koleske, 2009). Recent discoveries showed that Abl2 interacts with the regulators of the cytoskeleton to coordinate cell migration (Peacock et al., 2007). In response to extracellular stimuli through growth factor receptors and integrin receptors, activated Abl2 can directly phosphorylate actin nucleating promoting factors, such as cortactin and N-WASp, to increase the stabilized actin branching network (Courtemanche et al., 2015). The activated Abl2 also phosphorylates the p190RhoGAP to inhibit RhoA activity, attenuate actomyosin contractility and regulate adhesion dynamics (Bradley et al., 2006; Hernandez et al., 2004; Peacock et al., 2007). Even despite these many illustrated mechanisms, how Abl2 regulates MT dynamics and whether and how Abl2 mediates interactions between MTs and actin filaments in the cell migration are still unknown.

Summary

Abl family kinases mediated signaling events play fundamental roles in the development and function of the heart, vasculature, brain, and immune system, and inappropriate activation of these kinases causes leukemias and promotes solid tumor progression (Colicelli, 2010). Upon activation by growth factor or integrin adhesion receptors, Abl2 functions as a central hub for integrating signaling cues and cytoskeletal rearrangement. Inactivation of these mechanisms dysregulates cell migration, chemotaxis, and phagocytosis in fibroblasts and macrophages, impairs breast cancer cell invasion and metastasis, and causes defects in neuronal dendrite and dendritic spines development and stability (Bradley & Koleske, 2009).

Direct and indirect interactions of Abl family kinases with both actin filaments and MTs have been reported. The domains that medicate binding of Abl2 to actin filaments and their impact on actin stability and structure have been revealed. How Abl2 interacts with MTs or tubulin to regulate MT dynamics remains largely unclear.

Chapter 3 – Thesis aims and my contributions

Genetic studies in Drosophila revealed that Abl family kinases interact functionally with MTs through acting upstream of the microtubule stabilizer Orbit/CLASP and the microtubule polymerase and nucleator Msps/XMAP215, which mediates the proper control of axon guidance. Our previous colleague Yinxiang Wang firstly reported the striking finding that Abl2 directly binds MTs. Along with the two F-actin binding domains, Abl2 can act as a crosslinker of MTs and F-actin *in vitro*. Abl2 localizes to and is required for the formation of dynamic actin-rich cell edge protrusions in 3T3 fibroblasts, which are also enriched for MTs. Inhibition of either F-actin or MT network disrupts Abl2 localization to the cell periphery and eliminates the dynamic cell edge protrusions (Miller et al., 2004). Despite these compelling data that Abl family kinases interact functionally with MTs, the physical and mechanistic basis by which Abl family kinases interact with and regulate MTs remain elusive**. The main objective of my project was to characterize the physical and functional interactions between the Abl family kinases and dynamic MTs.** I provide evidence here that the Abl2 non-receptor tyrosine kinase regulates microtubule dynamics via direct binding to free tubulin and MT lattice, which is underlying the role of Abl2 in cell migration.

Aim 1. Characterization of the physical interactions between Abl2, MTs, and tubulin.

To examine which amino acid regions of Abl2 are important in mediating the Abl2 interactions with MTs and tubulin, I designed a library of Abl2 truncations to perform the functional assays for binding measurements. Different affinity tags are tested to obtain better protein quality and reduce the potential effect on protein functions in the assays. In collaboration with Daisy Duan, MT cosedimentation assays and TIRF microscopy were used to qualitatively and quantitatively measure binding of Abl2 fragments to taxol-stabilized MTs and GMPCPP-stabilized MTs. The preference of Abl2 for different nucleotide states of MTs was also analyzed. The size-exclusion chromatography profile of Abl2 mixed with tubulin indicated that Abl2 formed complexes with tubulin dimers. I further performed BioLayer Interferometry to quantify the tubulin binding affinity of Abl2 and Abl2 fragments, localize the tubulin binding regions, and evaluated how the ionic strength impacted Abl2 binding to tubulin.

Aim 2. Examination of how Abl2 regulates microtubule dynamics *in vitro* and in cells.

I performed the bulk tubulin turbidity assays to measure how Abl2 regulates MT nucleation and assembly. Interestingly, as a protein with an intrinsically disordered region, Abl2-eGFP undergoes phase separation under conditions thought to mimic the conditions of a crowded intracellular environment. I measured if Abl2 can co-condensate with tubulin to further regulate MT nucleation. My collaborator Yuhan

Hu performed in vitro fluorescence microscopy assay to visualize the dynamics of microtubules in the presence and absence of Abl2 or Abl2 fragments.

I then aimed to investigate how Abl2 regulates the cytoskeletal network in cells. I engineered CRISPR *abl2*$^{-/-}$ cells and re-constituted the *abl2*$^{-/-}$ cells with Abl2-eGFP or Abl2 fragments-eGFP. I used the microtubule tip tracking peptide MACF43, fused with a fluorescent marker as a reporter to visualize the plus-end growth of MTs in cells and measured the rate of microtubule growth in the absence or presence of Abl2 or Abl2 fragments. Previous work reported that Abl2 mainly localizes to the cell edge and regulates the cell edge protrusions through interacting with actin filaments and microtubules. I performed live cell imaging using TIRF and confocal microscopy to visualize the interaction of Abl2 and cytoskeleton in cells. Lastly, I analyzed how cell migration is regulated in WT and *abl2*$^{-/-}$ cells, and the reconstituted cells re-expressing different Abl2 fragments.

Chapter 4 – Characterization of the Physical Interactions between Abl2, MTs, and Tubulin

Abstract

Genetic studies in Drosophila indicate that Abl family kinases interact functionally with MTs, specifically with orbit/CLASP, which is the MT stabilizer that regulates the proper neuronal axon pathfinding (Lee et al., 2004). Previous work identified Abl2 as a direct interactor of both actin filaments and MTs (Y. Hu et al., 2019; Miller et al., 2004). Extensive studies of Abl2 interaction with actin filaments from our lab and others outlined the mechanism that Abl2 directly stabilizes actin filaments and cooperates with cortactin to regulate the actin branching. However, how Abl2 interacts with MTs remained mysterious for more than ten years. My collaborator Yuhan Hu in the Koleske Lab provided one piece of the puzzle that the binding of Abl2 to MT lattice is mainly mediated through the electrostatic interaction with the disordered E-hook of MTs (Y. Hu et al., 2019). There are many other questions that remain to be answered to unveil the comprehensive interaction mechanism, including a) what is the MT binding region inside Abl2? b) Does Abl2 recognizes different MT nucleotide states? c) Does Abl2 binds to tubulin dimers?

To answer these biochemical questions, I started from studies of the biophysical properties of Abl2 using Stokes' radius analysis and multi-angle light scattering coupled with size exclusion chromatography (SEC-MALS) analysis. I provide evidence here that Abl2 mainly exists as monomers *in vitro*. In the subsequent studies, I designed a panel of Abl2 fragments and performed microtubule cosedimentation assays to determine the minimal regions that bind MTs. My data suggest that the C-terminal region is required for strong binding of Abl2 to MTs, since truncations from both sides largely reduced the binding affinity.

Interestingly, even though the N-terminal half containing the kinase domain does not directly bind to MTs, the deletion of it reduces Abl2 binding affinity to MTs, which is likely mediated through the phosphorylation level or the conformational change. As I reviewed in Chapter 1, MTs have different ultra-structures when bound with different nucleotides, generally characterized as the GTP-cap and the GDP-MT lattice. Determination of where Abl2 binds on the MT lattice is critical for understanding the role of Abl2 in regulating the MT network. I found that Abl2 binds tightly to both taxol- and GMPCPP-stabilized MTs. My collaborator Daisy Duan showed that Abl2 has a preference for the GMPCPP-MTs over GDP-MTs using TIRF Microscopy. Strikingly, I also found that Abl2 directly binds to tubulin. Measurements of the tubulin binding using BioLayer Interferometry (BLItz) revealed that Abl2 binds to tubulin through the two different regions aa. 688-924 and aa. 1024-1090. The loss of aa. 688-790 eliminates the observable binding to tubulin. I reported that the interaction is mediated through electrostatic interactions and partly through the C-terminal tails of MTs. Taken together, our data indicate that Abl2 possesses binding abilities to GTP-MTs and tubulin, which may enable Abl2's function to regulate MT dynamics.

Purified Abl2 and Abl2 fragments exist primarily as monomers in solution.

The intrinsic disorder property of Abl2 impeded the yield and purity of Abl2 and Abl2 fragments' purification. Different affinity tags have been explored to obtain better protein quality and reduce the potential effect in the assays. The switch from MBP-tag to His_6-tag purification system produces much higher yields of the proteins. Interestingly, the purified His_6-tag cleaved Abl2 runs at an unexpected early elution volume in the size-exclusion chromatography, indicating either an extended conformation or the existence of oligomers (**Figure 4.1A**). I set out to determine the biophysical properties of Abl2 using the Stokes' radius analysis and SEC-MALS analysis.

The Stokes' radius (R_s) of Abl2 full-length and the C-terminus were determined by gel filtration chromatography. The standard proteins, Thyroglobulin (670 kDa, 86 Å), γ-globulin (150 kDa, 51 Å), Ovalbumin (44.3 kDa, 28 Å), and Ribonuclease A (13.7 kDa, 17.5 Å) were used to generate the standard curve for the estimation of Abl2's Stokes' radius (**Figure 4.1B**). Purified His_6-tag cleaved Abl2 full-length (122 kDa) eluted at about 10.66 mL with a Stokes' radius of 78 Å, corresponding to a globular protein at about 480 kDa. Purified His_6-tag cleaved Abl2-557-C (66 kDa) eluted at about 11.45 mL with a Stokes radius of 67.7 Å, corresponding to a globular protein at about 350 kDa. I went on to test if the extended Stokes radius is due to the oligomerization of Abl2 or the extended conformation.
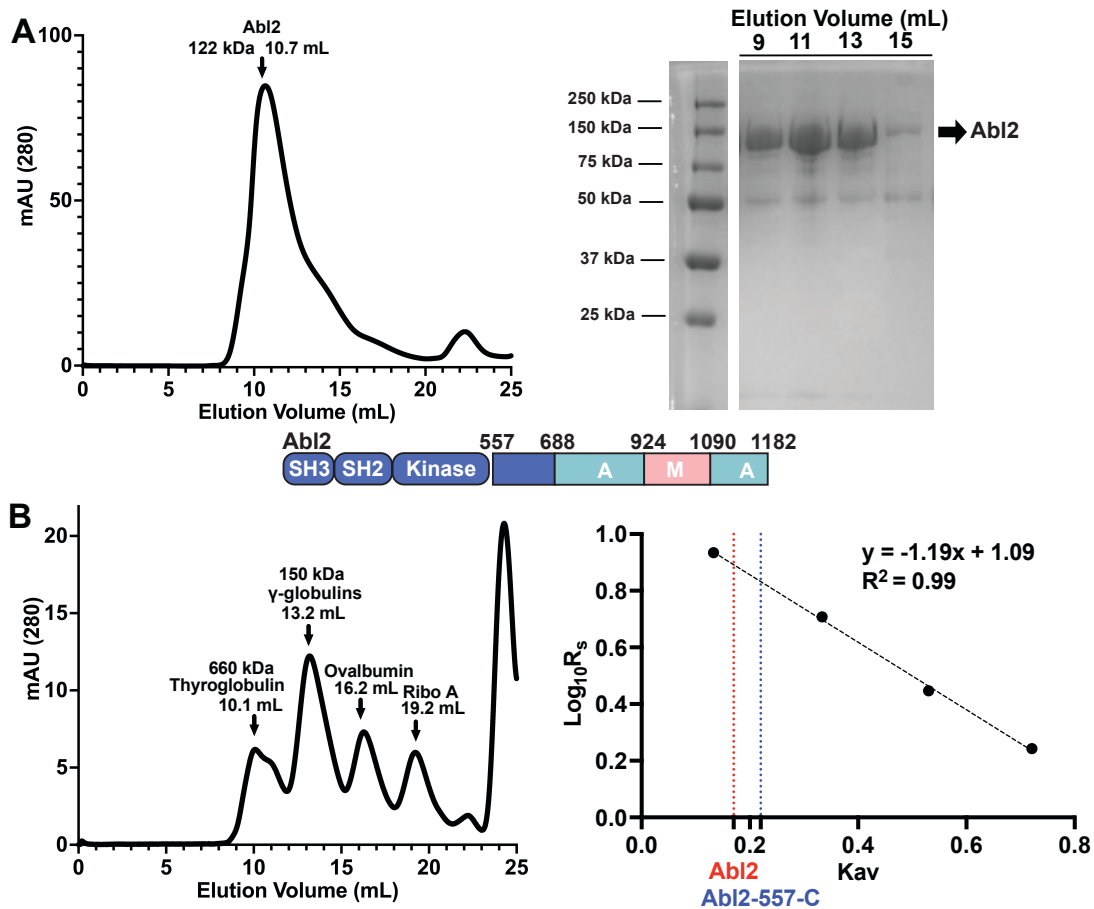
Figure 4.1 Purification of Abl2 and Stokes radius determination. A) Gel filtration chromatography of His$_6$-tag cleaved Abl2 and the corresponding SDS-PAGE of the purified Abl2. **B)** Gel filtration chromatography of the standard proteins and the standard curve of the Stokes' radius and the partition coefficient, K$_{av}$, a parameter calculated as $(V_e-V_0)/(V_t-V_0)$, where V_e represents the elution volume corresponding to the protein peak, V_0 is the void volume of the column, and V_t is total bed volume. The dotted lines indicate the positions of Abl2 and Abl2-557-C.

In collaboration with Dr. Chunxiang Wu in the Xiong lab, we utilized size-exclusion chromatography coupled to multi-angle light scattering (SEC-MALS) to confirm the native state of Abl2 and Abl2 fragments. Interestingly, SEC-MALS data reveal that the peak of Abl2 with 78 Å Stokes radius (Peak1) has a molecular weight of ~127 kDa, corresponding to the monomer state. The presence of the significantly large complex eluting at the void volume (Peak3) and the dimer peak eluting at 10.1 mL (Peak2) may underlie the oligomers formed under formaldehyde crosslinking. The analysis of Abl2-557-C, Abl2-N-688, and Abl2-688-C are all predominantly monomers, with a low population of dimers (**Figure 4.2**). The combining result of Stokes' radius analysis and SEC-MALS data indicate that Abl2 exists mainly as an extended monomer in solution. The attempts to solve the structure of Abl2 or Abl2-557-C using Electron Microscopy (EM) of negatively stained specimens failed due to the heterogeneity of the protein samples.
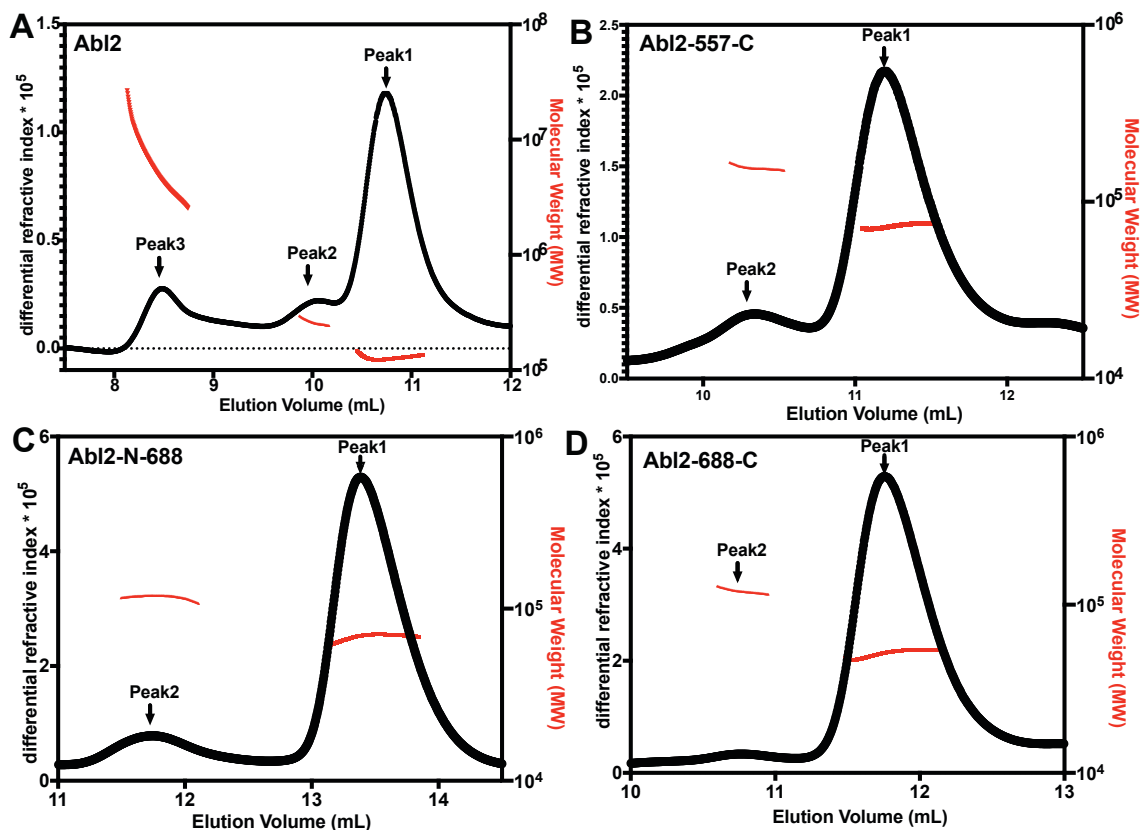
Figure 4.2 SEC-MALS analysis showed that Abl2 mainly exists as monomers in solution. The profiles of SEC-MALS of **A)** Abl2; **B)** Abl2-557-C; **C)** Abl2-N-688; **D)** Abl2-688-C. The left axis showed that differential refractive index and the right axis showed the calculated molecular weight based on the light scattering signals. In **A)** All 3 peaks were shown, in which Peak1 corresponds to the monomer, Peak2 corresponds to the dimer, and Peak3 corresponds to either aggregation or higher oligomers. In **B)**, **C)**, and **D)**, only Peak1 and Peak2 were shown.

Abl2 binds to the MT lattice mainly through the C-terminus.

We previously characterized MT binding of Abl2 fragments fused to dimeric glutathione-S-transferase (GST) fusion or the large molecular weight maltose binding protein (MBP) (Y. Hu et al., 2019; Miller et al., 2004). Concerned that these moieties may introduce artifacts, we purified monomeric Abl2 protein and fragments fused C-terminally to GFP via N-terminal His$_6$-tags, which were subsequently removed. Consistent with findings from our previous work (Y. Hu et al., 2019), His$_6$-cleaved Abl2-eGFP binds to taxol-stabilized MTs with a dissociation constant K$_D$ = 0.37 ± 0.12 µM (**Table I**) and the C-terminal half 557-C-eGFP binds to MTs with a slightly lower affinity (K$_D$ = 0.66 ± 0.16 µM, **Figure 4.3A**). Abl2-557-C is enriched with positively charged residues (12.8%, 80/626) and prolines (10.7%, 67/626), which is one of the conserved features in MT binding regions (Goode et al., 1997; Tajielyato et al., 2018). Abl2-557-1024-eGFP maintain binding ability to MTs, albeit with a lower affinity (K$_{D, 557-1024-eGFP}$ = 3.8 ± 1.5 µM, **Table I**). Further truncation to 557-930 still showed binding to MTs, however, the binding did not reach saturation, thus preventing us from estimating the affinity of this fragment for MTs accurately (K$_D$ > 3 µM). Smaller fragments including 557-688-eGFP, 688-924-eGFP, and 1024-1090-eGFP at 2 µM did not bind to rhodamine-labeled MTs imaged by TIRF microscopy (data not shown). Assessments of Abl2 fragments binding to MTs are summarized in **Table I**. Interestingly, Abl1 and a naturally existing Abl2 neuronal isoform lacking amino acids 688-790 (Abl2Δ688-790) (Perego et al., 2005) exhibit strong binding to MTs (K$_{D, Abl1}$ = 0.45 ± 0.17 µM; K$_{D, Abl2Δ688-790}$ = 0.40 ± 0.20 µM, **Figure 4.3B, C**).

Together, these data suggest that the C-terminal is required for strong binding of Abl2 to MTs.

Abl2-N-557-eGFP does not bind directly to MTs. However, truncation of Abl2 N-557 from Abl2-FL-eGFP decreases MT binding affinity. Phosphorylation of MTBPs has been shown to play an important role in mediating the interaction with MTs. Considering that there are abundant phosphorylated tyrosines in Abl2-N-557, Abl2 binding on MTs is likely regulated by the phosphorylation of the N-terminus. We added PD180970, a tyrosine kinase inhibitor, at the onset of Abl2-eGFP expression in Hi5 insect cells. Global phosphorylation of Abl2-eGFP was successfully controlled at low levels, as proven by western blot (**Figure 4.3D**). Co-sedimentation assays showed that tyrosine dephosphorylated Abl2-eGFP still binds MTs, but with weak affinity, K_D = 2.4 ± 1.4 µM (**Figure 4.3E**).

		K_D (µM)
Abl2-eGFP	SH3 SH2 Kinase 557 688 924 1090 1182 A M A	0.37 ± 0.13
N-557-eGFP	SH3 SH2 Kinase	N.B.
557-C-eGFP	A M A	0.66 ± 0.15
557-C	A M A	1.1 ± 0.26
Abl2Δ688-790	SH3 SH2 Kinase A M A	0.40 ± 0.20
557-688-eGFP		N.B.
557-1024-eGFP	A	3.8 ± 1.5
557-930	A	> 3
Dephosphorylated Abl2-eGFP	SH3 SH2 Kinase A M A	2.4 ± 1.4

Table I. Summary of Abl2 and Abl2 fragments binding to taxol-MTs. Disassociation constant (K_D) data are measured as means ± S.D., for each assay condition, n > 3. NB: Not Binding, NS: Not Saturating, binding did not reach saturation for the tested concentrations.
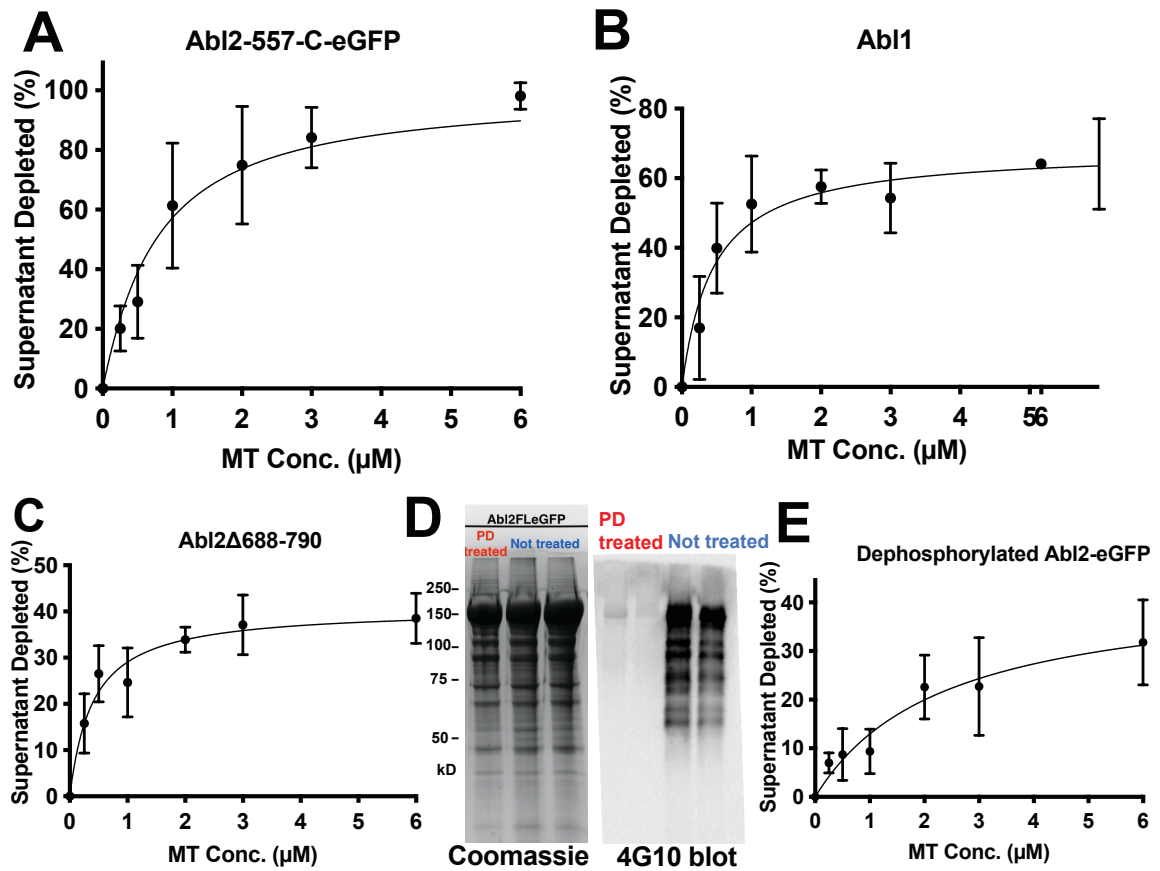
Figure 4.3 Abl2 binds to taxol-MTs via the C-terminal half. The plots of the percentage of **A)** 557-C-eGFP, **B)** Abl1, **C)** Abl2Δ688-790, and **E)** the dephosphorylated Abl2-eGFP bound versus MT concentration are shown. For each MT cosedimentation assay condition, n ≥ 4. **D)** Purified Abl2-eGFP and dephosphorylated Abl2-eGFP were run with SDS-PAGE, followed by Coomassie blue G250 staining in the left and by western blot using the phosphorylated tyrosine antibody 4G10.

Abl2 binds stronger to GMPCPP-MTs than GDP-MTs.

New tubulin dimers are added to the growing tips of MT protofilaments in complex with GTP, which undergoes hydrolysis into GDP. The growing MT contains a "cap" of GTP-polymerized tubulin that protects it from destabilization, which occurs when aged GDP-bound protofilament ends are exposed to solution. GMPCPP is a slowly hydrolyzed analog of GTP; hence, MTs polymerized from GMPCPP structurally mimic the GTP cap. To decipher the mechanism by which Abl2 regulates the MT network, it is critical to understand whether Abl2 binds preferentially to the GDP:MT lattice or the GTP:MT caps. Previously I showed that Abl2 binds to taxol-stabilized MTs with high affinity. Cosedimentation assays with MTs stabilized with GMPCPP showed that Abl2-eGFP binds to MTs stabilized with taxol ($K_D = 0.37 \pm 0.12$ µM) or with GMPCPP ($K_D = 0.33 \pm 0.15$ µM) with similar dissociation constants (**Figure 4.4A, B**). My collaborator Daisy established the MT segmentation assays to measure whether Abl2 preferentially binds to GDP- or GMPCPP-bound polymerized tubulin, which mimics the GTP-bound state (**Figure 4.4C**). GDP-MTs were grown from GMPCPP-seeds and capped with GMPCPP-polymerized tubulin to prevent catastrophe. Control specimens EB1-eGFP and tau-eGFP bound preferentially to GMPCCP-MTs and GDP-MTs, respectively as demonstrated previously (Castle et al., 2020; Reid et al., 2019; Zanic et al., 2009). Purified Abl2-eGFP and 557-C-eGFP bound preferentially to GMPCPP-MT segments over GDP-MT segments (**Figure 4.4D, E**), where they may facilitate tubulin addition or stabilize the MT lattice.
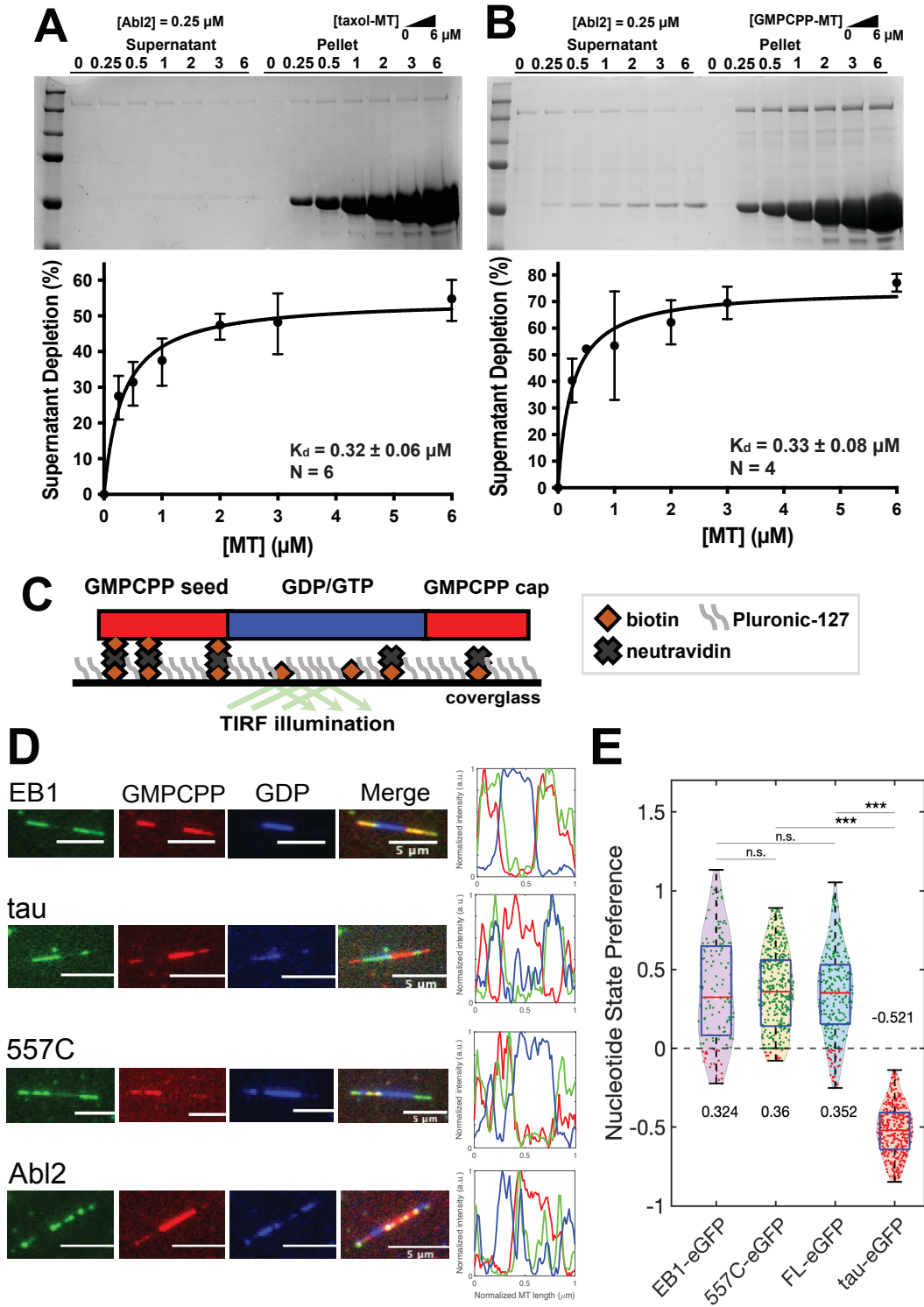
Figure 4.4 Abl2 binds the MT lattice, with a preference for GMPCPP-MTs over GDP-MTs.

(Figure caption on next page.)

Figure 4.4 Abl2 binds the MT lattice, with a preference for GMPCPP-MTs over GDP-MTs. A, B) Representative gels of the cosedimentation assays performed with **A)** taxol-stabilized MTs and **B)** GMPCPP-stabilized MTs and the plots of the percentage of Abl2 or Abl2 fragments bound versus MT concentration are shown. The fitted K_D values indicated that Abl2 binds similarly to taxol-MTs and GMPCPP-MTs. N indicates the replicates number of the experiments. **C)** Diagram of the experimental setup. The middle GDP-enriched segments labeled by Alexa Fluor 647-tubulin are capped by the GMPCPP-enriched segments labeled by rhodamine-tubulin. **D)** EB1-eGFP, Tau-eGFP, Abl2-eGFP, and 557-C-eGFP prefer different nucleotide-enriched segments, and the preferences of the GMPCPP-segments over the GDP-segments are quantified in **E)**, shown as the log scale. **E)** The binding intensity of proteins on GMPCPP- over GDP-MTs were plotted in log scale. The points above 0 indicate preferred binding to GMPCPP-MTs, and below 0 indicate preferred binding to GDP-MTs.

Abl2 binds to free tubulin dimers via the C-terminal half.

I next set out to test whether Abl2 binds tubulin dimers in solution using size-exclusion chromatography. Purified Abl2 and porcine tubulin were applied separately or after mixing for 30 min on ice to the Superdex 200 column and their elution profiles were measured. Interestingly, the mixture of Abl2 and tubulin shifted tubulin to the earlier fractions. As shown in the first section, purified Abl2-557-C (68 kDa) eluted at about 11.45 mL with a Stokes radius of 67.7 Å, corresponding to a globular protein at about 350 kDa. The incubation of His-Abl2-557-C and tubulin leads to the formation of a new peak with larger Stokes radius of 101 Å (**Figure 4.5A, B**).

To quantitatively measure the affinity of Abl2 binding to tubulin dimers, I performed biolayer interferometry (BLItz) using His-Abl2 and His-Abl2 fragments. His-Abl2 or His-Abl2 fragments were immobilized on a Ni-NTA affinity chip and the binding of a range of concentrations of tubulin were measured as a change in the binding signal (nm). Purified His-Abl2 bound tubulin dimers with a K_D = 42 ± 13 nM. His-Abl2-557-C is sufficient for high-affinity tubulin dimer binding, K_D = 17 ± 8 nM (**Figure 4.5C, D**), while the Abl2 N-terminal half, His-Abl2-N-557, did not detectably bind dimers (**Table II**). Interestingly, increase of the association buffer salt from 100 mM to 300 mM KCl largely reduced the binding signals (**Figure 4.5 E**). We further tested the binding affinity of His-Abl2-fragments to identify the tubulin dimer binding domain in Abl2 (**Table II**). Two distinct fragments, Abl2-688-924 and 1024-1090, each bound independently to tubulin dimers, but with greatly lower affinity ($K_{D, 688-924}$ = 118 ± 39 nM; $K_{D, 1024-1090}$ = 252 ± 123 nM). Strikingly, the naturally

expressing isoform His-Abl2Δ688-790 fails to bind tubulin but binds strongly to MTs ($K_{D, Abl2\Delta688-790}$ = 0.40 ± 0.20 μM, **Figure 4.4C**). This indicates that the MT-binding region and tubulin-binding region of Abl2 are not completely overlapping.
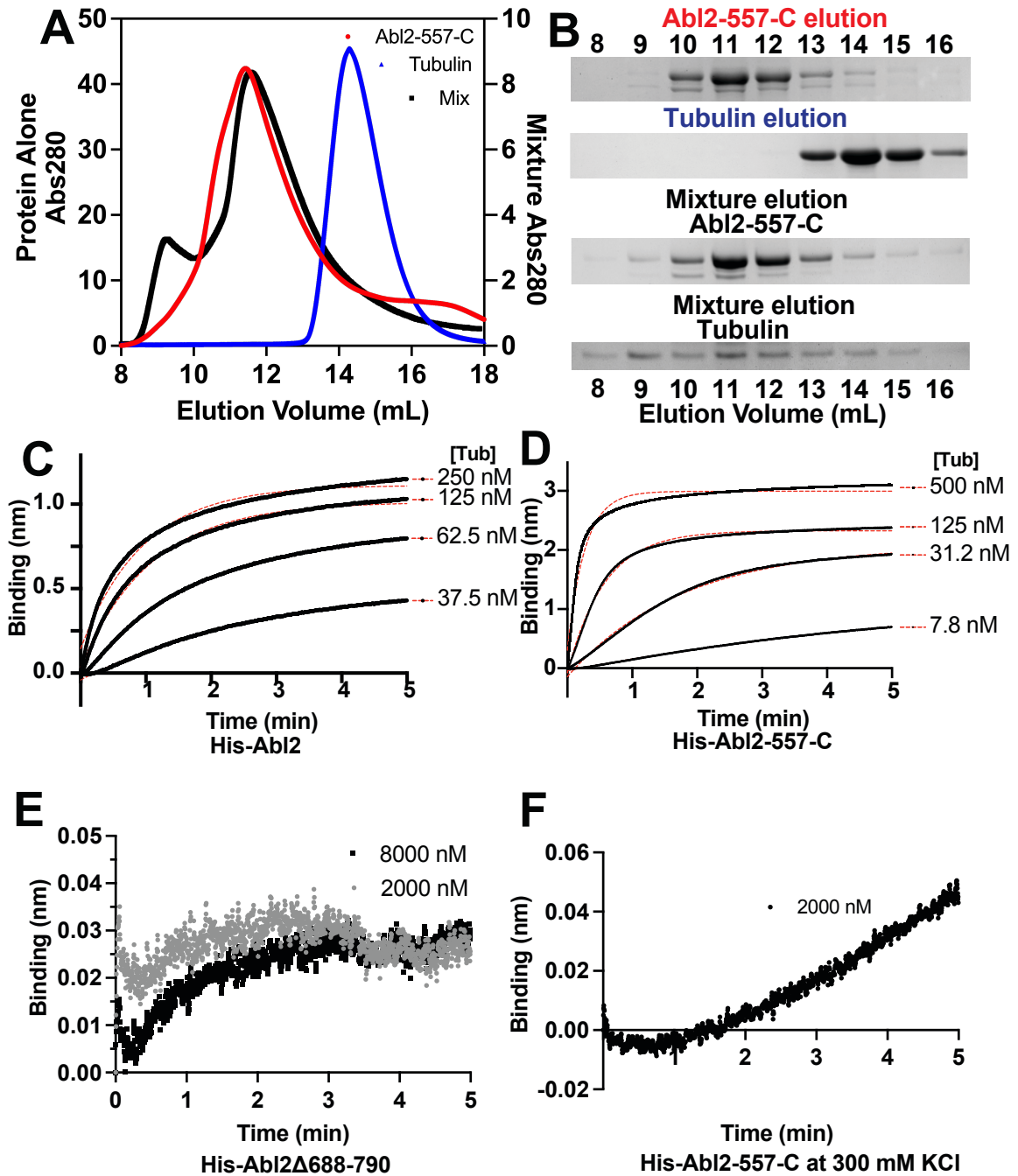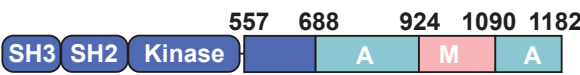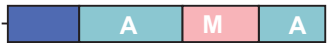
Figure 4.5 Abl2 binds tubulin via two regions in the C-terminal half.

(Figure caption on next page.)

Figure 4.5 Abl2 binds tubulin via two regions in the C-terminal half. A) SEC analysis of 557-C, tubulin, and the mixture of 557-C and mixture. The corresponding SDS-PAGE analysis of the SEC elution fractions is shown in **B)**. His-Abl2 **C)** or His-557-C **D)** were immobilized on a Ni-NTA biosensor and the association of different concentrations of tubulin was measured. Representative traces are shown, with data in black and one phase exponential fits in red dotted lines. Full concentration gradients (4 tubulin concentrations) were performed at least three independent times and used to calculate a K_D. **E)** Tubulin binding to His-Abl2Δ688-790 are not observable in the presence of 2000 nM and 8000 nM tubulin. **F)** The binding signals are significantly reduced for His-Abl2-557-C when the association buffer contains 300 mM KCl.

	K_D (nM)	k_{on} ($*10^6$ M^{-1}min^{-1})	k_{off} (min^{-1})
Abl2	42 ± 13	3.6 ± 1.1	0.14 ± 0.02
N-557	N.B.	N.B.	N.B.
557-C	17 ± 8	8.6 ± 2.1	0.15 ± 0.08
Δ688-790	N.B.	N.B.	N.B.
688-924	118 ± 39	5.4 ± 2.6	0.58 ± 0.15
930-1090	20 ± 3	12 ± 1.0	0.23 ± 0.02
924-1024	N.B.	N.B.	N.B.
1024-1090	252 ± 123	8.3 ± 0.83	1.5 ± 0.10

Table II. Summary of Abl2 and Abl2 fragments binding to tubulin. Disassociation constant (K_D) data are measured as means ± S.D., for each assay condition, n = 3. N.B.: Not Binding, the binding signals are not observable or really low that cannot be fit. The parameters are fitted using the GraphPad Prism 9 "Association Kinetics – Two or more ligand concentrations", which assumes a shared k_{off} and globally fits the data to the exponential association kinetic model to derive a single best-fit estimate for k_{on} and k_{off}.

Chapter 5 – Regulation of MT dynamics via Abl2 *in vitro* and in cells

Abstract

Abl family kinases-mediated signaling events and cytoskeletal rearrangements play fundamental roles in many cellular processes, including cell morphogenesis and migration, and neuronal dendrites stability. Previous work by Ann Miller showed that Abl2 localizes to and is required for the formation of dynamic actin-rich cell edge protrusions in 3T3 cells, which are also enriched for MTs. Inhibition of either F-actin or MT polymerization disrupts Abl2 localization to the cell periphery and eliminates these dynamic cell edge protrusions (Miller et al., 2004). In the previous chapter, I showed that Abl2 directly interacts with MTs and tubulin *in vitro*. The mechanistic functions of Abl2 through these interactions *in vitro* and in cells remain unknown. I provide evidence here that Abl2 promotes MT nucleation and assembly in the turbidity assays, which requires the interaction of Abl2 with tubulin. Interestingly, we found that Abl2 form co-condensates with tubulin in the presence of molecular crowding reagent dextran, which locally increases tubulin concentration and further enhances the nucleation of MTs. My collaborators Yuhan Hu and Daisy Duan showed that Abl2 increases MT elongation rates and reduces MT rescue frequency. I further set out to investigate how Abl2 regulates cytoskeletons in cells. I tracked the MT elongation rates using the MT plus-end binding peptide mKate-MACF43 and showed that loss of Abl2 slows down the MT elongation rates, which can be rescued by re-expressing Abl2 in the knockout cells. The effect of Abl2 on MT growth rates is mainly dependent on the function of the C-terminal half. Using live cell imaging, I found that Abl2 mainly co-localizes with actin structures in cells, with transient interactions with

MTs and with the MTOC. Lastly, I measured the random cell migration of WT and Abl2 KO cells. I showed that loss of Abl2 leads to aberrantly high migration speed, which can only be partially rescued by the expression of the C-terminal half. Together, our work demonstrates that Abl2 plays versatile roles in regulating MT dynamics *in vitro* and in cells, which can further coordinate with the actin network and the downstream signaling pathways to mediate cell migratory behaviors.

Abl2 promotes tubulin nucleation and assembly in vitro.

After determining the physical binding properties of Abl2 and MTs, I next sought to determine if the direct interactions of Abl2, MTs, and tubulin are responsible for regulating MT dynamics. I employed an in vitro MT turbidity assay to measure the impact of Abl2 on tubulin assembly. The concentration of MTs was monitored using absorbance at 350 nm; 18 µM tubulin was polymerized in the presence of GTP and reached the plateau after 120 mins. When incubating alone without tubulin, MBP-Abl2 and MBP did not significantly change the turbidity measurements (**Figure 5.1A**). When tubulin was incubated with 0.5 µM Abl2-N-557 or MBP the turbidity curves did not change compared with tubulin alone control (**Figure 5.1B**). The inclusion of 0.5 µM MBP-Abl2 or MBP-557-C led to a steeper increase in Abs. 350 nm that plateaued at a significantly higher level (**Figure 5.1B**). The reactions were ultracentrifuged to pellet the polymerized MTs, followed by SDS-PAGE and densitometry quantifications, to confirm that more tubulin was polymerized in the presence of Abl2 (**Figure 5.1C**). MBP-557-C promoted tubulin assembly in a concentration-dependent manner (**Figure 5.1D**). Samples taken from the end of turbidity experiments (T = 120 min) were visualized using EM of negatively stained specimens and revealed that tubulin was assembled into MTs (**Figure 5.1E**). I did not observe any significant MT bundles, as noted previously (Miller et al., 2004). Together, these results indicate that Abl2 COOH-terminal half is sufficient and necessary to promote MT assembly and Abl2 kinase domain (MBP-N-557) does not influence MT dynamics.
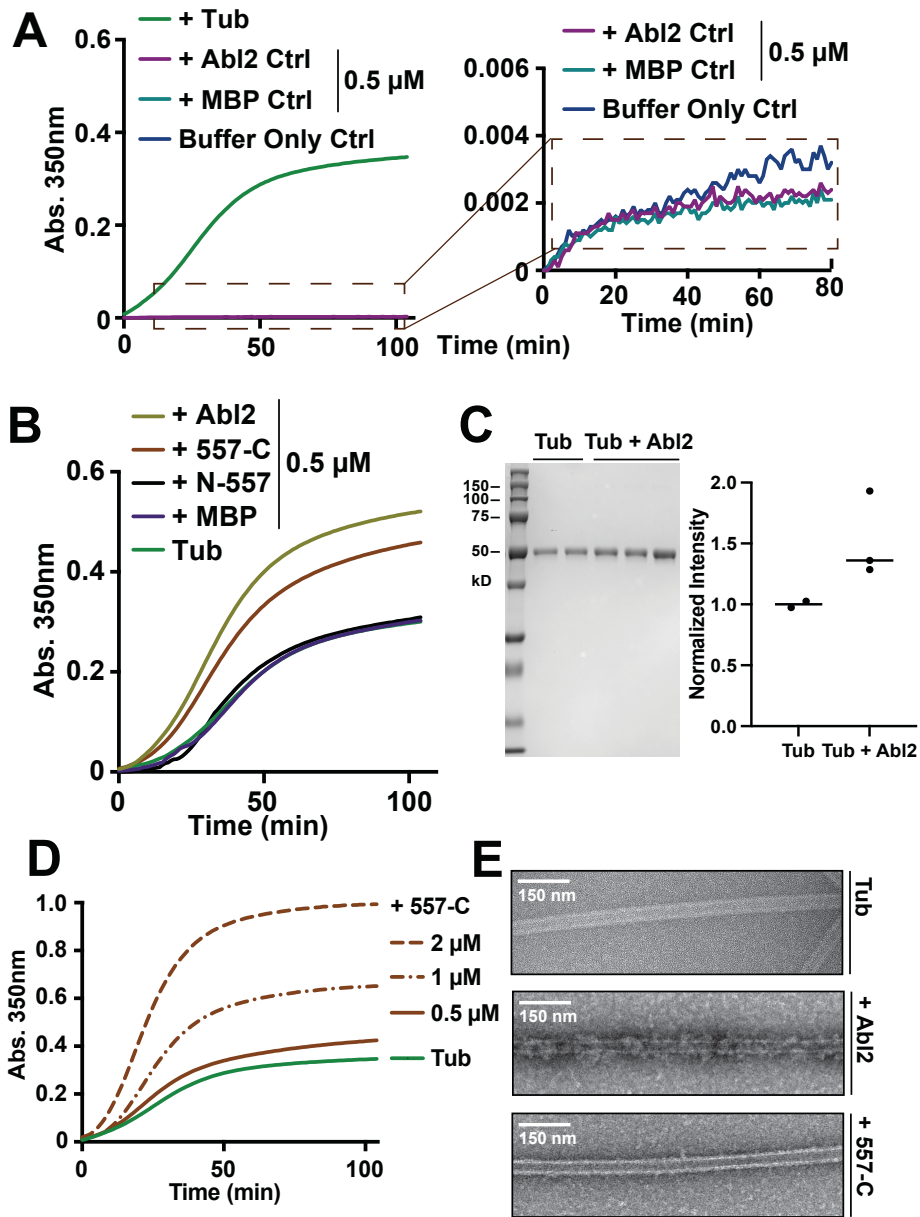
Figure 5.1 Abl2 promotes MT assembly via the C-terminal half.

(Figure caption on next page.)

Figure 5.1 Abl2 promotes MT assembly via the C-terminal half. A) 18 µM

tubulin assembly was measured by the change in turbidity. As control groups,

absorbance changes of the MBP-Abl2 alone and MBP-alone were also measured

in the absence of tubulin. **B)** Absorbance changes were measured when 18 µM

tubulin was incubated with 0.5 µM MBP-Abl2, 0.5 µM MBP-557-C, 0.5 µM MBP-

N-557, or 0.5 µM MBP. **C)** The tubulin assembly reactions with and without Abl2

were ultracentrifuged and the amount of the pellet MTs was quantified using SDS-

PAGE and densitometry. **D)** 18 µM tubulin was incubated in the presence of

increasing concentrations of 0.5-2 µM MBP-557-C. **E)** Representative negative

stain EM images of MTs or MTs with MBP-Abl2 or MBP-557-C at the end of

turbidity assay (T = 120 min).

I next measured the physiological Abl2 concentration in cells. Using purified recombinant MBP-Abl2 as blotting standards, I found that Abl2 represents 0.19% of total protein in WT mouse 3T3 fibroblast and COS-7 cell extracts. Assuming that the total cytoplasmic protein concentration is ~100 mg/ml (Albe et al., 1990; Finka & Goloubinoff, 2013) and the molecular weight of Abl2 is 128 kD, I estimated the physiological concentration of Abl2 to be ~1.5 µM (**Figure 5.2A, B**). This is within the concentration range at which Abl2 or Abl2 C-terminal half promotes tubulin assembly.

As noticed before, besides the total polymerized MTs, the inclusion of Abl2 leads to a steeper curve, which indicates the potential change in the nucleation phase. The critical concentrations required for MT formation and the lag time when one-tenth of the maximum turbidity is reached provide sensitive measures of MT nucleation, as reviewed in **Chapter 1**. After the optimization of the protein purification systems, I also switched the MBP-tagged proteins to tag-free Abl2 and Abl2 fragments. Consistent with what we observed before, the addition of the tag-free Abl2 leads to higher absorbance readings when plateau (**Figure 5.2C**), which is corresponded to the amount of polymerized MTs.

The plateau of the turbidity assays varied as a linear function of initial tubulin concentration, yielding critical concentrations (x intercept) of 5.5 ± 1.1 µM and 0.5 ± 1.8 µM in the absence and presence of Abl2, respectively (**Figure 5.2E**). The lag time decreased from 16 ± 2 min to 9 ± 3 min when Abl2 was added in the reactions (**Figure 5.2F**). I also found that Abl2Δ688-790, which loses the tubulin binding ability, did not promote MT nucleation in the turbidity assay, with a lag time of 16

± 2 min. The acceleration of nucleation was also confirmed by using negative-stain electron microscopy. Ten minutes after the onset of the reaction (T = 10 min), 4 µL of the reactions were retrieved and preserved as negative-stain samples to visualize the MT segments. Significant more MTs were assembled at the initial phase when Abl2 is included in the reaction (**Figure 5.2G**). We can also observe more large particles formed in the presence of Abl2, which is likely the tubulin oligomers that can further form the critical nucleus and elongate as MT segments.

A anti-Abl2: Ar11

B Ponceau S

C

D

E

F Reactions at T = 10 min

18 µM Tub

18 µM Tub
+ 1 µM Abl2
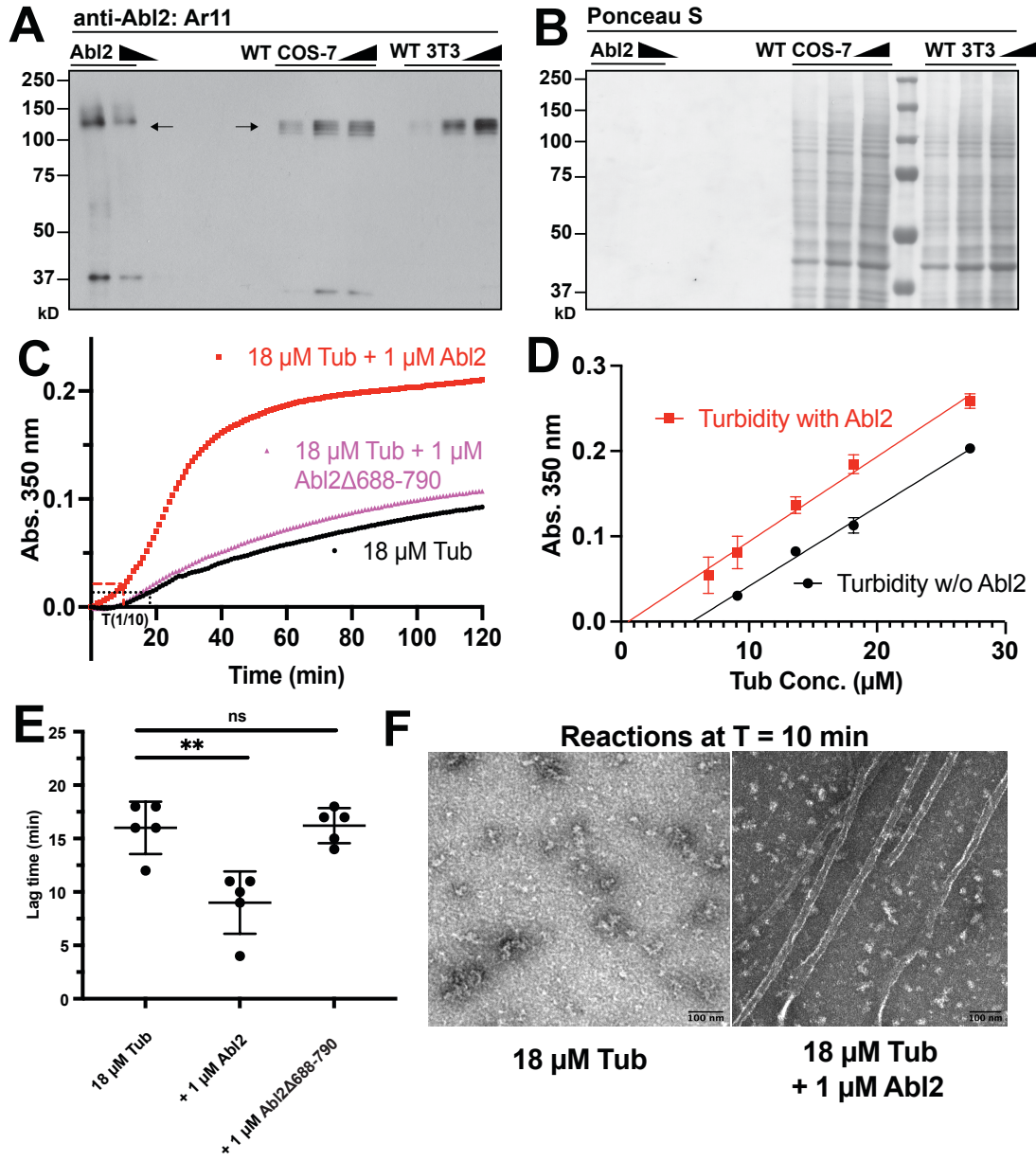
Figure 5.2 Abl2 promotes MT nucleation.

(Figure caption on next page.)

Figure 5.2 Abl2 promotes MT nucleation. (A) Ar11 immunoblot of recombinant

Abl2, WT COS-7 cell lysate, and WT mouse 3T3 fibroblast cell lysate. Ar11

recognizes the C-terminal half of Abl2. The expected bands of Abl2 (134 kD) are

indicated. **B)** Ponceau S staining reveals the total amount of the protein loaded in

each lane (purified recombinant Abl2: 0.08 and 0.053 µg, WT COS-7: 10, 20, 30

µg, WT 3T3: 10, 20, 30 µg). **C)** Absorbance changes were measured when 18 µM

tubulin was incubated in the absence or presence of 1 µM Abl2 or 1 µM Abl2Δ688-

790. **D)** Critical concentrations of tubulin were measured in the absence or

presence of 1 µM Abl2 by plotting the plateau absorbance change versus the

tubulin concentrations. **E)** The time that one-tenth of the maximum turbidity is

reached is quantified as a measure of MT nucleation efficiency. **F)** Representative

negative stain EM images of MTs or MTs with Abl2 at T = 10 min.

Abl2-eGFP undergoes phase separation and co-condenses with tubulin, which facilitates MT nucleation.

As reviewed in **Chapter 1**, several microtubule-binding proteins (MTBPs) regulate MT nucleation through phase separation (Hernandez-Vega et al., 2017; King & Petry, 2020), which occurs mostly in the highly disordered and multivalent proteins. The prediction software PONDR-FIT (Xue et al., 2010) and DISOPRED3 (Jones & Cozzetto, 2015), suggested that the Abl2 C-terminal half (PONDR-FIT: 0.6670; Diso-Pred3: 0.4391) contains significant disorder, relative to its N-terminal half (PONDR-FIT: 0.2670; Diso-Pred3: 0.1461, **Figure 5.3A**).

To investigate whether Abl2 could undergo phase separation, my collaborator Daisy observed solutions containing Abl2-eGFP under conditions thought to mimic the conditions of a crowded intracellular environment (5% dextran) (Andre & Spruijt, 2020). Abl2-eGFP underwent apparent phase separation: Abl2-eGFP puncta in the dense phase retained a spherical morphology that could be visualized in both the brightfield and fluorescence imaging (**Figure 5.3B**). The extent to which Abl2-eGFP partitions into the dense phase can be measured by the partition coefficient (PC), *i.e.*, the ratio of Abl2-eGFP concentration in the dense phase to the background solution phase. Fluorescence recovery after photobleaching (FRAP) of a single confocal plane within single Abl2-eGFP condensates demonstrated recovery of Abl2-eGFP fluorescence with an approximate half-life $t_{1/2}$=1.7 min (**Figure 5.3C**). The phase separation propensity, the threshold of which was set as PC ≥ 4, increased with increasing concentration of Abl2-eGFP but was attenuated by increasing salt (**Figure 5.3D,** phase diagram).

Control experiments revealed that eGFP alone did not similarly undergo phase separation. which reveals that Abl2 can form coacervates due to its own molecular grammar.

Given that Abl2-eGFP binds tubulin dimers and undergoes phase separation, we tested whether Abl2-eGFP could form coacervates with tubulin dimers. When incubated under conditions that promote Abl2-eGFP phase separation (50 mM KCl, 5% dextran), Alexa Fluor 647-tubulin dimers partitioned into Abl2-eGFP condensates. The Abl2 C-terminal half showed similar coacervation, while the Abl2 N-terminal did not undergo phase separation and did not bind tubulin dimers (**Figure 5.3E**). FRAP analysis revealed that the dimers could diffuse into an internally bleached region, with an approximate half-life $t_{1/2}$=0.833 min (**Figure 5.3F**).
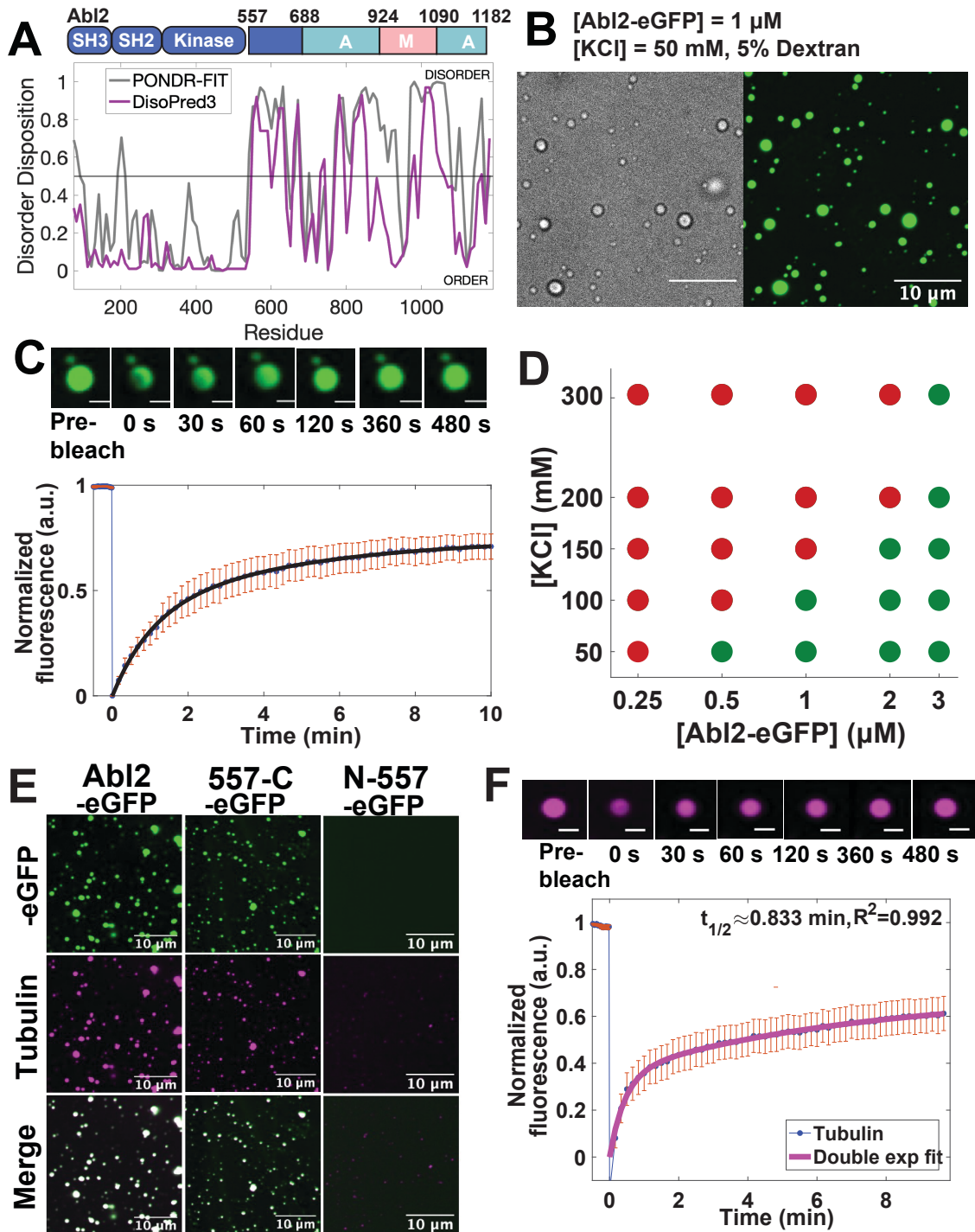
Figure 5.3 Abl2 undergoes phase separation and co-condenses with tubulin.

(Figure caption on next page.)

Figure 5.3 Abl2 undergoes phase separation and co-condenses with tubulin.

A) Probability of disorder along the sequence of Abl2 was predicted using PONDR-FIT (grey) and DISOPRED3 (magenta). **B)** 1 μM Abl2-eGFP undergoes phase separation in the buffer containing 50 mM KCl and 5% dextran, as shown in the brightfield (left) and fluorescence imaging (right). **C)** FRAP analysis of the Abl2-eGFP condensates showed that Abl2-eGFP can freely diffuse inside and outside of the condensates. The quantifications of the measurements are shown in the bottom panel as blue dots and the fitting is in black. **D)** Salt and concentration phase diagram of Abl2-eGFP is shown. The red dots represent PC < 4, considered as not phase separated. The green dots represent PC ≥ 4, considered as phase separated. **E)** Alexa Fluor 647 labeled-tubulin forms co-condensates with phase-separated Abl2-eGFP and 557-C-eGFP. N-557-eGFP does not form condensates and tubulin does not co-localize with N-557-eGFP signals. **F)** FRAP analysis of tubulin within the co-condensates showed that tubulin can freely diffuse inside and outside of the co-condensates. The quantifications of the measurements are shown in the bottom panel as blue dots and the fitting is in black.

I next set out to test if the co-condensation of Abl2 and tubulin further facilitates the nucleation process. Considering that phase separation of Abl2 may contribute to the turbidity measurement, we measured the non-templated MT nucleation using 8 μM of tubulin labeled with Alexa Fluor 647 and 1 μM Abl2-eGFP under the phase separation condition, 50 mM KCl and 3% dextran. As shown previously, Abl2-eGFP co-condenses with Alexa Fluor 647-tubulin at the beginning of the reaction. Polymerized MT segments were observed growing from the Abl2-tubulin co-condensates. In the absence of 3% dextran, Abl2-eGFP diffused in solution, and fewer MTs were observed after 1 hour-reaction (**Figure 5.4**).
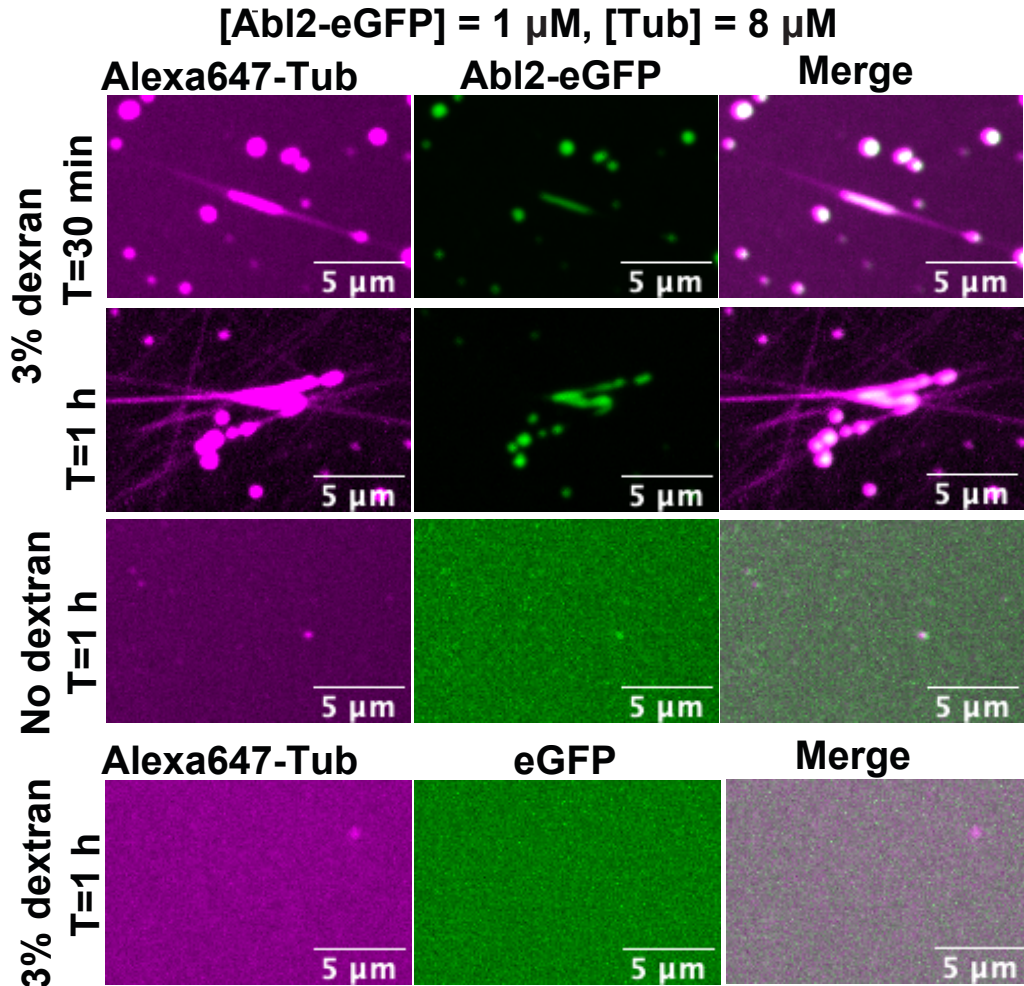
Figure 5.4 Abl2 and tubulin co-condensates promote MT nucleation. The confocal images of the Alexa Fluor 647-tubulin and Abl2-eGFP showed that MTs nucleate out of the co-condensates under phase separation conditions 30 min and 1 h after reactions started at 37°C. Under the same condition, eGFP does not form condensates. Without dextran, Abl2-eGFP is diffuse. Few MTs were observed assembled without dextran or with eGFP.

Abl2 increases MT elongation rate in TIRF single-filament assays.

My collaborator Yuhan Hu next used in vitro TIRF microscopy to measure Abl2 impacts MT dynamics at a single-filament resolution. The MT elongation rate was significantly higher in the presence of 0.5 or 1 µM MBP-Abl2 or MBP-557-C (**Figure 5.5A-C, E**). On the other hand, 1 µM MBP-688-C or 2 µM MBP-557-688 did not influence MT elongation (**Figure 5.5D**). These observations suggest the C-terminal half is required to allow Abl2's function in regulating MT elongation.
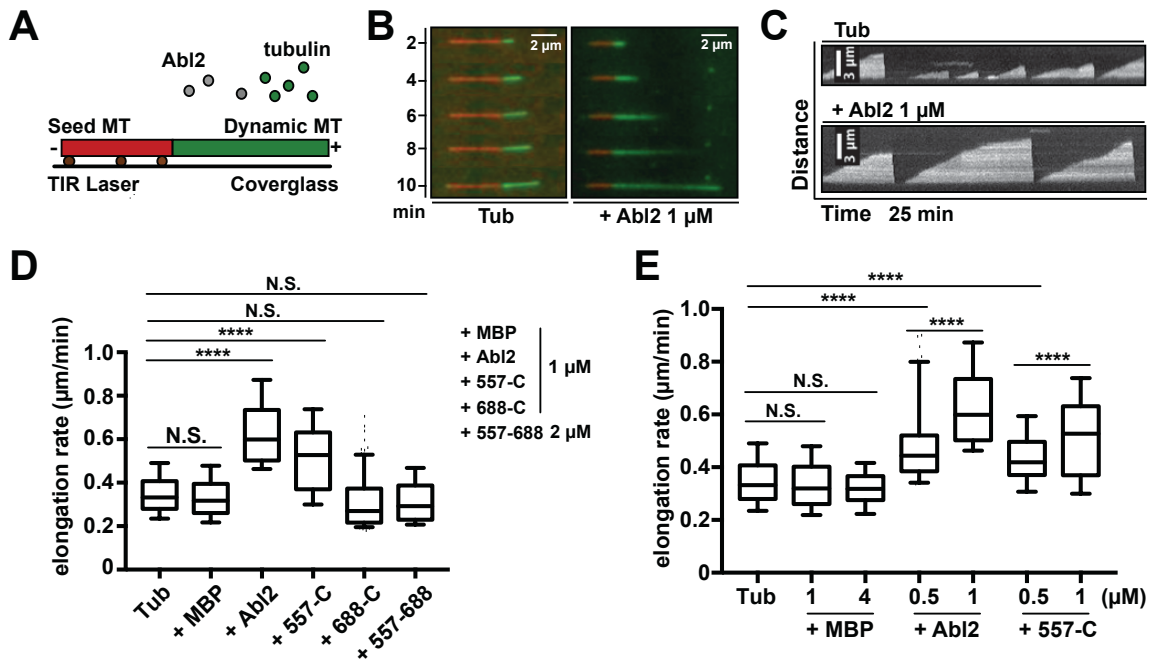
Figure 5.5 Abl2 increases MT elongation rate *in vitro*.

(Figure caption on next page.)

Figure 5.5 Abl2 increases MT elongation rate *in vitro*. A) Schematic of the experimental design. Alexa Fluor 488-labeled tubulin (green) polymerizes onto the ends of rhodamine-labeled GMPCPP-stabilized MTs (red) which are anchored to the coverslip with anti-rhodamine antibodies (brown), the flow chamber was observed using TIRF microscopy. **B-C)** Representative time stills and kymographs of 7 µM 15% Alexa Fluor 488-labeled tubulin elongation in the absence and presence of 1 µM Abl2**. D)** 7 µM tubulin were incubated with 1 µM MBP, 1 µM MBP-Abl2, 1 µM MBP-557-C, 1 µM MBP-688-C, or 2 µM MBP-557-688, and MT elongation rates were measured and quantified. **E)** MT elongation rates were measured with 7 µM tubulin incubated in the presence or absence of 0.5-1 µM Abl2, 0.5-1 µM 557-C, 1-4 µM MBP. Data points are means ± S.E.; **, $p<0.01$; ****, $p<0.0001$, for each in vitro MT dynamic assay condition n ≥ 100.

Loss of Abl2 reduces MT elongation rate in cells, which can be rescued by the C-terminal half.

Having demonstrated that purified Abl2 promotes elongation rate *in vitro*, I examined how the loss of Abl2 function impacts MT behaviors in cells. I generated CRISPR *abl2*$^{-/-}$ COS-7 cells and 3T3 fibroblasts. I used western blotting to confirm the expression levels of Abl2 in the WT and *abl2*$^{-/-}$ cells, and the transient re-expression levels of Abl2-GFP, Abl2-N-557-GFP, and Abl2-557-C-GFP in *abl2*$^{-/-}$ COS-7 cells, and the stably re-expression levels of Abl2-GFP, Abl2-N-557-GFP, and Abl2-557-C-GFP (**Figure 5.6**).
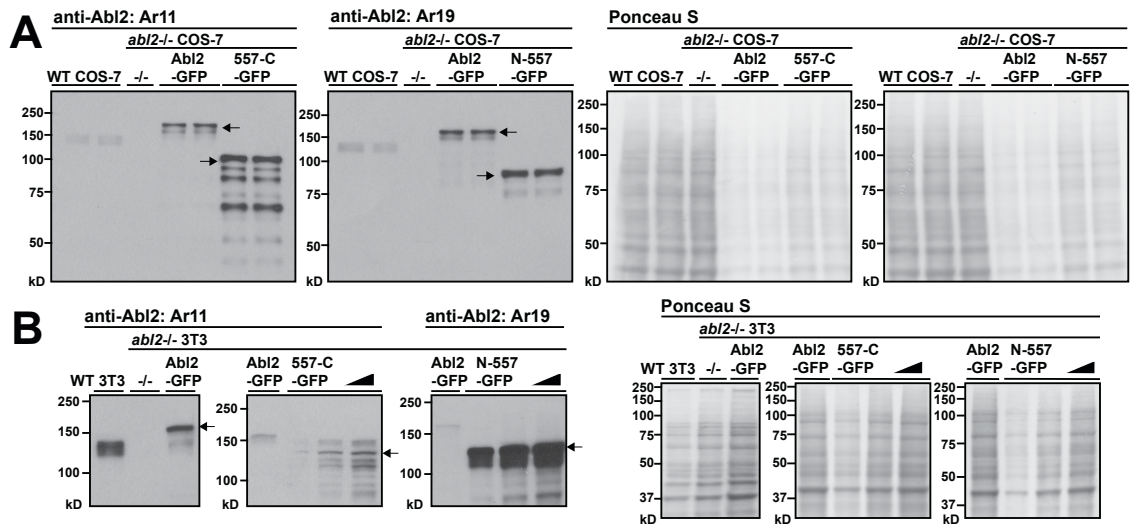
Figure 5.6 Expression levels of Abl2 in WT, *abl2*⁻/⁻, and the rescue cell lines.

A) Ar11 immunoblot of WT and *abl2*⁻/⁻ COS-7 cells, and *abl2*⁻/⁻ COS-7 cells re-expressing Abl2-GFP or Abl2-557-C-GFP. Ar11 recognizes the Abl2 C-terminal half. Ar19 immunoblot of WT and *abl2*⁻/⁻ COS-7 cells, and *abl2*⁻/⁻ COS-7 cells re-expressing Abl2-GFP and Abl2-N-557-GFP. Ar19 recognizes the Abl2 N-terminal half. The expected bands of Abl2, Abl2-GFP (161 kD), Abl2-557-C-GFP (96 kD), and Abl2-N-557-GFP (92 kD) are indicated. Ponceau S staining reveals the total amount of the protein loaded in each lane of the Ar11 blot (WT COS-7: 30, 30 µg, *abl2*⁻/⁻ COS-7: 30 µg, *abl2*⁻/⁻ COS-7 + Abl2-GFP: 5, 5 µg, *abl2*⁻/⁻ COS-7 + Abl2-557-C-GFP: 5, 5 µg) and the Ar19 blot (WT COS-7: 30, 30 µg, *abl2*⁻/⁻ COS-7: 30 µg, *abl2*⁻/⁻ COS-7 + Abl2-GFP: 5, 5 µg, *abl2*⁻/⁻ COS-7 + Abl2-N-557-GFP: 5, 5 µg). **B)** Left: Ar11 immunoblot of WT mouse 3T3 fibroblast cells, *abl2*⁻/⁻ 3T3 cells, and *abl2*⁻/⁻ 3T3 cells re-expressing Abl2-GFP. Center: Ar11 immunoblot of *abl2*⁻/⁻ 3T3 cells re-expressing Abl2-GFP or Abl2-557-C-GFP. Right: Ar19 immunoblot of *abl2*⁻/⁻ 3T3 cells re-expressing Abl2-GFP or Abl2-N-557-GFP. The expected bands of Abl2, Abl2-GFP, Abl2-557-C-GFP, and Abl2-N557-GFP are indicated.

Ponceau S staining reveals the total amount of the protein loaded in each lane of the left Ar11 blot (WT 3T3: 20 µg, $abl2^{-/-}$ 3T3: 20 µg, $abl2^{-/-}$ 3T3 + Abl2-GFP: 50 µg), the center Ar11 blot ($abl2^{-/-}$ 3T3 + Abl2-GFP: 30 µg, $abl2^{-/-}$ 3T3 + Abl2-557-C-GFP: 10, 20, 30 µg), and the right Ar19 blot ($abl2^{-/-}$ 3T3 + Abl2-GFP: 30 µg, Abl2-N-557-GFP: 10, 20, 30 µg).

I measured MT elongation rates by tracking the extension of MT plus-end

marker mCherry-MACF43 (**Figure 5.7A**). Because MT dynamics differ drastically

at the center compared to the periphery of a single cell, we separately analyzed

MT elongation rates in the cell center and the outermost 25% of the cells, based

on the distance from the observed MT-organization center (MTOC) to the cell

membrane. In control WT COS-7 cells, MTs grew at a rate of 6.1 ± 0.1 μm/ min at

the cell edge and 6.5 ± 0.2 μm/min at the cell center. In $abl2^{-/-}$ COS-7 cells, MT

growth slowed by 25% at the cell edge (4.6 ± 0.2 μm/min) and 21% at the cell

center (5.2 ± 0.2 μm/min; **Figure 5.7B-D**). Re-expression of Abl2-GFP in $abl2^{-/-}$

COS-7 cells increased MT growth rates to 8.3 ± 0.2 μm/min at the cell edge and

9.7 ± 0.2 μm/min at the cell center. Re-expression of 557-C-GFP also increased

MT growth rates to 8.5 ± 0.2 μm/min at the cell edge and 10.0 ± 0.3 μm/min at the

cell center (**Figure 5.7C, D**). The elevated rates of MT growth over those of WT

cells likely resulted from the overexpression of Abl2-GFP (14-fold) or 557-C-GFP

(18-fold; **Figure 5.6**). That said, this effect was specific to the re-expression of Abl2

or 557-C, as similar overexpression of N-557-GFP (12-fold), containing the

tyrosine kinase domain but not the MT-binding regions, did not rescue MT growth

at the cell edge (5.1 ± 0.2 μm/min) or the cell center (6.5 ± 0.2 μm/min). GFP

expression also did not impact MT growth in $abl2^{-/-}$ COS-7 cells (edge: 4.9 ± 0.1

μm/min; center: 5.4 ± 0.2 μm/min; **Figure 5.7C, D**). The COS-7 cell experiments

demonstrate that reduction of Abl2 levels slowed MT growth, and overexpression

of Abl2 or 557-C rescued this defect. We extended these results to 3T3 fibroblasts,

where we could achieve more physiological re-expression levels of Abl2 or 557-C

in *abl2*−/− 3T3 cells (**Figure 5.6**). In WT 3T3 cells, MTs grew at a rate of 11.5 ± 0.4 µm/ min at the cell edge and 14.6 ± 0.4 µm/min at the cell center. In *abl2*−/− 3T3 cells, MT growth was reduced by 26% at the cell edge (8.4 ± 0.3 µm/min) and 26% at the cell center (10.8 ± 0.4 µm/ min; **Figure 5.6E-G**). Stable re-expression of Abl2-GFP (0.25-fold of endogenous level) in *abl2*−/− 3T3 cells restored MT growth to levels observed in WT cells (edge: 11.1 ± 0.2 µm/min; center: 13.1 ± 0.2 µm/min). Stable re-expression of 557-C-GFP (0.34-fold) was sufficient to restore MT growth at the cell edge, but not at the cell center (**Figure 5.6F, G**). Re-expression of N-557-GFP (21-fold) did not rescue MT growth defect in *abl2*−/− 3T3 cells (edge: 7.9 ± 0.2 µm/min; center: 10.2 ± 0.3 µm/min).
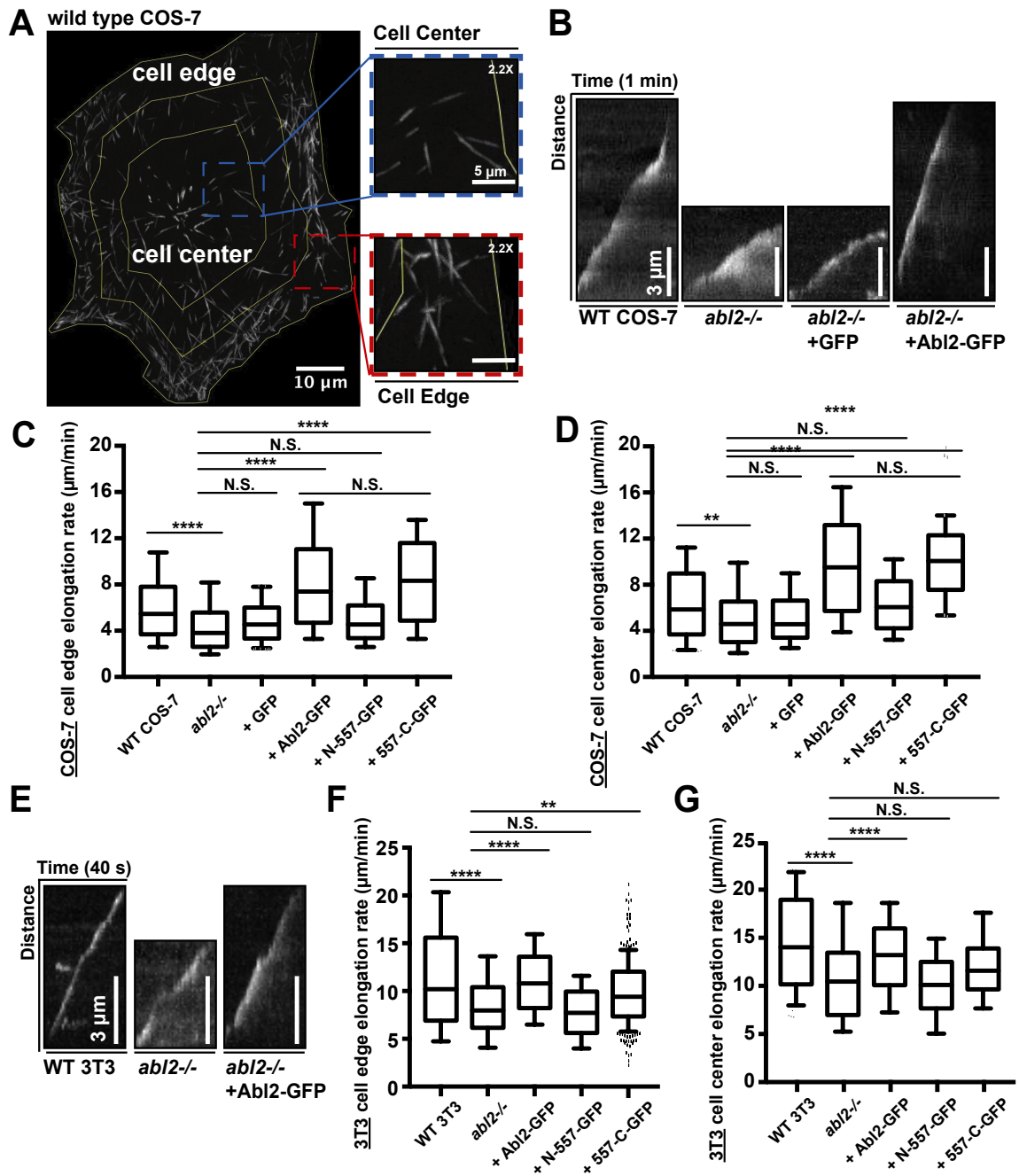
Figure 5.7 Abl2 is required for normal MT growth in cells.

(Figure caption on next page.)

Figure 5.7 Abl2 is required for normal MT growth in cells. A) Maximum intensity projection of mCherry-MACF43 time-lapse showed single MT tracks in a COS-7 cell. MT growth events in the inner one half of the cell, centered at the MTOC, were categorized as being within the cell center, and those in the outermost one-quarter region were categorized as being within the cell edge. **B)** Kymographs of the cell edge MT plus-tip growth in WT and $abl2^{-/-}$ COS-7 cells, and $abl2^{-/-}$ COS-7 cells re-expressing GFP or Abl2-GFP. **E)** Kymographs of the cell edge MT plus-tip growth in WT and $abl2^{-/-}$ 3T3 cells, and $abl2^{-/-}$ 3T3 cells re-expressing Abl2-, N-557-, 557-C-GFP. MT plus-tip growth at the cell center and the cell edge in **C)** and **D)** in COS-7 cells or **F)** and **G)** in 3T3 cells are quantified. n ≥ 150. ******, P < 0.01; ********, P < 0.0001. N.S., not significant.

Abl2 co-localizes with the cytoskeleton in cells.

To study Abl2 and cytoskeleton localization in COS-7 cells, I performed live-cell imaging of COS-7 *abl2*$^{-/-}$ expressing fluorescently labeled Abl2 and the fluorescent markers of MTs (EB3) or actin (LifeAct). Using dual-color TIRF imaging, I observed EB3-GFP-positive MT plus-tips approaching and traversing though Abl2-RFP puncta at the cell edge in COS-7 cells (**Figure 5.8A**). Consistent with my collaborator Ke Zhang's finding, more of the Abl2 signals were found to co-localize with actin in the wave-like structures near the cell edge (**Figure 5.8B**). Further inspection with spinning disk confocal microscopy confirmed that Abl2-GFP puncta co-localizes with actin (**Figure 5.8C**). Additionally, more interactions of Abl2 with the cellular MTs are observed in the dorsal plane via different behaviors: 1) Abl2 colocalizes with the aster EB3 signal in the cell center, which is potentially the MTOC in cells. 2) Abl2 transiently decorates MT lattice in cells (**Figure 5.8D**).

Abl2 regulates cell migration partially through interactions with the cytoskeleton.

Knowing that re-expression of Abl2-557-C rescued MT growth in cells, we next sought to test if Abl2-557-C regulates cell migration. Previously our laboratory showed that *abl2*$^{-/-}$ 3T3 cells had significantly higher migration speeds compared with WT 3T3 fibroblasts and that Abl2-GFP re-expression in *abl2*$^{-/-}$ 3T3 cells slowed migration to WT levels (Peacock et al., 2007). As before, we found that *abl2*$^{-/-}$ 3T3 cells showed a twofold increase in migration speed compared with WT 3T3 cells (WT: 11.88 ± 4.50 µm/h; *abl2*$^{-/-}$: 22.18 ± 8.14 µm/h). Re-expression of

Abl2-557-C-GFP in *abl2*$^{-/-}$ 3T3 cells partially slowed migration by 22.5% to 17.19 ± 9.01 µm/h, but unlike full-length Abl2, it did not slow migration to WT speeds (**Figure 5.9**). GFP alone did not impact the accelerated *abl2*$^{-/-}$ migratory behavior (20.00 ± 7.56 µm/h). These data indicate that the Abl2-557-C contributes to normal cell migration, likely in combination with other activities of the protein.
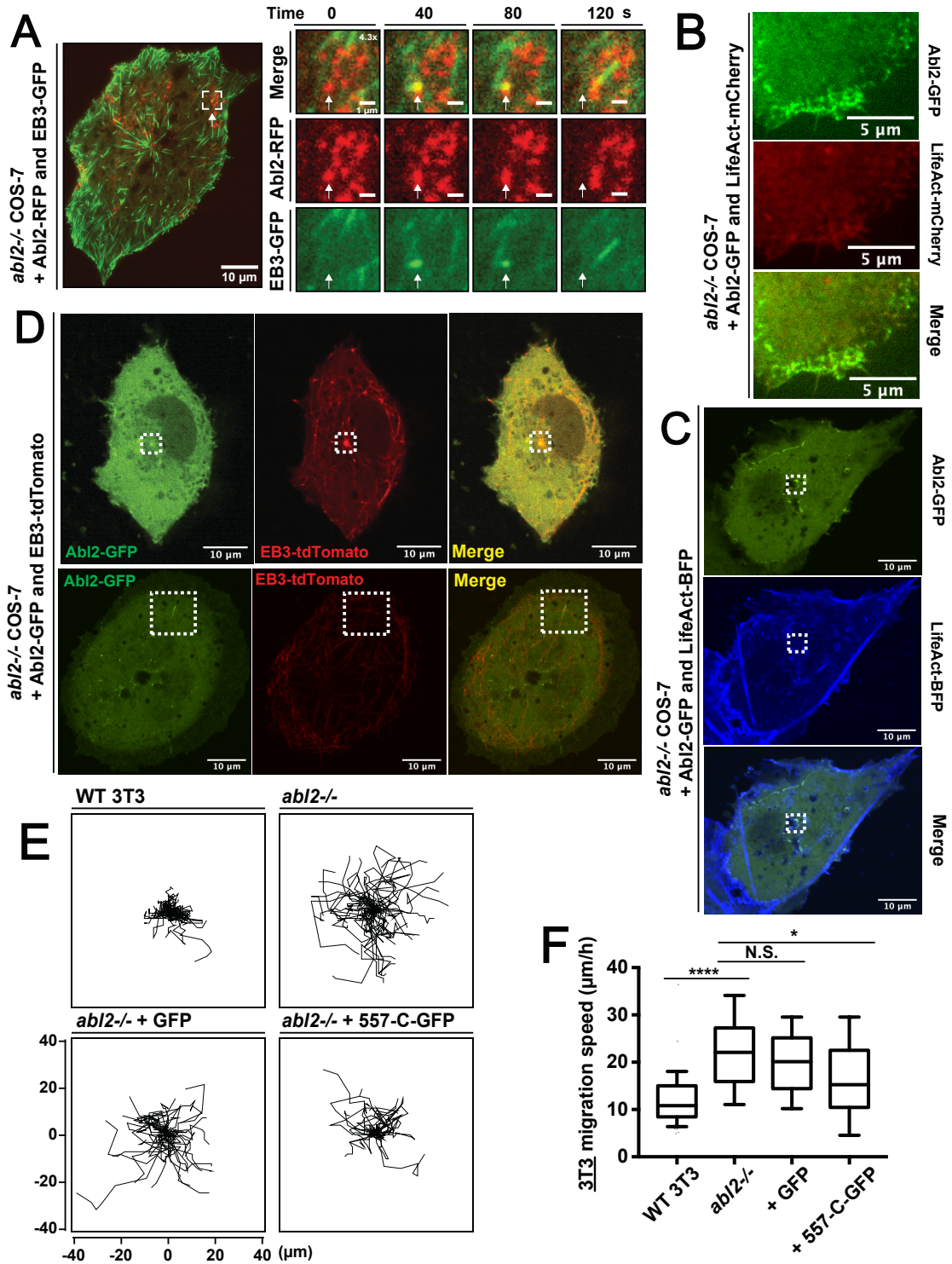
Figure 5.8 Abl2 interacts with the cytoskeleton in cells, which mediates cell migration.

(Figure caption on next page.)

Figure 5.8 Abl2 interacts with the cytoskeleton in cells, which mediates cell migration. A) Maximum intensity projection of a live cell TIRF video of an *abl2⁻/⁻* COS-7 cell expressing EB3-GFP and Abl2-RFP. Time-lapse shots showed MT plus-tip tracker EB3-GFP went through Abl2-RFP puncta. **B)** One frame of a live cell TIRF video of an *abl2⁻/⁻* COS-7 cell expressing Abl2-GFP and LifeAct-mCherry showed that Abl2-GFP co-localizes with actin in the ventral waves. **C)** Frames of live cell confocal videos of *abl2⁻/⁻* COS-7 cells expressing Abl2-GFP and EB3-tdTomato showed that Abl2-GFP co-localizes with actin. **E)** Cell migration tracks showed the displacements of WT and *abl2⁻/⁻* 3T3 fibroblasts, and *abl2⁻/⁻* 3T3 cells re-expressing Abl2- 557-C-GFP or GFP over 6 h. **F)** The plot showed the speed of migration. Error bars are presented as mean ± SD n ≥ 30. *, $P < 0.05$; ****, $P < 0.0001$. N.S., not significant.

Chapter 6 – Summary, Conclusions and Future Perspectives

To sum up, I provide evidence in the previous chapters that the non-receptor tyrosine kinase Abl2 regulates MT dynamics in vitro and in cells by directly interacting with the MT lattice and tubulin dimers. I demonstrated that Abl2-MT and Abl2-tubulin binding interactions are mediated by the disordered Abl2 C-terminal half through electrostatic forces. Abl2 recognizes unique MT lattice structures and prefers binding to GMPCPP-stabilized MTs. Abl2 interacts with free tubulin dimers through two regions, aa. 688-924 and aa. 1024-1090, both that reside within the C-terminal half. Interestingly, the alternative spliced Abl2 isoform, which lacks aa. 688-790, does not bind tubulin dimers, without affecting binding to MTs.

We then characterized the MT dynamics change under the regulation of Abl2. Using the turbidity assay to measure scattered light as a function of time, I showed that Abl2 decreases the critical concentration for spontaneous tubulin polymerization, promotes MT nucleation, and increases the total amount of the assembled MTs.

By TIRF microscopy, we observed that Abl2 regulates MT dynamics by increasing the plus-end elongation rate, which is in line with my cellular data that MT elongation rates were reduced when Abl2 was knocked out. I also demonstrated that the C-terminal half of Abl2 is necessary and sufficient to rescue MT growth rate. Furthermore, I showed that Abl2 interacts with the cytoskeleton in cells, which can further mediate the cell migratory behaviors.

Additionally, we observed that Abl2 undergoes phase separation and forms coacervates with tubulin to enhance the effect on MT nucleation.

Abl2 interacts with tubulin through two distinct regions.

We identified two tubulin-binding regions in Abl2, regions containing amino acids 688-924 (Site I) and 1024-1090 (Site II), each sufficient to bind tubulin dimers itself, albeit with weaker affinity than Abl2 and the C-terminal half. Curiously, the Abl2Δ688-790 splice isoform did not bind detectably to tubulin even though it retains site II (**Table II**). We speculate that Abl2 initially interacts with tubulin via Site I, which has a higher affinity to tubulin. The binding of tubulin to Site I may be required to expose Site II to an additional tubulin dimer and promote their interactions in a head-to-tail fashion (**Figure 6.1**). This model may help to explain why the naturally occurring splice isoform Abl2Δ688-790, which lacks all or part of Site I, significantly disrupt binding to tubulin and render it unable to promote MT nucleation. The protein sequence of the two tubulin-binding sites in Abl2 showed no significant alignment with known tubulin-binding domains, indicating novel interactions between tubulin and tubulin-binding proteins.

Interestingly, one of the processed 2D class averages from the negative stain EM samples of the Abl2-tubulin mixture appears as one proposed complex in the hypothesized binding model. I also observed that in the size-exclusion chromatography, tubulin was shifted to two earlier peaks upon pre-incubation with Abl2-557-C: one at an earlier elution volume and the other with similar position as Abl2-557-C only, indicating that there may be two populations of the tubulin bound with Abl2-557-C in different ratios, i.e., 2:1 in the first peak and 1:1 in the second peak. Inspection of the binding curves of His-Abl2 or His-557-C to tubulin (**Figure 4.5C, D**) also reveals that the simple 1:1 binding model does not perfectly fit the

curve, especially for the reactions with higher tubulin concentrations. The deviation in the fitting may be due to the presence of different binding rations of Abl2 and tubulin. The confirmation of the binding ratios will require the support from future experiments. Such follow-up validation experiments include running the gel samples together with previously known amounts of tubulin and Abl2-557-C to quantify the molar ratio using densitometry. Additionally, it will be necessary to perform SEC-MALS or analytical ultracentrifugation to determine the molecular mass of these two peaks.
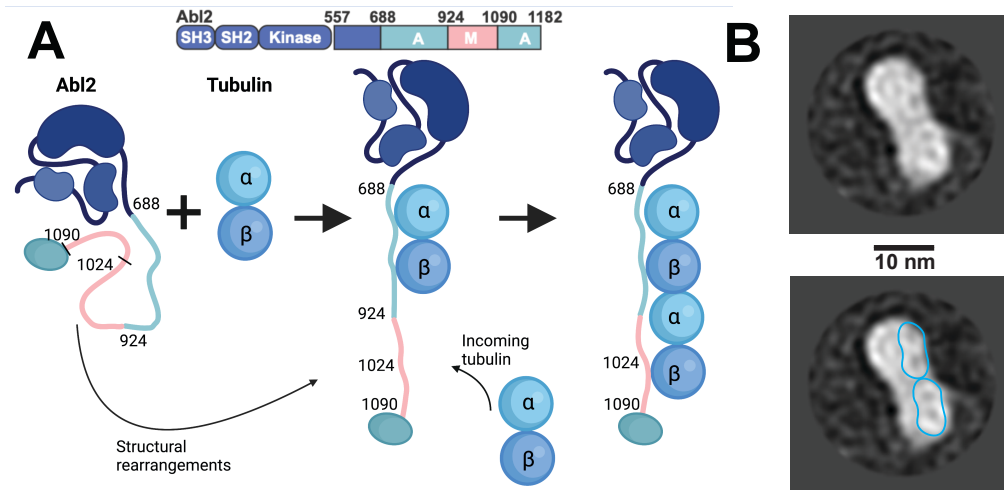
Figure 6.1 Abl2 interacts with tubulin through two tubulin-binding regions.

A) The hypothesized model of Abl2 interaction with tubulin: Abl2 uses the more exposed 688-924 region as the major site to interact with tubulin. The 1024-1090 region is less accessible in the native conformation. The interaction with the first tuulin dimers leads to the conformational change and the exposure of the second binding region, 1024-1090, which can further recruit additional dimers in a head-to-tail fashion. **B)** One class of the 2D averages of Abl2-tubulin negative stain EM samples. The bottom panel showed the drawing illustration. The blue peanut outlines the potential tubulin signals.

What is the biological importance of the alternatively spliced isoform AbI2Δ688-790 that loses tubulin binding ability?

As a naturally existing isoform, AbI2Δ688-790 lacks the ability to bind tubulin, but retains strong binding to MTs. The fragment aa. 688-924 contains an actin-binding domain, though the boundaries of which have not been accurately determined. Future studies will be required to measure how the loss of 688-790 affects AbI2 binding to actin. The loss of this region may disrupt the internal actin binding region and defect the cooperative binding of AbI2 to actin.

To figure out if AbI2 and AbI2Δ688-790 have different biological roles *in vivo*, I collaborated with Shaojie Ma in the Sestan lab to investigate if there is unique expression pattern for AbI2 and AbI2Δ688-790 in different tissues. Murine AbI2 shares highly conserved sequence with that of human AbI2, with almost identical sequence in the region of 688-790. Several human AbI2 transcripts also revealed lack of aa. 688-790. We extracted the RNA-sequencing data both in mouse neocortical regions (**Figure 6.2A**) and in human tissues (**Figure 6.2B**), and plotted the transcripts level. We found that AbI2 (aa. 1-1182) transcript has higher RNA levels in human (data from GTEx database) and AbI2Δ688-790 transcripts has higher level in mouse (data from (Tasic et al., 2018)), with no specific tissue localization. Follow-up studies will require the cross-confirmation from multiple databases and the quantitative reverse transcription PCR (RT-qPCR) and western blotting. After validating that these two isoforms have distinct expression levels between human and mouse, it would be interesting to investigate the evolutionary

roles of the 688-790 region and to study if these two isoforms have unique subcellular localizations and functions.

Figure 6.2 Transcripts levels of different Abl2 isoforms A) in mouse neocortical brains and **B)** in human tissues. The pink highlighted indicate Abl2 (1-1182) and the red rectangles indicate the isoforms with 688-790 missing.

Abl2 binding to MTs via the C-terminal half is likely to be mediated by the upstream signaling pathways.

Though there is no binding to MTs itself, the N-terminal half of Abl2 mediates Abl2 C-terminus binding to MTs. The N-terminal half of Abl2 is enriched with tyrosine residues through which the upstream signaling factors like the platelet-derived growth factor receptor (Boyle et al., 2007) and integrins (Warren et al., 2012) can modulate Abl2's kinase activity. Phosphorylation of MTBPs is reported to be an important switch to mediate their binding to MTs temporally and spatially in cells (Ramkumar et al., 2018). As reviewed in Chapter 1, most of the interactions between MTBPs and MTs is negatively correlated with the phosphorylation status of the MTBPs. For example, the hyperphosphorylation of tau abolishes MT binding. It is also the underlying cause of neurofibrillary tangles, which is its pathological aggregation form and is a hallmark of Alzheimer's disease (Gong & Iqbal, 2008). Intriguingly, I found that the dephosphorylated Abl2-eGFP has reduced binding affinity for MTs, as compared to highly tyrosine-phosphorylated Abl2-eGFP (**Figure 4.3D, E**). Previous colleague Yuhan Hu in our lab showed that Abl2 interacts with the MTs through electrostatic interactions between the positively charged C-terminal half of Abl2 and the negatively charged tubulin C-terminal tails, also known as E-hook, of MTs (Y. Hu et al., 2019). Dephosphorylation leads to an overall decrease of the negative charge in Abl2, which should result in higher binding affinity to MTs in theory. These contradictory results indicate the underlying MT-binding property of Abl2 is likely due to the structural rearrangements upon phosphorylation level change, rather than its electrostatics change by the

phosphorylation status. Recent results from the Reck-Peterson Lab and the Leschziner Lab on the cryo-EM structure of LRRK showed that the kinase domain conformation is likely to mediate MT binding (Deniston et al., 2020). Phosphorylation via autophosphorylation or upstream signaling factors activates Abl2 and posits the N terminus in an open conformation, as discussed in Chapter 2. However, how the conformation of the N-terminal SH3-SH2-kinase cassette affects the C terminus structural rearrangements remains unknown due to the lack of structural resolution. The highly disordered C-terminal region impedes the quality of the purified proteins and limits pursuit of the structural studies. Alpha-fold predicts the C-terminal of Abl2 is made up of flexible coils surrounding the conserved N terminus. I hypothesized that the open-up of the N-terminal core may change the exposed charge residues distribution, hence affects Abl2's binding to MTs. In collaboration with Matt Cook in the Xiong lab, we tried several conditions to prepare EM samples together with tubulin, however, the samples are too heterogeneous to achieve the three-dimensional reconstructions. The future validations of the hypothesized model will require the optimization of the Abl2 purification, or the stabilization of Abl2 with chemicals or binding partners to decrease the heterogeneity of the particles under EM. Structural insights into Abl2, especially the C terminus, will be critical for us to answer a lot of mechanical questions, e.g., where does Abl2 bind on MTs and tubulin? Does Abl2 undergo conformational changes upon binding to MTs and tubulin? Does the N-terminal conformational changes lead to differences in the accessibility of the MT-binding or tubulin binding sites?

In the other way, localization of Abl2 on the MTs through the C terminus may also affect the specificity of the kinase towards different substrates. I generated the retroviral vector to stably express Abl2-BioID2-HA in cells. Immediate next steps following proximity labelling include mass spectrometry, which will reveal the interactome profile of Abl2 and changes of substrates under different cell status, e.g., cells treated with nocodazole for loss of MT structures or taxol for stabilized MT structures. Data analysis on the interactome profile changes will shed lights on how the downstream pathways are mediated through Abl2 binding to MTs.

Abl2 may have different interaction behaviors with MTs under certain cellular contexts.

Abl family kinases have been reported to play critical roles in coordinating multiple cellular behaviors including protrusion and migration. Previous work from our laboratory has demonstrated that Abl2 binds cooperatively to actin and promotes formation of actin-based protrusions, including lamellipodia in fibroblasts and invadopodia in invasive cancer cells (Gil-Henn et al., 2013; Mader et al., 2011; Miller et al., 2004; Peacock et al., 2007; Wang et al., 2001). In these contexts, Abl2 stably co-localizes primarily with actin, and transiently interacts with MTs. Interestingly, the destabilization of the actin filaments in COS-7 does not release Abl2 to the MT lattice. The possible reason is that Abl2 possesses strong binding affinity to free tubulin, which is highly concentrated in the cytoplasm. Abl2 released from actin filaments may prefer binding to tubulin, instead of on MTs. The

hypothesis is in line with my observation that Abl2 showed significant colocalization with MTs when the cellular MTs are more stabilized and appears as bundles (data not shown). In addition to the transient interaction with the filamentous MTs, Abl2 is also found to enrich in the area near the microtubule-organization center (MTOC). Recent work from Cao lab and Liu lab showed that c-Abl/Abl1 directly binds and phosphorylates γ-tubulin, which is important for the γ-TuRC assembly and centrosome maturation (Wang et al., 2022). My preliminary results showed that Abl1 functions similarly to Abl2 in MTs (**Figure 4.3B**) and tubulin binding (data not shown), therefore, Abl1 and Abl2 is likely to play compensatory roles in cells. Our collective data indicate the model that Abl family kinases can firstly interact with γ-tubulin promote the γ-TuRC formation. Thereafter, the interaction with α/β-tubulins via the C terminus can promote the elongation of the MTs from the templates.

Future studies of Abl2 interactions with cytoskeleton in specific cell types, e.g., epithelial cells which have classic cell-cell adhesion structures, or in specific cell cycles, e.g., the mitosis, especially the prophase and the metaphase, will help us understand Abl2's regulation mechanism on the cellular MT network and what are the physiological roles of Abl2 interaction with MTs.

Abl2 serves as the central crosslinker between MT and actin in cells.

In collaboration with Dr. Ke Zhang, we showed that Abl2 is recruited to ventral actin waves to promote lamellipodium extension, and MT plus tips do not extend beyond the Abl2:actin waves (K. Zhang et al., 2018). Using confocal microscopy, I

observed that Abl2 also colocalizes with the actin coated vesicle-like structures (**Figure 5.9B, C**), indicating that Abl2 may assist in the endocytosis and/or other related trafficking processes by coupling actin and MTs. Previous work from the Pendergast lab showed that inhibition of Abl kinases signaling through the kinase inhibitor STI571 treatment induced the accumulation of autophagosomes and lysosomes (Yogalingam & Pendergast, 2008). As we discussed before, MT binding is likely to be mediated by the kinase domain conformation. STI571 treatment could also cause the direct changes in the cytoskeletal interactions, besides the indirect roles through downstream signaling. Dr. Miguel A Del Pozo's Lab also reported that Abl family kinases regulate the early stages of caveolin-1 inward trafficking (Echarri et al., 2012). Both endocytosis and trafficking require the exquisite collaboration between actin filaments and MTs (Apodaca, 2001; Nolte et al., 2021). It would be interesting to set up the experimental systems to measure Abl family kinases' effect in these processes and determine how different fragments of Abl family kinases will alter the functions.

Recruitment of tubulin dimers to MTs or oligomers may be a common mechanism underlying MT nucleation, growth, and lattice repair.

In **Chapter 5**, I showed that Abl2 decreases the lag time for MTs to initiate processive growth **(Figure 5.2)**, and increases the total amount of the polymerized MTs in the equilibrated reactions **(Figure 5.1)**. Tubulin-binding deficient Abl2Δ688-790 has no effect on the lag time **(Figure 5.2)**. Analysis of the MT plus-end dynamics using TIRF microscopy revealed that Abl2 promotes MT elongation both

in vitro and in cells. My discovery that Abl2 can both interact with MT lattice and tubulin encouraged us to look into the other roles Abl2 may play in regulating MT network. Inspired by the recent findings that new tubulin can be incorporated into the MT lattice defects or gaps for self-repair, my collaborator Daisy Duan obtained the preliminary data that Abl2 structurally recognizes damaged sites and localizes at areas directly adjacent to lattice defects (data not shown). As the functional readout, more repair events of the taxol-damaged MTs were observed in the presence of Abl2-eGFP (data not shown). Together, our discoveries shown here and in Chapter 5 suggest that Abl2 binds tubulin dimers to promote nucleation, increase MT growth and lifetime, and promote MT lattice repair. The versatile functions of Abl2 in the regulation of MT networks appear as lots of puzzle pieces, which can be unified together by a hypothesized mechanism.

Under our hypothesized working model, Abl2 can clamp down onto the MT growing ends, lattice defects boundaries, or the tubulin oligomer to facilitate the incorporation of new tubulin dimers **(Figure 6.3)**. The accurate ultrastructure of MT growing ends, MT lattice segments containing damage sites, and tubulin oligomers remain unclear due to the difficulties in capturing such heterogeneous intermediate structures. However, recent cryo-EM analysis on the growing ends of the MTs showed the presence of various structures including straight ends, curled multi-protofilaments sheet, and flared or ragged ends **(Figure 1.5)**. Certain lattice defects like "holes" may be akin to corners on protofilaments along growing ends. We postulate that Abl2 docks onto ends of protofilaments to promote rapid tubulin dimer addition (growth rates increase) – analogous to Abl2 localization on

boundaries of the damaged MT segments (repair promotion) **(Figure 6.3)**. As a support of this model, many of the identified MT nucleators like XMAP215 (Brouhard et al., 2008; Thawani et al., 2018) and CLASP2α (Aher et al., 2020; Al-Bassam et al., 2010; Lawrence et al., 2018) also have been reported to participate in plus-end elongation rate promotion and/or lattice repair, indicating these processes may share similar underlying mechanisms.

The nucleation process seems difficult to fit in the scenario since the process has been a puzzling question for almost a century. As reviewed in **Chapter 1**, classical models for MT nucleation proposed that new MTs form via a nucleation-elongation mechanism, in which the formation of a critical nucleus is the rate-limiting step. Recent studies demonstrated that 'the critical nuclei' are first formed as 2D layers of a growing lattice prior to its maturation into a cylindrical tube[91,92]. Enlargement of 2D lattices is energetically favorable but kinetically impeded by the difficulty in adding new protofilament layers (Brouhard & Rice, 2018; Rice et al., 2021). This new model connects the nucleation with the growing ends, both dependent on the addition of new tubulins onto the existing structures. We propose that Abl2 may facilitate this by binding a nascent protofilament and recruiting and condensing tubulin dimers to promote layer formation. In addition, Abl2 may then bind to the lattice and facilitate tubulin addition at corners of 2D lattices, which may be structurally akin to the corners at growing MT ends and damaged holes **(Figure 6.3)**.
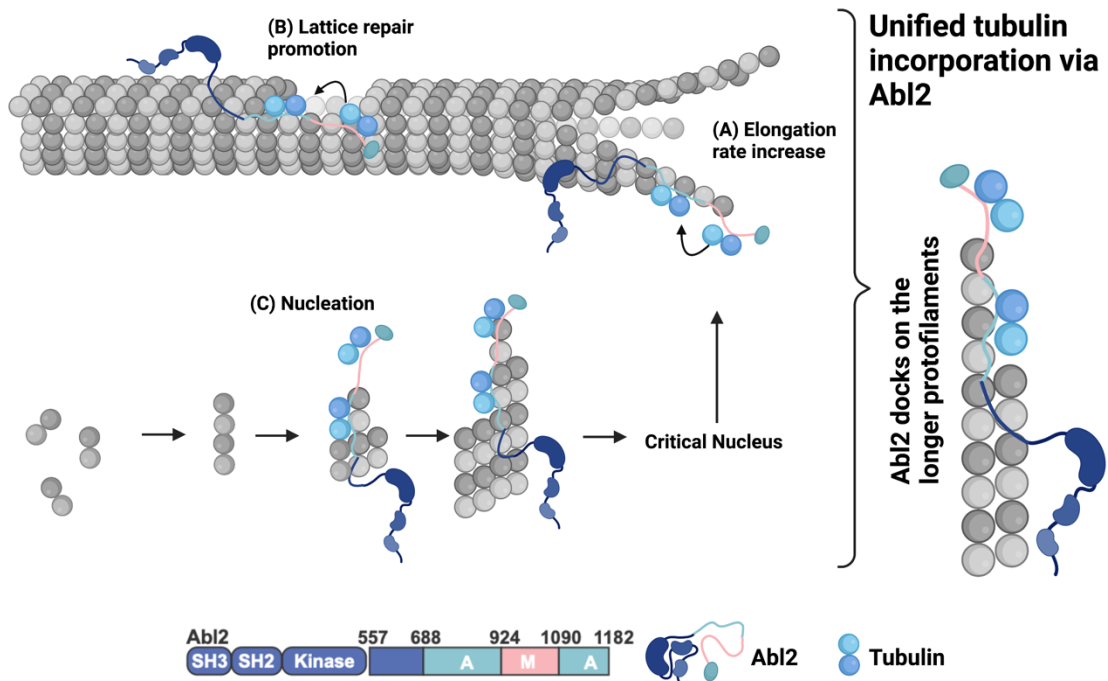
Figure 6.3 The hypothesized model that Abl2 interacts with tubulin and MTs to regulate dynamics. Abl2 can dock onto the longer protofilaments **A)** in the MT growing ends, **B)** MT lattice defects boundaries, and **C)** the tubulin oligomers to facilitate the incorporation of new tubulin dimers, resulting in the facilitation of the MT elongation, lattice damage repair, and nucleation.

Phase separation of Abl2 facilitates MT nucleation.

Biomolecules that can form condensates generally contain intrinsically disordered regions (IDRs) and multivalent binding regions. These sequence features generate the driving forces for the condensate formation (Alberti et al., 2019; Feng et al., 2019; Wang et al., 2018). The multivalency and the inherent disordered C-terminal half of Abl2 led us to determine whether Abl2 can undergo phase separation. Strikingly, we found that Abl2 form coacervates in the presence of 5% dextran, which is thought to mimic the conditions of a crowded intracellular environment. The phase separation behavior is mainly mediated through the disordered C-terminal half and can recruit the interacting tubulin into the dense phase (**Figure 5.3**). Recent studies on several MTBPs including TPX2 (King & Petry, 2020), tau (Hernandez-Vega et al., 2017; Tan et al., 2019), and CLIP-170 (Wu et al., 2021) reveal that phase separation allows MTBPs to conduct various MT-associated functions, which include enhancing nucleation, protecting existing MTs from severing enzymes, and spatially condensing tubulin dimers for MT growth. I showed that new MTs nucleated from Abl2-eGFP:tubulin co-condensates. Under the same conditions, tubulin mixing with eGFP did not have filaments assembled (**Figure 5.4**). Unlike the homogeneous behaviors of MT bundles growing from tau:tubulin co-condensates (Hernandez-Vega et al., 2017) and the branched MT network growing from the TPX2:tubulin co-condensates (King & Petry, 2020), both single/bundle filament or aster MTs were observed in the presence of Abl2-eGFP. In addition, there were some Abl2:tubulin co-condensates whereby new MT polymers did not nucleate out. One potential explanation is that the purified Abl2-

eGFP is not pure enough. The impurities in the phase separation system causes the formation of the "sticky balls" that cannot be fused together *in vitro* (Wang et al., 2018), which is consistent with Daisy's observations in pilot dual optical-trap fusion experiments. Depending on biophysical properties, the condensates *in vitro* can 'mature' into a more viscous-gel- or solid-like state that differs in aging speeds (J.B. Woodruff, et al., 2017). This may also reduce the exchange of the molecules inside and outside of condensates which will negatively impact the protein function inside condensates. Hence, clusters of Abl2 within these sticky, aged condensates may have lost the pre-mature liquid-like properties and trapped tubulin in the inactive fractions.

Our in vitro experiments require molecular crowders to drive the formation of Abl2 drops at physiological salt concentrations. We do not know whether similar mechanisms of nucleation via Abl2:tubulin co-condensates operate *in vivo*. Tubulin condensation has been proposed to be a mechanism driving the nucleation of microtubules in C. elegans centrosomes (Woodruff et al., 2017). Considering my observations that Abl2 colocalizes with the MTOC in cells, Abl2 is likely to participate in the condensates, probably at certain cell cycle phases to promote the MT nucleation and growth from the centrosome. It would be interesting to determine if Abl2 undergoes phase separation in cells and if the phase separation behavior of Abl2 can be modulated by signaling cues or localization of Abl2.

Summary

As a summary of my thesis, my results demonstrated that Abl2 is a novel regulator of MT dynamics by directly binding to tubulin dimers and MT lattice. In our hypothesized working model, Abl2 co-condenses with tubulin and recruits fresh GTP-tubulin to specific sites, as listed in the following contexts, to promote dynamics: **a)** In the context of MT nucleation, Abl2 is likely to interact with tubulin oligomers or the ultrastructure before the critical nucleus and recruit dimers from solution to form the critical nucleus. **b)** When Abl2 is enriched at damaged MT boundaries, fresh GTP-tubulin is recruited and the new protofilaments nucleated out from the damaged sites. The repaired lattice is enriched with GTP-tubulin, thereby increasing opportunities for the MT to switch back into its growth state after which it enters a state of shrinkage. **c)** Abl2 can also recognize the newly-formed MT GTP-caps to increase the plus-end elongation rates. Together, the ability of Abl2 to promote MT growth, rescue, and nucleation stems from co-condensation with tubulin, where Abl2-tubulin complexes serve as compartmentalized reactors for Abl2 to function locally on MTOC, MT shafts and/or at growing ends.

Chapter 7 – Materials and Methods

Molecular cloning and purification of recombinant proteins

Full-length murine Abl2 (residues 74-1182), Abl2-eGFP, N terminus (N-557), N-557-eGFP, C terminus (557-C), 557-C-eGFP, 688-790, 688-924, 688-924-eGFP, 1024-1090 were cloned with an N-terminal 6XHis tag into the pFastBac1 vector (Invitrogen) for insect cell expression. Abl2Δ688-790 and Abl2Δ688-790-eGFP was generated were generated using PCR-based mutagenesis and confirmed by DNA sequencing. Abl2 and Abl2Δ688-790 were cloned into pN1-EGFP expression vector for mammalian cell expression. Recombinant baculoviruses expressing Abl2 or Abl2 fragments in pFastBac vector constructs were generated using the Bac-to-Bac expression system in Sf9 insect cells according to the manufacturer's instructions (ThermoFisher, Waltham, MA). After 36-48hr infection with baculoviruses, Hi5 cells were collected and centrifuged for 3,000 rpm for 5min at 4°C. Cells were lysed using buffer containing 20 mM HEPES pH7.25, 5% glycerol, 500 mM KCl, 20 mM imidazole, 1 mM DTT, 1 mM PMSF, 1X protease inhibitor cocktail, 1% Triton-X100 and left to incubate at 4°C on a rotisserie stand for 5-10min. Lysates were ultracentrifuged using Ti70.1 rotor for 45 min, 40K rpm at 4°C. After collecting and 0.45 μm filtering the supernatant, proteins were passed through disposable columns with Ni-NTA resin beads via gravity flow 3x. Resin was washed with the following buffers in the following order: wash A (20 mM HEPES pH7.25, 5% glycerol, 500 mM KCl, 20 mM imidazole, 1 mM DTT, 1 mM PMSF, 1X protease inhibitor cocktail); B (20 mM HEPES pH7.25, 5% glycerol, 1 M KCl, 20 mM imidazole, 1 mM DTT, 1 mM PMSF, 1X protease inhibitor cocktail), A, and C (20 mM HEPES pH7.25, 5% glycerol, 300 mM KCl, 20 mM imidazole, 1

mM DTT, 1 mM PMSF, 1X protease inhibitor cocktail). Bound proteins were bump-eluted off the Ni-NTA resin (Invitrogen) using wash C buffer containing 300 mM imidazole in 5 1mL fractions. His-Abl2 and Abl2 fragments for biolayer interferometry assays were exchanged into storage buffer containing 20 mM HEPES pH7.25, 5% glycerol, 100 mM KCl, 1 mM DTT using either Superdex 75 increase 10/300 GL column for proteins with MW < 75kDa, or Supderdex 200 increase 10/300 GL column for proteins with MW ≥ 75kDa. For His-tag cleavage, tags on Abl2 and tau proteins were removed using 1:60 units of TEV protease and were incubated on rotisserie stand at 4°C for 2.5-4 hrs. His-tag cleaved proteins were exchanged into the storage buffer containing 20 mM HEPES, 5% glycerol, 300 mM KCl, 1 mM DTT using either Superdex 75 increase 10/300 GL column or Supderdex 200 increase 10/300 GL column. Peak fractions were collected, snap frozen, and stored at -80°C until use. EB1-eGFP and tau-eGFP were prepared with the same procedures.

The plasmid pRK793 TEV S219V was obtained as a gift from the Boggon Lab and transformed into BL21 E. coli for purification. The protein was expressed in 2L of BL21 E. coli culture followed by isopropylβ-D-thiogalactopyranoside (IPTG) (0.2 mM) induction at 37°C for 3 hrs. Cells were sonicated in buffer containing 20 mM Tris pH 8, 5 mM βME, 500 mM NaCl, 4 mM imidazole, 1 mM DTT, 1 mM PMSF, 1X protease inhibitor cocktail. Lysates were ultracentrifuged using Ti70.1 rotor for 45 min, 40K rpm at 4°C. After collecting and 0.45mm filtering the supernatant, proteins were passed through disposable columns with Ni-NTA resin beads via gravity flow 3X. Resin was washed with the following buffers in the following order:

wash A (20 mM Tris pH 8, 5 mM βME, 500 mM NaCl, 4 mM imidazole, 1 mM DTT, 1 mM PMSF), B (20 mM Tris pH 8, 5 mM βME, 250 mM NaCl, 40 mM imidazole, 1 mM DTT, 1 mM PMSF), and C (20 mM Tris pH 8, 5 mM βME, 40 mM Imidazole, 100 mM NaCl, 1 mM DTT, 1 mM PMSF). Bound proteins were eluted off the Ni-NTA resin using elution buffer (20 mM Tris pH 8, 5 mM βME, 400 mM Imidazole, 100 mM NaCl, 1 mM DTT, 1 mM PMSF, and 1X protease inhibitor cocktail). The eluted fractions were then applied to a mono S cation exchange column for cleanup using buffer A (20 mM HEPES pH 7.25, 5% Glycerol, 1 mM DTT) and buffer B (20 mM HEPES pH 7.25, 5% Glycerol, 1 M KCl, 1 mM DTT). The eluted fractions containing TEV were pooled, flash-frozen in liquid nitrogen, and stored at 80°C.

Tubulin purification and labelling

Porcine brain tubulin was purified as described previously (Castoldi and Popov, 2003). Cycled tubulin was labeled with Alexa Fluor 647 (Alexa Fluor™ 647 NHS Ester (Succinimidyl Ester)), ThermoFisher, Waltham, MA and rhodamine (TAMRA, SE; 5-(and-6)-Carboxytetramethylrhodamine, Succinimidyl Ester, Invitrogen, Carlsbad, CA) as described (Brouhard et al., 2008). Biotinylated porcine brain tubulin was obtained from Cytoskeleton, Denver, CO.

Microtubule cosedimentation assays and quantification

Cosedimentation assays were performed as previously described (Campbell and Slep, 2011; Miller et al., 2004). Double-cycled GMPCPP (Jena Bioscience,

Thuringia, Germany) stabilized MTs were grown as described (Vemu et al., 2020). Taxol-MTs was polymerized at a final concentration of 60 µM at 37°C in polymerization buffer [80 mM PIPES, pH 6.8, 1 mM MgCl2, 1 mM EGTA, 1 mM GTP, and 15 nM paclitaxel (taxol)]. The taxol-stabilized MTs and GMPCPP-stabilized MTs were set aside for cosedimentation. For MT cosedimentation assays, 0.2 µM Abl2 or Abl2 fragments were mixed with increasing concentration of MTs (0 to 6 µM) at 37°C for 20 minutes in binding buffer [80 mM PIPES, pH 6.8, 70 mM KCl, 1 mM GTP, 5 nM taxol (100 µL reaction volume)]. Mixtures were pelleted by high-speed centrifugation at 120,000 X g for 20 minutes at 37°C. Pellet and supernatant fractions were recovered and separated by SDS-PAGE, stained with Coomassie Blue G-250 (Bio-Rad Laboratories, Hercules, CA) then destained in water. The SDS-PAGE gels were then scanned with Bio-Rad ChemiDoc™ Touch Imaging System and quantified by densitometry using ImageJ software. Binding affinity was quantified either as the percentage of Abl2/Abl2 fragments bound to MTs over total amount of Abl2/Abl2 fragments in the reaction for each concentration or as the amount of Abl2 bound to MTs for each concentration of Abl2. Experiments were repeated at least 4 times for each experimental condition (n $\geq$ 4). A specific binding curve with equation $y = B_{max} \times x / (K_D + x)$ was used to fit the curve, where y is specific binding, x is the concentration of the ligand, B_{max} is the maximal binding in the same units as y, and K_D is the binding affinity in the same units as x (Pollard, 2010). Binding curves, affinities (K_D), and R^2 value for curve fitting were calculated using Prism 9 (GraphPad).

Tubulin binding analysis with size-exclusion chromatography

Size-exclusion chromatography used a Supderdex 200 increase 10/300 GL column equilibrated in 20 mM HEPES pH 7.25, 5% glycerol, 100 mM KCl, 1 mM DTT. The column was calibrated with standard proteins of known Stokes radii (Sigma-Aldrich, St. Louis, MO). Abl2 or Abl2-557-C and tubulin were mixed with tubulin at a ratio of 1:4 and incubated for 30 min on ice, and then injected onto the column. Control experiments were performed with each protein alone. The collected fractions were analyzed by SDS-PAGE, stained with Coomassie brilliant blue G250 (Sigma-Aldrich, St. Louis, MO), and scanned.

Tubulin binding affinity measurements using biolayer Interferometry

The biolayer interferometry technique using the BLItz system (ForteBio) was used to measure binding kinetics for the tubulin interaction with His-Abl2 and His-Abl2 fragments. Anti-His biosensors (for the His_6-tag fusions) were hydrated in binding buffer (20 mM HEPES pH 7.25, 5% glycerol, 100 mM KCl, 1 mM DTT, 0.02% Tween) for 10 min. For each tubulin concentration (ranging from 7 nM to 2000 nM), the following procedure was performed. An initial baseline was collected by immersing the biosensor in binding buffer for 1 min, and then 4 µl of fixed concentrations of His_6-Abl2 or His_6-Abl2 fragments (0.3 µM or 1 µM) were loaded to the biosensor for 5 min. The Abl2-loaded biosensor was returned to binding buffer for collection of a second baseline for 1 min and then placed in 4 µl of tubulin for a 5-min association step. For each data point, the background binding was also measured. For each tubulin concentration, the difference in the signal (in nm) just

prior to the association step and that at the end of the association step was subtracted from the difference in signal for background binding. These values were plotted, and the curves were fit using GraphPad Prism to obtain a dissociation constant.

Turbidity assay and preparation of Abl2-MT sample grids for EM imaging

18 µM porcine brain tubulin in BRB80 was incubated with the MT polymerization buffer (2 mM of GTP, 1 mM DTT, 15% Glycerol) alone or in the presence of Abl2 and Abl2 fragments at 37°C. Tubulin assembly was monitored by measuring turbidity at 350 nm (A350) for 2 hours using SpectraMax M6 Multi-Mode Microplate Reader recording spectrophotometer. Control experiments were done by monitoring A350 for buffer alone with 0.5 µM Abl2 and Abl2 fragments without tubulin. 4 µL reactions at 10 min were taken out and visualized using electron microscopy (EM) of negatively stained samples. A 400-mesh copper grid (Ted Pella, Redding, CA) overlaid with a very thin continuous carbon layer was gently glow discharged and 4 µL of the diluted protein was applied to the grid. After a 30 s adsorption, the reactions were blotted away from the grid with filter paper (Whatman No.1) leaving a thin layer of solution on the grid. 4 µL of 2% uranyl-acetate solution were applied to the grid for 30 s before blotting twice. After blotting, the grid was left to dry for 2 min. The negative stain samples of the turbidity assays were imaged using a Tecnai12 transmission electron microscope (TEM) and images recorded on a Gatan CCD camera at ~−2-3 µm defocus.

Condensate (phase separation) analysis

To measure the phase diagram of Abl2-eGFP as a function of [salt] and its concentration, condensates were prepared by mixing Abl2-eGFP with 5% dextran 70, at the protein and salt concentrations indicated. A particular [salt]:[Abl2-eGFP] condition was scored to have phase-separated condensates if the average signal in apparent condensates was at least four times higher than background (i.e., partition coefficient ≥ 4). Conditions were scored to not contain condensates if they fell below this cutoff or if no apparent condensates were observed. Partition coefficient is defined as the difference in mean intensity of a condensate compared with the background, i.e., apparent relative enrichment. The "Color Threshold" (Otsu thresholding) and "Particle Analyzer" functions on FIJI were used to identify and quantify condensate intensity, respectively. For each concentration, construct, and condition, at least 30 condensates were analyzed. All statistical analysis and graph generation was carried out in MATLAB.

To measure FRAP, condensates were prepared and were allowed to settle for 10 min. Focus was set just above the coverslip and three regions of interest (ROIs) of equal size and geometry were placed (1) within the condensate to be photobleached, (2) the background, and (3) within a nearby condensate. Photobleaching was carried out and the intensity of each ROI recorded every second for the first 10 s and every 10 s thereafter over a 10 min acquisition. Recovery in the photobleached ROI was normalized to any changes in intensity in the background and nearby condensate ROI due to global bleaching. Global photobleaching in excess of 5% of the starting intensity was never observed. If the

intensity in the nearby condensate ROI changed, that FRAP acquisition was discarded.

Microtubule nucleation under phase separation conditions

8 µM 10% Alexa Fluor 647-labeled porcine brain tubulin in BRB80 was incubated with the MT polymerization buffer (2 mM of GTP, 1 mM DTT, 10% Glycerol), 1 µM Abl2-eGFP, 3% Dextran at 37°C. Reactions were added to a 384-well glass-bottom plate (Corning, Corning, NY), which was acid-washed and coated with 2% F-127 for 30 min. Tubulin nucleation was monitored using Nikon CSU-W1 SoRa spinning disk confocal 30 min and 1 h after the start of the reactions.

Microtubule segmentation and dynamic assays *in vitro*

Silanization of cover glasses and preparation of flow-cells was previously described (Y. Hu et al., 2019) and coated with 1 mg/mL biotin for 10 min, 2% F-127 for 30 min, and neutravidin for 5 min. To create the GDP-enriched islands, 6-12% rhodamine-labeled, 10% biotinylated GMPCPP seeds were immobilized on glass cover slips in flow chambers. 8 µM of 6-12% Alexa Fluor 647-labeled tubulin supplemented with 1 mM GTP was flowed into the chamber to allow for the MTs elongation for 2 min. The flow chamber was washed with BRB80 and immediately flew in 8 µM of 6-12% rhodamine-labeled supplemented with 1 mM GMPCPP to prevent the catastrophe of the GTP-MTs, which will further age into GDP-enriched MT islands. After 2 min equilibration, Abl2-eGFP, 557-C-eGFP, EB1-eGFP or tau-eGFP was flowed into the chamber in the imaging buffer containing BRB80

supplemented with 50 mM KCl, 40 mM glucose, 40 mg/ml glucose-oxidase, 16 µg/ml catalase, 0.16 mg/ml casein, 1% DTT, and 0.01% Tween-20. For all the experiments an objective heater was used to warm the sample to 34°C.

Dynamic MT assays using rhodamine-labeled seeds and Alexa Fluor 488-labeled dynamic extension were performed as describe previously (Brouhard et al., 2008; Zanic et al., 2009). The imaging buffer consisted of BRB80 (80 mM PIPES, 1 mM $MgCl_2$, 1 mM EGTA, pH 6.8), supplemented with 40 mM glucose, 40 µg/ml glucose oxidase, 16 µg/ml catalase, 0.1 mg/ml casein, 1 mM DTT, 1 mM GTP, and 100 mM KCl. For elongation rate measurements, images were acquired in the TIRF channel every 5 s for 25-40 minutes on a Nikon Ti-E microscope with a 100x/1.49 oil objective, an Andor Zyla 4.2 sCMOS camera, and Nikon Elements software. An objective heater was used to heat the sample to 34℃. Data were analyzed by making kymographs from acquired images using Fiji software, which were then used to measure the parameters of MT dynamics. Elongation rates were determined by measuring the change in length of a single MT over time.

Cells, cell culture, and construct transfection

Mycoplasma free COS-7 cell lines (ATCC) were grown in DMEM supplemented with 10% FBS, 100 units/mL penicillin, 100 µg/mL streptomycin, and 2 mM L-glutamine. *abl2*−/− COS-7 cells were generated using CRPISPR/Cas9. A guide sequence of 5′-GAGAAAGTGAGAGTAGCCCT-3′ with an adjacent PAM (GGG) targeting the fourth exon of Abl2 was inserted into lentiCRISPR plasmid then transfected into HEK293T cells to generate lentivirus. COS-7 cells were infected

with the generated lentivirus and then selected with 2 µg/mL puromycin for 72 hours. *abl2⁻/⁻* COS-7 cells were transfected with Abl2, N-557, or 557-C in pN1-EGFP using polyethylenimine (PEI). Transfection was performed 24 to 48 hours prior to imaging according to the manufacturer's instructions. The same strategy was used to inactivate Abl2 in WT mouse 3T3 fibroblasts, using the guide sequence of 5'- CATGTAAAGTAACACGACGG-3' with an adjacent PAM (CGG). Resistant Abl2-GFP, N-557-GFP, or 557-C-GFP were cloned into pLXSN vector and then transfected into HEK293T cells to generate retrovirus. *abl2⁻/⁻* 3T3 cells were infected with the retrovirus then selected with 400 µg/mL G418 for 7 days. Abl2 or Abl2 variants expressing cells were obtained by fluorescence-activated cell sorting using *abl2⁻/⁻* 3T3 cells as a negative reference. Cell lysates were collected to determine the expression levels of Abl2 or Abl2 variants via immunoblotting.

Western Blot analysis

Cells were lysed with 1x LSB buffer (8% SDS, 20% Glycerol, 100 mM Tris pH= 6.8, 8% 2-Mercaptoethanol, and complete protease inhibitors) at 95°C. Lysates were run on SDS-PAGE then transferred to nitrocellulose, blocked using 5% milk or BSA and immunoblotted with Ar11, which specifically recognizes Abl2 C-terminal half (residues 766–1182), or Ar19, which recognizes Abl2 N-terminal half (Ar11 and Ar19 were gifts from Peter Davies, Albert Einstein Medical College, Bronx, NY), or 4G10, which recognizes the phosphorylated tyrosine residues. The intensity of each band was quantified using ImageJ and controlled by the intensity of Ponceau S stain image for each lane. *abl2-/-* COS-7 cells exhibited >92% loss of Abl2 signal

and *abl2-/-* 3T3 fibroblasts exhibited > 95% loss of Abl2 signal by blotting with Ar11 and Ar19.

Time-lapse live-cell microscopy and quantification

For cellular MT growth tracking, cells were imaged on 30 mm #1.5 coverslips in an interchangeable dish (Bioptechs). Coverslips were plasma cleaned for 2 minutes with H_2/O_2. Coverslips were coated with 50 µg/ml Poly-D-Lysine (Sigma-Aldrich, St. Louis, MO) for 20 minutes at room temperature. Cells were seeded at 50,000 cells per coverslip. Cell dishes were maintained at 34°C in phenol red-free DMEM supplemented with 10% FBS and 20 mM HEPES (pH 7.3) while imaging. Images were acquired in TIRF mode every 1 second (1 FPS) for 2 minutes. Cell areas were divided by 15° radial lines centered at the observed MT organization center (MTOC). Cell centers were defined as the area within the inner half region of a cell determined by connecting the midpoints of all radial lines, cell edges were defined as the outer most one quarter of a cell. Kymographs were generated by plotting the track of MT plus-tip marker fluorescence, mCherry-MACF43, as a function of time. MT plus-end growth rates were determined by measuring the displacement of MT plus-tip tracker over time. At least 150 tracks of mCherry-MACF43 were quantified for each assay condition (n $\geq$ 150).

For visualization of Abl2 and the cytoskeleton interactions, cells were imaged on MetTek dishes (35 mm Dish, No. 1.5 Uncoated Coverslip, 14 mm Glass Diameter). The dishes were coated with 50 µg/ml Poly-D-Lysine (Sigma-Aldrich, St. Louis, MO) for 20 minutes at room temperature and 10 µg/ml human fibronectin

(Gibco) for 1 h at 37°C. Cells were seeded at 50,000 cells per coverslip. *abl2*^{-/-} COS-7 cells were transfected with fluorescently labeled Abl2 and LifeAct or EB3, as indicated, using polyethylenimine (PEI). Transfection was performed 24 to 48 hours prior to imaging according to the manufacturer's instructions. Cell dishes were maintained at 37°C in phenol red-free DMEM supplemented with 10% FBS and 20 mM HEPES (pH 7.2) while imaging. Images were acquired using TIRF and Nikon CSU-W1 SoRa spinning disk confocal Microscopy.

Single-cell migration assay and quantification

WT and *abl2*^{-/-} 3T3 fibroblasts, or *abl2*^{-/-} 3T3 cells re-expressing GFP, or Abl2-557-C-GFP were plated at a sub-confluence on 6-well plates coated with 10 µg/ml fibronectin (Sigma-Aldrich, St. Louis, MO). Phase-contrast images were acquired every 40 minutes for 6 hours on a Keyence BZ-X710 All-in-One Fluorescence Microscope with a 4x/0.1 objective. Movies were analyzed with the Manual Tracking function in ImageJ, using one of the nucleoli to track the cells in each frame. At least 30 cells were tracked for each experimental condition ($n \geq 30$). The cell migration tracking data was analyzed as described (Gorelik and Gautreau, 2014).

Statistical analyses

Comparisons of MT elongation rates were made with unpaired, two-tailed Student's *t*-tests, as appropriate. Significance was defined as *, $p<0.05$, **, $p<0.01$; ***, $p<0.001$; ****, $p<0.0001$. For binding experiments, values of K_D are expressed

as mean ± S.D., N.B. (not binding), or N.S. (not saturating). Error bars of the binding curves are presented as standard deviation (mean ± S.D.). Calculations were performed in Prism8 (GraphPad).

Bibliography

Abelson, H. T., & Rabstein, L. S. (1970). Influence of prednisolone on Moloney leukemogenic virus in BALB-c mice. *Cancer Res*, *30*(8), 2208-2212. https://www.ncbi.nlm.nih.gov/pubmed/4918190

Aher, A., Rai, D., Schaedel, L., Gaillard, J., John, K., Liu, Q., Altelaar, M., Blanchoin, L., Thery, M., & Akhmanova, A. (2020). CLASP Mediates Microtubule Repair by Restricting Lattice Damage and Regulating Tubulin Incorporation. *Curr Biol*, *30*(11), 2175-2183 e2176. https://doi.org/10.1016/j.cub.2020.03.070

Akhmanova, A., & Steinmetz, M. O. (2015). Control of microtubule organization and dynamics: two ends in the limelight. *Nat Rev Mol Cell Biol*, *16*(12), 711-726. https://doi.org/10.1038/nrm4084

Al-Bassam, J., Kim, H., Brouhard, G., van Oijen, A., Harrison, S. C., & Chang, F. (2010). CLASP promotes microtubule rescue by recruiting tubulin dimers to the microtubule. *Dev Cell*, *19*(2), 245-258. https://doi.org/10.1016/j.devcel.2010.07.016

Albe, K. R., Butler, M. H., & Wright, B. E. (1990). Cellular Concentrations of Enzymes and Their Substrates. *Journal of Theoretical Biology*, *143*(2), 163-195. https://doi.org/Doi 10.1016/S0022-5193(05)80266-8

Alberti, S., Gladfelter, A., & Mittag, T. (2019). Considerations and Challenges in Studying Liquid-Liquid Phase Separation and Biomolecular Condensates. *Cell*, *176*(3), 419-434. https://doi.org/10.1016/j.cell.2018.12.035

Alushin, G. M., Lander, G. C., Kellogg, E. H., Zhang, R., Baker, D., & Nogales, E. (2014). High-resolution microtubule structures reveal the structural transitions in alphabeta-tubulin upon GTP hydrolysis. *Cell*, *157*(5), 1117-1129. https://doi.org/10.1016/j.cell.2014.03.053

Amos, L. A., & Schlieper, D. (2005). Microtubules and maps. *Adv Protein Chem*, *71*, 257-298. https://doi.org/10.1016/S0065-3233(04)71007-4

Andre, A. A. M., & Spruijt, E. (2020). Liquid-Liquid Phase Separation in Crowded Environments. *Int J Mol Sci*, *21*(16). https://doi.org/10.3390/ijms21165908

Apodaca, G. (2001). Endocytic traffic in polarized epithelial cells: Role of the actin and microtubule cytoskeleton. *Traffic*, *2*(3), 149-159. https://doi.org/DOI 10.1034/j.1600-0854.2001.020301.x

Aumeier, C., Schaedel, L., Gaillard, J., John, K., Blanchoin, L., & Thery, M. (2016). Self-repair promotes microtubule rescue. *Nat Cell Biol*, *18*(10), 1054-1064. https://doi.org/10.1038/ncb3406

Backert, S., Feller, S. M., & Wessler, S. (2008). Emerging roles of Abl family tyrosine kinases in microbial pathogenesis. *Trends Biochem Sci*, *33*(2), 80-90. https://doi.org/10.1016/j.tibs.2007.10.006

Baratier, J., Peris, L., Brocard, J., Gory-Faure, S., Dufour, F., Bosc, C., Fourest-Lieuvin, A., Blanchoin, L., Salin, P., Job, D., & Andrieux, A. (2006). Phosphorylation of microtubule-associated protein STOP by calmodulin kinase II. *J Biol Chem*, *281*(28), 19561-19569. https://doi.org/10.1074/jbc.M509602200

Barila, D., & Superti-Furga, G. (1998). An intramolecular SH3-domain interaction regulates c-Abl activity. *Nature Genetics*, *18*(3), 280-282. https://doi.org/DOI 10.1038/ng0398-280

Beffert, U., Dillon, G. M., Sullivan, J. M., Stuart, C. E., Gilbert, J. P., Kambouris, J. A., & Ho, A. (2012). Microtubule plus-end tracking protein CLASP2 regulates neuronal polarity and synaptic function. *J Neurosci*, *32*(40), 13906-13916. https://doi.org/10.1523/JNEUROSCI.2108-12.2012

Beissert, T., Hundertmark, A., Kaburova, V., Travaglini, L., Mian, A. A., Nervi, C., & Ruthardt, M. (2008). Targeting of the N-terminal coiled coil oligomerization interface by a helix-2 peptide inhibits unmutated and imatinib-resistant BCR/ABL. *Int J Cancer*, *122*(12), 2744-2752. https://doi.org/10.1002/ijc.23467

Ben-Neriah, Y., Daley, G. Q., Mes-Masson, A. M., Witte, O. N., & Baltimore, D. (1986). The chronic myelogenous leukemia-specific P210 protein is the product of the bcr/abl hybrid gene. *Science*, *233*(4760), 212-214. https://doi.org/10.1126/science.3460176

Bodakuntla, S., Jijumon, A. S., Villablanca, C., Gonzalez-Billault, C., & Janke, C. (2019). Microtubule-Associated Proteins: Structuring the Cytoskeleton. *Trends Cell Biol*, *29*(10), 804-819. https://doi.org/10.1016/j.tcb.2019.07.004

Bosc, C., Andrieux, A., & Job, D. (2003). STOP proteins. *Biochemistry*, *42*(42), 12125-12132. https://doi.org/10.1021/bi0352163

Boyle, S. N., Michaud, G. A., Schweitzer, B., Predki, P. F., & Koleske, A. J. (2007). A critical role for cortactin phosphorylation by Abl-family kinases in PDGF-induced dorsal-wave formation. *Current Biology*, *17*(5), 445-451. https://doi.org/10.1016/j.cub.2007.01.057

Bradley, W. D., Hernandez, S. E., Settleman, J., & Koleske, A. J. (2006). Integrin signaling through arg activates p190RhoGAP by promoting its binding to p120RasGAP and recruitment to the membrane. *Molecular Biology of the Cell*, *17*(11), 4827-4836. https://doi.org/10.1091/mbc.E06-02-0132

Bradley, W. D., & Koleske, A. J. (2009). Regulation of cell migration and morphogenesis by Abl-family kinases: emerging mechanisms and physiological contexts. *Journal of Cell Science*, *122*(19), 3441-3454. https://doi.org/10.1242/jcs.039859

Brasher, B. B., & Van Etten, R. A. (2000). c-Abl has high intrinsic tyrosine kinase activity that is stimulated by mutation of the Src homology 3 domain and by autophosphorylation at two distinct regulatory tyrosines. *J Biol Chem*, *275*(45), 35631-35637. https://doi.org/10.1074/jbc.M005401200

Brouhard, G. J., & Rice, L. M. (2014). The contribution of alphabeta-tubulin curvature to microtubule dynamics. *J Cell Biol*, *207*(3), 323-334. https://doi.org/10.1083/jcb.201407095

Brouhard, G. J., & Rice, L. M. (2018). Microtubule dynamics: an interplay of biochemistry and mechanics. *Nat Rev Mol Cell Biol*, *19*(7), 451-463. https://doi.org/10.1038/s41580-018-0009-y

Brouhard, G. J., Stear, J. H., Noetzel, T. L., Al-Bassam, J., Kinoshita, K., Harrison, S. C., Howard, J., & Hyman, A. A. (2008). XMAP215 is a processive microtubule polymerase. *Cell*, *132*(1), 79-88. https://doi.org/10.1016/j.cell.2007.11.043

Brugg, B., & Matus, A. (1991). Phosphorylation determines the binding of microtubule-associated protein 2 (MAP2) to microtubules in living cells. *J Cell Biol*, *114*(4), 735-743. https://doi.org/10.1083/jcb.114.4.735

Cahu, J., Olichon, A., Hentrich, C., Schek, H., Drinjakovic, J., Zhang, C., Doherty-Kirby, A., Lajoie, G., & Surrey, T. (2008). Phosphorylation by Cdk1 increases the binding of Eg5 to microtubules in vitro and in Xenopus egg extract spindles. *PLoS One*, *3*(12), e3936. https://doi.org/10.1371/journal.pone.0003936

Cao, C., Leng, Y. M., Li, C. F., & Kufe, D. (2003). Functional interaction between the c-Abl and Arg protein-tyrosine kinases in the oxidative stress response. *Journal of Biological Chemistry*, *278*(15), 12961-12967. https://doi.org/10.1074/jbc.M300058200

Cao, C., Li, Y. P., Leng, Y. M., Li, P., Ma, Q. J., & Kufe, D. (2005). Ubiquitination and degradation of the Arg tyrosine kinase is regulated by oxidative stress. *Oncogene*, *24*(15), 2433-2440. https://doi.org/10.1038/sj.onc.1208454

Castle, B. T., McKibben, K. M., Rhoades, E., & Odde, D. J. (2020). Tau Avoids the GTP Cap at Growing Microtubule Plus-Ends. *Iscience*, *23*(12). https://doi.org/ARTN 101782
10.1016/j.isci.2020.101782

Chaaban, S., & Brouhard, G. J. (2017). A microtubule bestiary: structural diversity in tubulin polymers. *Mol Biol Cell*, *28*(22), 2924-2931. https://doi.org/10.1091/mbc.E16-05-0271

Chretien, D., Fuller, S. D., & Karsenti, E. (1995). Structure of growing microtubule ends: two-dimensional sheets close into tubes at variable rates. *J Cell Biol*, *129*(5), 1311-1328. https://doi.org/10.1083/jcb.129.5.1311

Chretien, D., & Wade, R. H. (1991). New data on the microtubule surface lattice. *Biol Cell*, *71*(1-2), 161-174. https://doi.org/10.1016/0248-4900(91)90062-r

Chrzanowska-Wodnicka, M., & Burridge, K. (1996). Rho-stimulated contractility drives the formation of stress fibers and focal adhesions. *J Cell Biol*, *133*(6), 1403-1415. https://doi.org/10.1083/jcb.133.6.1403

Cicchetti, P., Mayer, B. J., Thiel, G., & Baltimore, D. (1992). Identification of a Protein That Binds to the Sh3 Region of Abl and Is Similar to Bcr and Gap-Rho. *Science*, *257*(5071), 803-806. https://doi.org/DOI 10.1126/science.1379745

Cleary, J. M., & Hancock, W. O. (2021). Molecular mechanisms underlying microtubule growth dynamics. *Curr Biol*, *31*(10), R560-R573. https://doi.org/10.1016/j.cub.2021.02.035

Colicelli, J. (2010). ABL tyrosine kinases: evolution of function, regulation, and specificity. *Sci Signal*, *3*(139), re6. https://doi.org/10.1126/scisignal.3139re6

Conde, C., & Caceres, A. (2009). Microtubule assembly, organization and dynamics in axons and dendrites. *Nat Rev Neurosci*, *10*(5), 319-332. https://doi.org/10.1038/nrn2631

Courtemanche, N., Gifford, S. M., Simpson, M. A., Pollard, T. D., & Koleske, A. J. (2015). Abl2/Abl-related gene stabilizes actin filaments, stimulates actin branching by actin-related protein 2/3 complex, and promotes actin filament severing by

cofilin. *J Biol Chem*, *290*(7), 4038-4046. https://doi.org/10.1074/jbc.M114.608117

David-Cordonnier, M. H., Hamdane, M., Bailly, C., & D'Halluin, J. C. (1998). Determination of the human c-Abl consensus DNA binding site. *FEBS Lett*, *424*(3), 177-182. https://doi.org/10.1016/s0014-5793(98)00169-0

Dehmelt, L., & Halpain, S. (2005). The MAP2/Tau family of microtubule-associated proteins. *Genome Biol*, *6*(1), 204. https://doi.org/10.1186/gb-2004-6-1-204

Deniston, C. K., Salogiannis, J., Mathea, S., Snead, D. M., Lahiri, I., Matyszewski, M., Donosa, O., Watanabe, R., Bohning, J., Shiau, A. K., Knapp, S., Villa, E., Reck-Peterson, S. L., & Leschziner, A. E. (2020). Structure of LRRK2 in Parkinson's disease and model for microtubule interaction. *Nature*, *588*(7837), 344-349. https://doi.org/10.1038/s41586-020-2673-2

Downing, K. H., & Nogales, E. (1998). Tubulin structure: insights into microtubule properties and functions. *Curr Opin Struct Biol*, *8*(6), 785-791. https://doi.org/10.1016/s0959-440x(98)80099-7

Echarri, A., Muriel, O., Pavon, D. M., Azegrouz, H., Escolar, F., Terron, M. C., Sanchez-Cabo, F., Martinez, F., Montoya, M. C., Llorca, O., & del Pozo, M. A. (2012). Caveolar domain organization and trafficking is regulated by Abl kinases and mDia1 (vol 125, pg 3097, 2012). *Journal of Cell Science*, *125*(18), 4413-4413. https://doi.org/10.1242/jcs.120816

Elie-Caille, C., Severin, F., Helenius, J., Howard, J., Muller, D. J., & Hyman, A. A. (2007). Straight GDP-tubulin protofilaments form in the presence of taxol. *Curr Biol*, *17*(20), 1765-1770. https://doi.org/10.1016/j.cub.2007.08.063

Engel, U., Zhan, Y., Long, J. B., Boyle, S. N., Ballif, B. A., Dorey, K., Gygi, S. P., Koleske, A. J., & Vanvactor, D. (2014). Abelson phosphorylation of CLASP2 modulates its association with microtubules and actin. *Cytoskeleton (Hoboken)*, *71*(3), 195-209. https://doi.org/10.1002/cm.21164

Eot-Houllier, G., Venoux, M., Vidal-Eychenie, S., Hoang, M. T., Giorgi, D., & Rouquier, S. (2010). Plk1 Regulates Both ASAP Localization and Its Role in Spindle Pole Integrity. *Journal of Biological Chemistry*, *285*(38), 29556-29568. https://doi.org/10.1074/jbc.M110.144220

Estevez-Gallego, J., Josa-Prado, F., Ku, S., Buey, R. M., Balaguer, F. A., Prota, A. E., Lucena-Agell, D., Kamma-Lorger, C., Yagi, T., Iwamoto, H., Duchesne, L., Barasoain, I., Steinmetz, M. O., Chretien, D., Kamimura, S., Diaz, J. F., & Oliva, M. A. (2020). Structural model for differential cap maturation at growing microtubule ends. *Elife*, *9*. https://doi.org/ARTN e50155
10.7554/eLife.50155

Ettinger, A., van Haren, J., Ribeiro, S. A., & Wittmann, T. (2016). Doublecortin Is Excluded from Growing Microtubule Ends and Recognizes the GDP-Microtubule Lattice. *Current Biology*, *26*(12), 1549-1555. https://doi.org/10.1016/j.cub.2016.04.020

Fees, C. P., & Moore, J. K. (2018). Regulation of microtubule dynamic instability by the carboxy-terminal tail of beta-tubulin. *Life Sci Alliance*, *1*(2). https://doi.org/10.26508/lsa.201800054

Feng, Z., Chen, X., Wu, X., & Zhang, M. (2019). Formation of biological condensates via phase separation: Characteristics, analytical methods, and physiological implications. *J Biol Chem*, *294*(40), 14823-14835. https://doi.org/10.1074/jbc.REV119.007895

Finka, A., & Goloubinoff, P. (2013). Proteomic data from human cell cultures refine mechanisms of chaperone-mediated protein homeostasis. *Cell Stress Chaperones*, *18*(5), 591-605. https://doi.org/10.1007/s12192-013-0413-3

Fourest-Lieuvin, A., Peris, L., Gache, V., Garcia-Saez, I., Juillan-Binard, C., Lantez, V., & Job, D. (2006). Microtubule regulation in mitosis: tubulin phosphorylation by the cyclin-dependent kinase Cdk1. *Mol Biol Cell*, *17*(3), 1041-1050. https://doi.org/10.1091/mbc.e05-07-0621

Galkin, V. E., Orlova, A., Koleske, A. J., & Egelman, E. H. (2005). The Arg non-receptor tyrosine kinase modifies F-actin structure. *J Mol Biol*, *346*(2), 565-575. https://doi.org/10.1016/j.jmb.2004.11.078

Gaskin, F., Cantor, C. R., & Shelanski, M. L. (1974). Turbidimetric studies of the in vitro assembly and disassembly of porcine neurotubules. *J Mol Biol*, *89*(4), 737-755. https://doi.org/10.1016/0022-2836(74)90048-5

Gebremichael, Y., Chu, J. W., & Voth, G. A. (2008). Intrinsic bending and structural rearrangement of tubulin dimer: molecular dynamics simulations and coarse-grained analysis. *Biophys J*, *95*(5), 2487-2499. https://doi.org/10.1529/biophysj.108.129072

Gell, C., Friel, C. T., Borgonovo, B., Drechsel, D. N., Hyman, A. A., & Howard, J. (2011). Purification of tubulin from porcine brain. *Methods Mol Biol*, *777*, 15-28. https://doi.org/10.1007/978-1-61779-252-6_2

Gertler, F. B., Bennett, R. L., Clark, M. J., & Hoffmann, F. M. (1989). Drosophila abl tyrosine kinase in embryonic CNS axons: a role in axonogenesis is revealed through dosage-sensitive interactions with disabled. *Cell*, *58*(1), 103-113. https://doi.org/10.1016/0092-8674(89)90407-8

Gifford, S. M., Liu, W. Z., Mader, C. C., Halo, T. L., Machida, K., Boggon, T. J., & Koleske, A. J. (2014). Two Amino Acid Residues Confer Different Binding Affinities of Abelson Family Kinase Src Homology 2 Domains for Phosphorylated Cortactin. *Journal of Biological Chemistry*, *289*(28), 19704-19713. https://doi.org/10.1074/jbc.M114.556480

Gil-Henn, H., Patsialou, A., Wang, Y., Warren, M. S., Condeelis, J. S., & Koleske, A. J. (2013). Arg/Abl2 promotes invasion and attenuates proliferation of breast cancer in vivo. *Oncogene*, *32*(21), 2622-2630. https://doi.org/10.1038/onc.2012.284

Ginger, M. L., Portman, N., & McKean, P. G. (2008). Swimming with protists: perception, motility and flagellum assembly. *Nat Rev Microbiol*, *6*(11), 838-850. https://doi.org/10.1038/nrmicro2009

Gittes, F., Mickey, B., Nettleton, J., & Howard, J. (1993). Flexural rigidity of microtubules and actin filaments measured from thermal fluctuations in shape. *J Cell Biol*, *120*(4), 923-934. https://doi.org/10.1083/jcb.120.4.923

Goff, S. P., Gilboa, E., Witte, O. N., & Baltimore, D. (1980). Structure of the Abelson murine leukemia virus genome and the homologous cellular gene: studies with

cloned viral DNA. *Cell*, *22*(3), 777-785. https://doi.org/10.1016/0092-8674(80)90554-1

Gong, C. X., & Iqbal, K. (2008). Hyperphosphorylation of microtubule-associated protein tau: a promising therapeutic target for Alzheimer disease. *Curr Med Chem*, *15*(23), 2321-2328. https://doi.org/10.2174/092986708785909111

Goode, B. L., Denis, P. E., Panda, D., Radeke, M. J., Miller, H. P., Wilson, L., & Feinstein, S. C. (1997). Functional interactions between the proline-rich and repeat regions of tau enhance microtubule binding and assembly. *Molecular Biology of the Cell*, *8*(2), 353-365. https://doi.org/DOI 10.1091/mbc.8.2.353

Goodson, H. V., & Jonasson, E. M. (2018). Microtubules and Microtubule-Associated Proteins. *Cold Spring Harb Perspect Biol*, *10*(6). https://doi.org/10.1101/cshperspect.a022608

Goodson, H. V., Valetti, C., & Kreis, T. E. (1997). Motors and membrane traffic. *Curr Opin Cell Biol*, *9*(1), 18-28. https://doi.org/10.1016/s0955-0674(97)80147-0

Gotoh, A., Miyazawa, K., Ohyashiki, K., Tauchi, T., Boswell, H. S., Broxmeyer, H. E., & Toyama, K. (1995). Tyrosine phosphorylation and activation of focal adhesion kinase (p125FAK) by BCR-ABL oncoprotein. *Exp Hematol*, *23*(11), 1153-1159. https://www.ncbi.nlm.nih.gov/pubmed/7556524

Grafmuller, A., & Voth, G. A. (2011). Intrinsic bending of microtubule protofilaments. *Structure*, *19*(3), 409-417. https://doi.org/10.1016/j.str.2010.12.020

Gudimchuk, N. B., & McIntosh, J. R. (2021). Regulation of microtubule dynamics, mechanics and function through the growing tip. *Nat Rev Mol Cell Biol*, *22*(12), 777-795. https://doi.org/10.1038/s41580-021-00399-x

Guesdon, A., Bazile, F., Buey, R. M., Mohan, R., Monier, S., Garcia, R. R., Angevin, M., Heichette, C., Wieneke, R., Tampe, R., Duchesne, L., Akhmanova, A., Steinmetz, M. O., & Chretien, D. (2016). EB1 interacts with outwardly curved and straight regions of the microtubule lattice. *Nat Cell Biol*, *18*(10), 1102-1108. https://doi.org/10.1038/ncb3412

Gundersen, G. G. (2002a). Evolutionary conservation of microtubule-capture mechanisms. *Nat Rev Mol Cell Biol*, *3*(4), 296-304. https://doi.org/10.1038/nrm777

Gundersen, G. G. (2002b). Microtubule capture: IQGAP and CLIP-170 expand the repertoire. *Curr Biol*, *12*(19), R645-647. https://doi.org/10.1016/s0960-9822(02)01156-9

Hantschel, O. (2012). Structure, regulation, signaling, and targeting of abl kinases in cancer. *Genes Cancer*, *3*(5-6), 436-446. https://doi.org/10.1177/1947601912458584

Harrison, S. C. (2003). Variation on an Src-like theme. *Cell*, *112*(6), 737-740. https://doi.org/10.1016/s0092-8674(03)00196-x

Hernandez, S. E., Krishnaswami, M., Miller, A. L., & Koleske, A. J. (2004). How do Abl family kinases regulate cell shape and movement? *Trends in Cell Biology*, *14*(1), 36-44. https://doi.org/10.1016/j.tcb.2003.11.003

Hernandez, S. E., Settleman, J., & Koleske, A. J. (2004a). Adhesion-dependent regulation of p190RhoGAP in the developing brain by the Abl-related gene tyrosine kinase. *Curr Biol*, *14*(8), 691-696. https://doi.org/10.1016/j.cub.2004.03.062

Hernandez, S. E., Settleman, J., & Koleske, A. J. (2004b). Adhesion-dependent regulation of p190RhoGAP in the developing brain by the Abl-related gene tyrosine kinase. *Current Biology*, *14*(8), 691-696. https://doi.org/10.1016/j.cub.2004.03.062

Hernandez-Vega, A., Braun, M., Scharrel, L., Jahnel, M., Wegmann, S., Hyman, B. T., Alberti, S., Diez, S., & Hyman, A. A. (2017). Local Nucleation of Microtubule Bundles through Tubulin Concentration into a Condensed Tau Phase. *Cell reports*, *20*(10), 2304-2312. https://doi.org/10.1016/j.celrep.2017.08.042

Howell, B., Larsson, N., Gullberg, M., & Cassimeris, L. (1999). Dissociation of the tubulin-sequestering and microtubule catastrophe-promoting activities of oncoprotein 18/stathmin. *Mol Biol Cell*, *10*(1), 105-118. https://doi.org/10.1091/mbc.10.1.105

Howes, S. C., Geyer, E. A., LaFrance, B., Zhang, R., Kellogg, E. H., Westermann, S., Rice, L. M., & Nogales, E. (2017). Structural differences between yeast and mammalian microtubules revealed by cryo-EM. *Journal of Cell Biology*, *216*(9), 2669-2677. https://doi.org/10.1083/jcb.201612195

Hu, Y., Lyu, W., Lowery, L. A., & Koleske, A. J. (2019). Regulation of MT dynamics via direct binding of an Abl family kinase. *J Cell Biol*, *218*(12), 3986-3997. https://doi.org/10.1083/jcb.201812144

Hu, Y. H., Lyu, W. Q., Lowery, L. A., & Koleske, A. J. (2019). Regulation of MT dynamics via direct binding of an Abl family kinase. *Journal of Cell Biology*, *218*(12), 3986-3997. https://doi.org/10.1083/jcb.201812144

Hyman, A. A., Salser, S., Drechsel, D. N., Unwin, N., & Mitchison, T. J. (1992). Role of GTP hydrolysis in microtubule dynamics: information from a slowly hydrolyzable analogue, GMPCPP. *Mol Biol Cell*, *3*(10), 1155-1167. https://doi.org/10.1091/mbc.3.10.1155

Igaev, M., & Grubmuller, H. (2018). Microtubule assembly governed by tubulin allosteric gain in flexibility and lattice induced fit. *Elife*, *7*. https://doi.org/10.7554/eLife.34353

Jones, D. T., & Cozzetto, D. (2015). DISOPRED3: precise disordered region predictions with annotated protein-binding activity. *Bioinformatics*, *31*(6), 857-863. https://doi.org/10.1093/bioinformatics/btu744

Kain, K. H., & Klemke, R. L. (2001). Inhibition of cell migration by Abl family tyrosine kinases through uncoupling of Crk-CAS complexes. *Journal of Biological Chemistry*, *276*(19), 16185-16192. https://doi.org/DOI 10.1074/jbc.M100095200

Kaverina, I., Rottner, K., & Small, J. V. (1998). Targeting, capture, and stabilization of microtubules at early focal adhesions. *Journal of Cell Biology*, *142*(1), 181-190. https://doi.org/DOI 10.1083/jcb.142.1.181

Kellogg, E. H., Hejab, N. M. A., Howes, S., Northcote, P., Miller, J. H., Diaz, J. F., Downing, K. H., & Nogales, E. (2017). Insights into the Distinct Mechanisms of Action of Taxane and Non-Taxane Microtubule Stabilizers from Cryo-EM Structures.

Journal of Molecular Biology, *429*(5), 633-646.
https://doi.org/10.1016/j.jmb.2017.01.001

Kerrisk, M. E., & Koleske, A. J. (2013). Arg kinase signaling in dendrite and synapse stabilization pathways: Memory, cocaine sensitivity, and stress. *International Journal of Biochemistry & Cell Biology*, *45*(11), 2496-2500. https://doi.org/10.1016/j.biocel.2013.07.018

King, M. R., & Petry, S. (2020). Phase separation of TPX2 enhances and spatially coordinates microtubule nucleation. *Nat Commun*, *11*(1), 270. https://doi.org/10.1038/s41467-019-14087-0

Kirschner, M., & Mitchison, T. (1986). Beyond self-assembly: from microtubules to morphogenesis. *Cell*, *45*(3), 329-342. https://doi.org/10.1016/0092-8674(86)90318-1

Kirschner, M. W., Williams, R. C., Weingarten, M., & Gerhart, J. C. (1974). Microtubules from mammalian brain: some properties of their depolymerization products and a proposed mechanism of assembly and disassembly. *Proc Natl Acad Sci U S A*, *71*(4), 1159-1163. https://doi.org/10.1073/pnas.71.4.1159

Kodama, A., Karakesisoglou, I., Wong, E., Vaezi, A., & Fuchs, E. (2003). ACF7: an essential integrator of microtubule dynamics. *Cell*, *115*(3), 343-354. https://doi.org/10.1016/s0092-8674(03)00813-4

Koleske, A. J., Gifford, A. M., Scott, M. L., Nee, M., Bronson, R. T., Miczek, K. A., & Baltimore, D. (1998). Essential roles for the Abl and Arg tyrosine kinases in neurulation. *Neuron*, *21*(6), 1259-1272. https://doi.org/Doi 10.1016/S0896-6273(00)80646-7

Komarova, Y., De Groot, C. O., Grigoriev, I., Gouveia, S. M., Munteanu, E. L., Schober, J. M., Honnappa, S., Buey, R. M., Hoogenraad, C. C., Dogterom, M., Borisy, G. G., Steinmetz, M. O., & Akhmanova, A. (2009). Mammalian end binding proteins control persistent microtubule growth. *J Cell Biol*, *184*(5), 691-706. https://doi.org/10.1083/jcb.200807179

Kruh, G. D., Perego, R., Miki, T., & Aaronson, S. A. (1990). The complete coding sequence of arg defines the Abelson subfamily of cytoplasmic tyrosine kinases. *Proc Natl Acad Sci U S A*, *87*(15), 5802-5806. https://doi.org/10.1073/pnas.87.15.5802

Kuchnir Fygenson, D., Flyvbjerg, H., Sneppen, K., Libchaber, A., & Leibler, S. (1995). Spontaneous nucleation of microtubules. *Phys Rev E Stat Phys Plasmas Fluids Relat Interdiscip Topics*, *51*(5), 5058-5063. https://doi.org/10.1103/physreve.51.5058

Kufer, T. A., Sillje, H. H. W., Korner, R., Gruss, O. J., Meraldi, P., & Nigg, E. A. (2002). Human TPX2 is required for targeting Aurora-A kinase to the spindle. *Journal of Cell Biology*, *158*(4), 617-623. https://doi.org/10.1083/jcb.200204155

Kumar, N. (1981). Taxol-induced polymerization of purified tubulin. Mechanism of action. *J Biol Chem*, *256*(20), 10435-10441. https://www.ncbi.nlm.nih.gov/pubmed/6116707

Lapetina, S., Mader, C. C., Machida, K., Mayer, B. J., & Koleske, A. J. (2009). Arg interacts with cortactin to promote adhesion-dependent cell edge protrusion. *Journal of Cell Biology*, *185*(3), 503-519. https://doi.org/10.1083/jcb.200809085

Laurent, C. E., Delfino, F. J., Cheng, H. Y., & Smithgall, T. E. (2004). The human c-Fes tyrosine kinase binds tubulin and microtubules through separate domains and promotes microtubule assembly. *Mol Cell Biol*, *24*(21), 9351-9358. https://doi.org/10.1128/MCB.24.21.9351-9358.2004

Lawrence, E. J., Arpag, G., Norris, S. R., & Zanic, M. (2018). Human CLASP2 specifically regulates microtubule catastrophe and rescue. *Mol Biol Cell*, *29*(10), 1168-1177. https://doi.org/10.1091/mbc.E18-01-0016

Lee, H., Engel, U., Rusch, J., Scherrer, S., Sheard, K., & Van Vactor, D. (2004). The microtubule plus end tracking protein Orbit/MAST/CLASP acts downstream of the tyrosine kinase Abl in mediating axon guidance. *Neuron*, *42*(6), 913-926. https://doi.org/10.1016/j.neuron.2004.05.020

Lefevre, J., Savarin, P., Gans, P., Hamon, L., Clement, M. J., David, M. O., Bosc, C., Andrieux, A., & Curmi, P. A. (2013). Structural basis for the association of MAP6 protein with microtubules and its regulation by calmodulin. *J Biol Chem*, *288*(34), 24910-24922. https://doi.org/10.1074/jbc.M113.457267

Li, H., DeRosier, D. J., Nicholson, W. V., Nogales, E., & Downing, K. H. (2002). Microtubule structure at 8 A resolution. *Structure*, *10*(10), 1317-1328. https://doi.org/10.1016/s0969-2126(02)00827-4

Lin, Y. C., Yeckel, M. F., & Koleske, A. J. (2013). Abl2/Arg controls dendritic spine and dendrite arbor stability via distinct cytoskeletal control pathways. *J Neurosci*, *33*(5), 1846-1857. https://doi.org/10.1523/JNEUROSCI.4284-12.2013

Liu, B. A., & Machida, K. (2017). Introduction: History of SH2 Domains and Their Applications. In K. Machida & B. A. Liu (Eds.), *SH2 Domains: Methods and Protocols* (pp. 3-35). Springer New York. https://doi.org/10.1007/978-1-4939-6762-9_1

Liu, G., Huang, Y. J., Xiao, R., Wang, D., Acton, T. B., & Montelione, G. T. (2010). NMR structure of F-actin-binding domain of Arg/Abl2 from Homo sapiens. *Proteins*, *78*(5), 1326-1330. https://doi.org/10.1002/prot.22656

Liu, W., MacGrath, S. M., Koleske, A. J., & Boggon, T. J. (2012). Lysozyme contamination facilitates crystallization of a heterotrimeric cortactin-Arg-lysozyme complex. *Acta Crystallogr Sect F Struct Biol Cryst Commun*, *68*(Pt 2), 154-158. https://doi.org/10.1107/S1744309111056132

Lowery, L. A., Lee, H., Lu, C., Murphy, R., Obar, R. A., Zhai, B., Schedl, M., Van Vactor, D., & Zhan, Y. (2010). Parallel genetic and proteomic screens identify Msps as a CLASP-Abl pathway interactor in Drosophila. *Genetics*, *185*(4), 1311-1325. https://doi.org/10.1534/genetics.110.115626

Mader, C. C., Oser, M., Magalhaes, M. A., Bravo-Cordero, J. J., Condeelis, J., Koleske, A. J., & Gil-Henn, H. (2011). An EGFR-Src-Arg-cortactin pathway mediates functional maturation of invadopodia and breast cancer cell invasion. *Cancer Res*, *71*(5), 1730-1741. https://doi.org/10.1158/0008-5472.CAN-10-1432

Maiani, E., Diederich, M., & Gonfloni, S. (2011). DNA damage response: the emerging role of c-Abl as a regulatory switch? *Biochem Pharmacol*, *82*(10), 1269-1276. https://doi.org/10.1016/j.bcp.2011.07.001

Mandelkow, E. M., Mandelkow, E., & Milligan, R. A. (1991). Microtubule dynamics and microtubule caps: a time-resolved cryo-electron microscopy study. *J Cell Biol*, *114*(5), 977-991. https://doi.org/10.1083/jcb.114.5.977

Manka, S. W., & Moores, C. A. (2018a). Microtubule structure by cryo-EM: snapshots of dynamic instability. *Essays Biochem*, *62*(6), 737-751. https://doi.org/10.1042/EBC20180031

Manka, S. W., & Moores, C. A. (2018b). The role of tubulin-tubulin lattice contacts in the mechanism of microtubule dynamic instability. *Nature Structural & Molecular Biology*, *25*(7), 607-+. https://doi.org/10.1038/s41594-018-0087-8

Marantz, R., & Shelanski, M. L. (1970). Structure of microtubular crystals induced by vinblastine in vitro. *J Cell Biol*, *44*(1), 234-238. https://doi.org/10.1083/jcb.44.1.234

Martin, M., Ahern-Djamali, S. M., Hoffmann, F. M., & Saxton, W. M. (2005). Abl tyrosine kinase and its substrate Ena/VASP have functional interactions with kinesin-1. *Mol Biol Cell*, *16*(9), 4225-4230. https://doi.org/10.1091/mbc.e05-02-0116

McVicker, D. P., Millette, M. M., & Dent, E. W. (2015). Signaling to the microtubule cytoskeleton: an unconventional role for CaMKII. *Dev Neurobiol*, *75*(4), 423-434. https://doi.org/10.1002/dneu.22227

Mcwhirter, J. R., Galasso, D. L., & Wang, J. Y. J. (1993). A Coiled-Coil Oligomerization Domain of Bcr Is Essential for the Transforming Function of Bcr-Abl Oncoproteins. *Molecular and Cellular Biology*, *13*(12), 7587-7595. https://doi.org/Doi 10.1128/Mcb.13.12.7587

McWhirter, J. R., & Wang, J. Y. (1993). An actin-binding function contributes to transformation by the Bcr-Abl oncoprotein of Philadelphia chromosome-positive human leukemias. *EMBO J*, *12*(4), 1533-1546. https://www.ncbi.nlm.nih.gov/pubmed/8467803

Meltser, V., Ben-Yehoyada, M., & Shaul, Y. (2011). c-Abl tyrosine kinase in the DNA damage response: cell death and more. *Cell Death Differ*, *18*(1), 2-4. https://doi.org/10.1038/cdd.2010.132

Mendoza, M. C. (2013). Phosphoregulation of the WAVE regulatory complex and signal integration. *Semin Cell Dev Biol*, *24*(4), 272-279. https://doi.org/10.1016/j.semcdb.2013.01.007

Miller, A. L., Wang, Y., Mooseker, M. S., & Koleske, A. J. (2004). The Abl-related gene (Arg) requires its F-actin-microtubule cross-linking activity to regulate lamellipodial dynamics during fibroblast adhesion. *J Cell Biol*, *165*(3), 407-419. https://doi.org/10.1083/jcb.200308055

Miller, M. M., Lapetina, S., MacGrath, S. M., Sfakianos, M. K., Pollard, T. D., & Koleske, A. J. (2010). Regulation of actin polymerization and adhesion-dependent cell edge protrusion by the Abl-related gene (Arg) tyrosine kinase and N-WASp. *Biochemistry*, *49*(10), 2227-2234. https://doi.org/10.1021/bi901721u

Mitchison, T., & Kirschner, M. (1984). Dynamic instability of microtubule growth. *Nature*, *312*(5991), 237-242. https://doi.org/10.1038/312237a0

Mitchison, T. J. (1988). Microtubule dynamics and kinetochore function in mitosis. *Annu Rev Cell Biol*, *4*, 527-549. https://doi.org/10.1146/annurev.cb.04.110188.002523

Moresco, E. M., Donaldson, S., Williamson, A., & Koleske, A. J. (2005). Integrin-mediated dendrite branch maintenance requires Abelson (Abl) family kinases. *J Neurosci*, *25*(26), 6105-6118. https://doi.org/10.1523/JNEUROSCI.1432-05.2005

Moresco, E. M., & Koleske, A. J. (2003). Regulation of neuronal morphogenesis and synaptic function by Abl family kinases. *Curr Opin Neurobiol*, *13*(5), 535-544. https://doi.org/10.1016/j.conb.2003.08.002

Muller, R., Slamon, D. J., Tremblay, J. M., Cline, M. J., & Verma, I. M. (1982). Differential Expression of Cellular Oncogenes during Prenatal and Postnatal-Development of the Mouse. *Nature*, *299*(5884), 640-644. https://doi.org/DOI 10.1038/299640a0

Muller-Reichert, T., Chretien, D., Severin, F., & Hyman, A. A. (1998). Structural changes at microtubule ends accompanying GTP hydrolysis: Information from a slowly hydrolyzable analogue of GTP, guanylyl (alpha,beta)methylenediphosphonate. *Molecular Biology of the Cell*, *9*, 271a-271a. <Go to ISI>://WOS:000076906701574

Nagar, B., Hantschel, O., Young, M. A., Scheffzek, K., Veach, D., Bornmann, V., Clarkson, B., Superti-Furga, G., & Kuriyan, J. (2003). Structural basis for the autoinhibition of c-Abl tyrosine kinase. *Cell*, *112*(6), 859-871. https://doi.org/Doi 10.1016/S0092-8674(03)00194-6

Nehme, A., Lee, B. L., Baskaran, R., Zhang, Q., Lin, X., & Christen, R. D. (2000). Effect of c-Abl tyrosine kinase on the cellular response to paclitaxel-induced microtubule damage. *Br J Cancer*, *83*(10), 1360-1366. https://doi.org/10.1054/bjoc.2000.1440

Nogales, E., Wolf, S. G., & Downing, K. H. (1998). Structure of the alpha beta tubulin dimer by electron crystallography (vol 391, pg 199, 1998). *Nature*, *393*(6681), 191-191. https://doi.org/Doi 10.1038/30288

Nolte, M. A., Nolte-'t Hoen, E. N. M., & Margadant, C. (2021). Integrins Control Vesicular Trafficking; New Tricks for Old Dogs. *Trends Biochem Sci*, *46*(2), 124-137. https://doi.org/10.1016/j.tibs.2020.09.001

Nourbakhsh, K., Ferreccio, A. A., Bernard, M. J., & Yadav, S. (2021). TAOK2 is an ER-localized kinase that catalyzes the dynamic tethering of ER to microtubules. *Dev Cell*, *56*(24), 3321-3333 e3325. https://doi.org/10.1016/j.devcel.2021.11.015

Omar, M. H., Kerrisk Campbell, M., Xiao, X., Zhong, Q., Brunken, W. J., Miner, J. H., Greer, C. A., & Koleske, A. J. (2017). CNS Neurons Deposit Laminin α5 to Stabilize Synapses. *Cell reports*, *21*(5), 1281-1292. https://doi.org/10.1016/j.celrep.2017.10.028

Ori-McKenney, K. M., McKenney, R. J., Huang, H. H., Li, T., Meltzer, S., Jan, L. Y., Vale, R. D., Wiita, A. P., & Jan, Y. N. (2016). Phosphorylation of beta-Tubulin by the Down Syndrome Kinase, Minibrain/DYRK1a, Regulates Microtubule Dynamics and Dendrite Morphogenesis. *Neuron*, *90*(3), 551-563. https://doi.org/10.1016/j.neuron.2016.03.027

Peacock, J. G., Miller, A. L., Bradley, W. D., Rodriguez, O. C., Webb, D. J., & Koleske, A. J. (2007). The Abl-related gene tyrosine kinase acts through p190RhoGAP to inhibit actomyosin contractility and regulate focal adhesion dynamics upon adhesion to fibronectin. *Mol Biol Cell*, *18*(10), 3860-3872. https://doi.org/10.1091/mbc.e07-01-0075

Pendergast, A. M. (2006). Role of Abl Family Kinases in Growth Factor-Mediated Signaling. In *Abl Family Kinases in Development and Disease* (pp. 11-15). Springer New York. https://doi.org/10.1007/978-0-387-68744-5_2

Perego, R. A., Corizzato, M., Bianchi, C., Eroini, B., & Bosari, S. (2005). N- and C-terminal isoforms of Arg quantified by real-time PCR are specifically expressed in human normal and neoplastic cells, in neoplastic cell lines, and in HL-60 cell differentiation. *Mol Carcinog*, *42*(4), 229-239. https://doi.org/10.1002/mc.20085

Peters, J. D., Furlong, M. T., Asai, D. J., Harrison, M. L., & Geahlen, R. L. (1996). Syk, activated by cross-linking the B-cell antigen receptor, localizes to the cytosol where it interacts with and phosphorylates alpha-tubulin on tyrosine. *J Biol Chem*, *271*(9), 4755-4762. https://doi.org/10.1074/jbc.271.9.4755

Pisabarro, M. T., Serrano, L., & Wilmanns, M. (1998). Crystal structure of the abl-SH3 domain complexed with a designed high-affinity peptide ligand: implications for SH3-ligand interactions. *J Mol Biol*, *281*(3), 513-521. https://doi.org/10.1006/jmbi.1998.1932

Plattner, R., Irvin, B. J., Guo, S. L., Blackburn, K., Kazlauskas, A., Abraham, R. T., York, J. D., & Pendergast, A. M. (2003). A new link between the c-Abl tyrosine kinase and phosphoinositide signalling through PLC-gamma 1. *Nature Cell Biology*, *5*(4), 309-319. https://doi.org/10.1038/ncb949

Plattner, R., Kadlec, L., DeMali, K. A., Kazlauskas, A., & Pendergast, A. M. (1999). c-Abl is activated by growth factors and Src family kinases and has a role in the cellular response to PDGF. *Genes & Development*, *13*(18), 2400-2411. https://doi.org/DOI 10.1101/gad.13.18.2400

Plattner, R., Koleske, A. J., Kazlauskas, A., & Pendergast, A. M. (2004). Bidirectional signaling links the Abelson kinases to the platelet-derived growth factor receptor. *Molecular and Cellular Biology*, *24*(6), 2573-2583. https://doi.org/10.1128/mcb.24.6.2573-2583.2004

Pollard, T. D. (2007). Regulation of actin filament assembly by Arp2/3 complex and formins. *Annu Rev Biophys Biomol Struct*, *36*, 451-477. https://doi.org/10.1146/annurev.biophys.35.040405.101936

Pollard, T. D. (2010). A guide to simple and informative binding assays. *Mol Biol Cell*, *21*(23), 4061-4067. https://doi.org/10.1091/mbc.E10-08-0683

Ramkumar, A., Jong, B. Y., & Ori-McKenney, K. M. (2018). ReMAPping the microtubule landscape: How phosphorylation dictates the activities of microtubule-associated proteins. *Developmental Dynamics*, *247*(1), 138-155. https://doi.org/10.1002/dvdy.24599

Reid, T. A., Coombes, C., & Gardner, M. K. (2017). Manipulation and quantification of microtubule lattice integrity. *Biol Open*, *6*(8), 1245-1256. https://doi.org/10.1242/bio.025320

Reid, T. A., Coombes, C., Mukherjee, S., Goldblum, R. R., White, K., Parmar, S., McClellan, M., Zanic, M., Courtemanche, N., & Gardner, M. K. (2019). Structural state recognition facilitates tip tracking of EB1 at growing microtubule ends. *Elife*, *8*. https://doi.org/ARTN e48117
10.7554/eLife.48117

Ren, R., Mayer, B. J., Cicchetti, P., & Baltimore, D. (1993). Identification of a ten-amino acid proline-rich SH3 binding site. *Science*, *259*(5098), 1157-1161. https://doi.org/10.1126/science.8438166

Renshaw, M. W., Capozza, M. A., & Wang, Y. J. (1988). Differential Expression of Type-Specific C-Abl Messenger-Rnas in Mouse-Tissues and Cell-Lines. *Molecular and Cellular Biology*, *8*(10), 4547-4551. https://doi.org/Doi 10.1128/Mcb.8.10.4547

Rice, L. M., Montabana, E. A., & Agard, D. A. (2008). The lattice as allosteric effector: Structural studies of alpha beta- and gamma-tubulin clarify the role of GTP in microtubule assembly. *Proceedings of the National Academy of Sciences of the United States of America*, *105*(14), 5378-5383. https://doi.org/10.1073/pnas.0801155105

Rice, L. M., Moritz, M., & Agard, D. A. (2021). Microtubules form by progressively faster tubulin accretion, not by nucleation-elongation. *Journal of Cell Biology*, *220*(5). https://doi.org/ARTN e202012079

10.1083/jcb.202012079

Robinson, J., & Engelborghs, Y. (1982). Tubulin polymerization in dimethyl sulfoxide. *J Biol Chem*, *257*(10), 5367-5371. https://www.ncbi.nlm.nih.gov/pubmed/7068596

Rockmill, B., & Fogel, S. (1988). DIS1: a yeast gene required for proper meiotic chromosome disjunction. *Genetics*, *119*(2), 261-272. https://doi.org/10.1093/genetics/119.2.261

Rodriguez, O. C., Schaefer, A. W., Mandato, C. A., Forscher, P., Bement, W. M., & Waterman-Storer, C. M. (2003). Conserved microtubule-actin interactions in cell movement and morphogenesis. *Nat Cell Biol*, *5*(7), 599-609. https://doi.org/10.1038/ncb0703-599

Roostalu, J., & Surrey, T. (2017). Microtubule nucleation: beyond the template. *Nat Rev Mol Cell Biol*, *18*(11), 702-710. https://doi.org/10.1038/nrm.2017.75

Salgia, R., Brunkhorst, B., Pisick, E., Li, J. L., Lo, S. H., Chen, L. B., & Griffin, J. D. (1995). Increased tyrosine phosphorylation of focal adhesion proteins in myeloid cell lines expressing p210BCR/ABL. *Oncogene*, *11*(6), 1149-1155. https://www.ncbi.nlm.nih.gov/pubmed/7566975

Schaedel, L., John, K., Gaillard, J., Nachury, M. V., Blanchoin, L., & Thery, M. (2015). Microtubules self-repair in response to mechanical stress. *Nat Mater*, *14*(11), 1156-1163. https://doi.org/10.1038/nmat4396

Schwartzberg, P. L., Goff, S. P., & Robertson, E. J. (1989). Germ-line transmission of a c-abl mutation produced by targeted gene disruption in ES cells. *Science*, *246*(4931), 799-803. https://doi.org/10.1126/science.2554496

Schwartzberg, P. L., Stall, A. M., Hardin, J. D., Bowdish, K. S., Humaran, T., Boast, S., Harbison, M. L., Robertson, E. J., & Goff, S. P. (1991). Mice Homozygous for the Ablm1 Mutation Show Poor Viability and Depletion of Selected B-Cell and T-Cell Populations. *Cell*, *65*(7), 1165-1175. https://doi.org/Doi 10.1016/0092-8674(91)90012-N

Seetharaman, S., & Etienne-Manneville, S. (2020). Cytoskeletal Crosstalk in Cell Migration. *Trends Cell Biol*, *30*(9), 720-735. https://doi.org/10.1016/j.tcb.2020.06.004

Sept, D., Baker, N. A., & McCammon, J. A. (2003). The physical basis of microtubule structure and stability. *Protein Sci*, *12*(10), 2257-2261. https://doi.org/10.1110/ps.03187503

Shaul, Y., & Ben-Yehoyada, M. (2005). Role of c-Abl in the DNA damage stress response. *Cell Research*, *15*(1), 33-35. https://doi.org/DOI 10.1038/sj.cr.7290261

Shaw, J. E., Kilander, M. B. C., Lin, Y. C., & Koleske, A. J. (2021). Abl2:Cortactin Interactions Regulate Dendritic Spine Stability via Control of a Stable Filamentous Actin Pool. *J Neurosci*, *41*(14), 3068-3081. https://doi.org/10.1523/JNEUROSCI.2472-20.2021

Shelanski, M. L., Gaskin, F., & Cantor, C. R. (1973). Microtubule assembly in the absence of added nucleotides. *Proc Natl Acad Sci U S A*, *70*(3), 765-768. https://doi.org/10.1073/pnas.70.3.765

Simon, J. R., & Salmon, E. D. (1990). The structure of microtubule ends during the elongation and shortening phases of dynamic instability examined by negative-stain electron microscopy. *J Cell Sci*, *96 (Pt 4)*, 571-582. https://doi.org/10.1242/jcs.96.4.571

Simpson, M. A., Bradley, W. D., Harburger, D., Parsons, M., Calderwood, D. A., & Koleske, A. J. (2015). Direct interactions with the integrin beta1 cytoplasmic tail activate the Abl2/Arg kinase. *J Biol Chem*, *290*(13), 8360-8372. https://doi.org/10.1074/jbc.M115.638874

Smith, K. M., Yacobi, R., & Van Etten, R. A. (2003). Autoinhibition of Bcr-Abl through Its SH3 Domain. *Molecular Cell*, *12*(1), 27-37. https://doi.org/https://doi.org/10.1016/S1097-2765(03)00274-0

Song, Y., & Brady, S. T. (2015). Post-translational modifications of tubulin: pathways to functional diversity of microtubules. *Trends Cell Biol*, *25*(3), 125-136. https://doi.org/10.1016/j.tcb.2014.10.004

Songyang, Z., Shoelson, S. E., Chaudhuri, M., Gish, G., Pawson, T., Haser, W. G., King, F., Roberts, T., Ratnofsky, S., Lechleider, R. J., & et al. (1993). SH2 domains recognize specific phosphopeptide sequences. *Cell*, *72*(5), 767-778. https://doi.org/10.1016/0092-8674(93)90404-e

Srayko, M., O'Toole E, T., Hyman, A. A., & Muller-Reichert, T. (2006). Katanin disrupts the microtubule lattice and increases polymer number in C. elegans meiosis. *Curr Biol*, *16*(19), 1944-1949. https://doi.org/10.1016/j.cub.2006.08.029

Srinivasan, D., & Plattner, R. (2006). Activation of Abl tyrosine kinases promotes invasion of aggressive breast cancer cells. *Cancer Research*, *66*(11), 5648-5655. https://doi.org/10.1158/0008-5472.Can-06-0734

Stradal, T., Courtney, K. D., Rottner, K., Hahne, P., Small, J. V., & Pendergast, A. M. (2001). The Abl interactor proteins localize to sites of actin polymerization at the tips of lamellipodia and filopodia. *Curr Biol*, *11*(11), 891-895. https://doi.org/10.1016/s0960-9822(01)00239-1

Strothman, C., Farmer, V., Arpag, G., Rodgers, N., Podolski, M., Norris, S., Ohi, R., & Zanic, M. (2019). Microtubule minus-end stability is dictated by the tubulin off-rate. *J Cell Biol*, *218*(9), 2841-2853. https://doi.org/10.1083/jcb.201905019

Tajielyato, N., Li, L., Peng, Y., Alper, J., & Alexov, E. (2018). E-hooks provide guidance and a soft landing for the microtubule binding domain of dynein. *Sci Rep*, *8*(1), 13266. https://doi.org/10.1038/s41598-018-31480-9

Tan, R., Lam, A. J., Tan, T., Han, J., Nowakowski, D. W., Vershinin, M., Simo, S., Ori-McKenney, K. M., & McKenney, R. J. (2019). Microtubules gate tau condensation to spatially regulate microtubule functions. *Nat Cell Biol*, *21*(9), 1078-1085. https://doi.org/10.1038/s41556-019-0375-5

Tanaka, T., Koizumi, H., & Gleeson, J. G. (2006). The doublecortin and doublecortin-like kinase 1 genes cooperate in murine hippocampal development. *Cereb Cortex*, *16 Suppl 1*, i69-73. https://doi.org/10.1093/cercor/bhk005

Tang, D. D., & Gerlach, B. D. (2017). The roles and regulation of the actin cytoskeleton, intermediate filaments and microtubules in smooth muscle cell migration. *Respir Res*, *18*(1), 54. https://doi.org/10.1186/s12931-017-0544-7

Tanis, K. Q., Veach, D., Duewel, H. S., Bornmann, W. G., & Koleske, A. J. (2003). Two distinct phosphorylation pathways have additive effects on Abl family kinase activation. *Molecular and Cellular Biology*, *23*(11), 3884-3896. https://doi.org/10.1128/Mcb.23.11.3884-3896.2003

Tasic, B., Yao, Z., Graybuck, L. T., Smith, K. A., Nguyen, T. N., Bertagnolli, D., Goldy, J., Garren, E., Economo, M. N., Viswanathan, S., Penn, O., Bakken, T., Menon, V., Miller, J., Fong, O., Hirokawa, K. E., Lathia, K., Rimorin, C., Tieu, M., . . . Zeng, H. (2018). Shared and distinct transcriptomic cell types across neocortical areas. *Nature*, *563*(7729), 72-78. https://doi.org/10.1038/s41586-018-0654-5

Teixido-Travesa, N., Roig, J., & Luders, J. (2012). The where, when and how of microtubule nucleation - one ring to rule them all. *J Cell Sci*, *125*(Pt 19), 4445-4456. https://doi.org/10.1242/jcs.106971

Thawani, A., Kadzik, R. S., & Petry, S. (2018). XMAP215 is a microtubule nucleation factor that functions synergistically with the gamma-tubulin ring complex. *Nature Cell Biology*, *20*(5), 575-+. https://doi.org/10.1038/s41556-018-0091-6

Tinti, M., Kiemer, L., Costa, S., Miller, M. L., Sacco, F., Olsen, J. V., Carducci, M., Paoluzi, S., Langone, F., Workman, C. T., Blom, N., Machida, K., Thompson, C. M., Schutkowski, M., Brunak, S., Mann, M., Mayer, B. J., Castagnoli, L., & Cesareni, G. (2013). The SH2 domain interaction landscape. *Cell Rep*, *3*(4), 1293-1305. https://doi.org/10.1016/j.celrep.2013.03.001

Tong, D., & Voth, G. A. (2020). Microtubule Simulations Provide Insight into the Molecular Mechanism Underlying Dynamic Instability. *Biophys J*, *118*(12), 2938-2951. https://doi.org/10.1016/j.bpj.2020.04.028

Tournebize, R., Popov, A., Kinoshita, K., Ashford, A. J., Rybina, S., Pozniakovsky, A., Mayer, T. U., Walczak, C. E., Karsenti, E., & Hyman, A. A. (2000). Control of microtubule dynamics by the antagonistic activities of XMAP215 and XKCM1 in Xenopus egg extracts. *Nat Cell Biol*, *2*(1), 13-19. https://doi.org/10.1038/71330

Triclin, S., Inoue, D., Gaillard, J., Htet, Z. M., DeSantis, M. E., Portran, D., Derivery, E., Aumeier, C., Schaedel, L., John, K., Leterrier, C., Reck-Peterson, S. L., Blanchoin, L., & Thery, M. (2021). Self-repair protects microtubules from destruction by

molecular motors. *Nat Mater*, *20*(6), 883-891. https://doi.org/10.1038/s41563-020-00905-0

Tybulewicz, V. L. J., Crawford, C. E., Jackson, P. K., Bronson, R. T., & Mulligan, R. C. (1991). Neonatal Lethality and Lymphopenia in Mice with a Homozygous Disruption of the C-Abl Protooncogene. *Cell*, *65*(7), 1153-1163. https://doi.org/Doi 10.1016/0092-8674(91)90011-M

van de Willige, D., Hoogenraad, C. C., & Akhmanova, A. (2016). Microtubule plus-end tracking proteins in neuronal development. *Cell Mol Life Sci*, *73*(10), 2053-2077. https://doi.org/10.1007/s00018-016-2168-3

Vemu, A., Szczesna, E., & Roll-Mecak, A. (2020). In Vitro Reconstitution Assays of Microtubule Amplification and Lattice Repair by the Microtubule-Severing Enzymes Katanin and Spastin. *Methods Mol Biol*, *2101*, 27-38. https://doi.org/10.1007/978-1-0716-0219-5_3

Vitre, B., Coquelle, F. M., Heichette, C., Garnier, C., Chretien, D., & Arnal, I. (2008). EB1 regulates microtubule dynamics and tubulin sheet closure in vitro. *Nat Cell Biol*, *10*(4), 415-421. https://doi.org/10.1038/ncb1703

von Loeffelholz, O., Venables, N. A., Drummond, D. R., Katsuki, M., Cross, R., & Moores, C. A. (2017). Nucleotide- and Mal3-dependent changes in fission yeast microtubules suggest a structural plasticity view of dynamics. *Nat Commun*, *8*(1), 2110. https://doi.org/10.1038/s41467-017-02241-5

Voter, W. A., & Erickson, H. P. (1984). The kinetics of microtubule assembly. Evidence for a two-stage nucleation mechanism. *J Biol Chem*, *259*(16), 10430-10438. https://www.ncbi.nlm.nih.gov/pubmed/6469971

Voter, W. A., Obrien, E. T., & Erickson, H. P. (1991). Dilution-Induced Disassembly of Microtubules - Relation to Dynamic Instability and the Gtp Cap. *Cell Motility and the Cytoskeleton*, *18*(1), 55-62. https://doi.org/DOI 10.1002/cm.970180106

Wagner, M. J., Stacey, M. M., Liu, B. A., & Pawson, T. (2013). Molecular Mechanisms of SH2-and PTB-Domain-Containing Proteins in Receptor Tyrosine Kinase Signaling. *Cold Spring Harbor Perspectives in Biology*, *5*(12). https://doi.org/ARTN a008987 10.1101/cshperspect.a008987

Wang, G. F., Dong, Q., Bai, Y., Gu, J., Tao, Q., Yue, J., Zhou, R., Niu, X., Zhu, L., Song, C., Zheng, T., Wang, D., Jin, Y., Liu, H., Cao, C., & Liu, X. (2022). c-Abl kinase-mediated phosphorylation of gamma-tubulin promotes gamma-tubulin ring complexes assembly and microtubule nucleation. *J Biol Chem*, 101778. https://doi.org/10.1016/j.jbc.2022.101778

Wang, J., Choi, J. M., Holehouse, A. S., Lee, H. O., Zhang, X., Jahnel, M., Maharana, S., Lemaitre, R., Pozniakovsky, A., Drechsel, D., Poser, I., Pappu, R. V., Alberti, S., & Hyman, A. A. (2018). A Molecular Grammar Governing the Driving Forces for Phase Separation of Prion-like RNA Binding Proteins. *Cell*, *174*(3), 688-699 e616. https://doi.org/10.1016/j.cell.2018.06.006

Wang, Y. X., Miller, A. L., Mooseker, M. S., & Koleske, A. J. (2001). The Abl-related gene (Arg) nonreceptor tyrosine kinase uses two F-actin-binding domains to bundle F-actin. *Proceedings of the National Academy of Sciences of the United States of America*, *98*(26), 14865-14870. https://doi.org/DOI 10.1073/pnas.251249298

Wang, Z., & Sheetz, M. P. (2000). The C-terminus of tubulin increases cytoplasmic dynein and kinesin processivity. *Biophys J*, *78*(4), 1955-1964. https://doi.org/10.1016/S0006-3495(00)76743-9

Warren, M. S., Bradley, W. D., Gourley, S. L., Lin, Y. C., Simpson, M. A., Reichardt, L. F., Greer, C. A., Taylor, J. R., & Koleske, A. J. (2012). Integrin beta 1 Signals through Arg to Regulate Postnatal Dendritic Arborization, Synapse Density, and Behavior. *Journal of Neuroscience*, *32*(8), 2824-2834. https://doi.org/10.1523/Jneurosci.3942-11.2012

Waterman-Storer, C. M., Worthylake, R. A., Liu, B. P., Burridge, K., & Salmon, E. D. (1999). Microtubule growth activates Rac1 to promote lamellipodial protrusion in fibroblasts. *Nat Cell Biol*, *1*(1), 45-50. https://doi.org/10.1038/9018

Wessler, S., & Backert, S. (2011). Abl family of tyrosine kinases and microbial pathogenesis. *Int Rev Cell Mol Biol*, *286*, 271-300. https://doi.org/10.1016/B978-0-12-385859-7.00006-9

Westphal, R. S., Soderling, S. H., Alto, N. M., Langeberg, L. K., & Scott, J. D. (2000). Scar/WAVE-1, a Wiskott-Aldrich syndrome protein, assembles an actin-associated multi-kinase scaffold. *EMBO J*, *19*(17), 4589-4600. https://doi.org/10.1093/emboj/19.17.4589

Wills, Z., Bateman, J., Korey, C. A., Comer, A., & Van Vactor, D. (1999). The tyrosine kinase Abl and its substrate Enabled collaborate with the receptor phosphatase Dlar to control motor axon guidance. *Neuron*, *22*(2), 301-312. https://doi.org/Doi 10.1016/S0896-6273(00)81091-0

Wills, Z., Marr, L., Zinn, K., Goodman, C. S., & Van Vactor, D. (1999). Profilin and the Abl tyrosine kinase are required for motor axon outgrowth in the Drosophila embryo. *Neuron*, *22*(2), 291-299. https://doi.org/10.1016/s0896-6273(00)81090-9

Wolanin, K., Magalska, A., Kusio-Kobialka, M., Podszywalow-Bartnicka, P., Vejda, S., McKenna, S. L., Mosieniak, G., Sikora, E., & Piwocka, K. (2010). Expression of oncogenic kinase Bcr-Abl impairs mitotic checkpoint and promotes aberrant divisions and resistance to microtubule-targeting agents. *Mol Cancer Ther*, *9*(5), 1328-1338. https://doi.org/10.1158/1535-7163.MCT-09-0936

Woodring, P. J., Litwack, E. D., O'Leary, D. D., Lucero, G. R., Wang, J. Y., & Hunter, T. (2002). Modulation of the F-actin cytoskeleton by c-Abl tyrosine kinase in cell spreading and neurite extension. *J Cell Biol*, *156*(5), 879-892. https://doi.org/10.1083/jcb.200110014

Woodruff, J. B., Gomes, B. F., Widlund, P. O., Mahamid, J., Honigmann, A., & Hyman, A. A. (2017). The Centrosome Is a Selective Condensate that Nucleates Microtubules by Concentrating Tubulin. *Cell*, *169*(6), 1066-+. https://doi.org/10.1016/j.cell.2017.05.028

Wu, Y. F. O., Bryant, A. T., Nelson, N. T., Madey, A. G., Fernandes, G. F., & Goodson, H. V. (2021). Overexpression of the microtubule-binding protein CLIP-170 induces a plus TIP network superstructure consistent with a biomolecular condensate. *PLoS One*, *16*(12). https://doi.org/ARTN e0260401

10.1371/journal.pone.0260401

Xue, B., Dunbrack, R. L., Williams, R. W., Dunker, A. K., & Uversky, V. N. (2010). PONDR-FIT: A meta-predictor of intrinsically disordered amino acids. *Biochimica Et Biophysica Acta-Proteins and Proteomics*, *1804*(4), 996-1010. https://doi.org/10.1016/j.bbapap.2010.01.011

Yogalingam, G., & Pendergast, A. M. (2008). Abl kinases regulate autophagy by promoting the trafficking and function of lysosomal components. *J Biol Chem*, *283*(51), 35941-35953. https://doi.org/10.1074/jbc.M804543200

Yue, J., & Wu, X. (2014). Microtubules Regulate Focal Adhesion Dynamics through MAP4K4. *Molecular Biology of the Cell*, *25*. <Go to ISI>://WOS:000352094105247

Zanic, M., Stear, J. H., Hyman, A. A., & Howard, J. (2009). EB1 recognizes the nucleotide state of tubulin in the microtubule lattice. *PLoS One*, *4*(10), e7585. https://doi.org/10.1371/journal.pone.0007585

Zhang, K., Lyu, W. Q., Yu, J., & Koleske, A. J. (2018). Abl2 is recruited to ventral actin waves through cytoskeletal interactions to promote lamellipodium extension. *Molecular Biology of the Cell*, *29*(23), 2863-2873. https://doi.org/10.1091/mbc.E18-01-0044

Zhang, R., Alushin, G. M., Brown, A., & Nogales, E. (2015). Mechanistic Origin of Microtubule Dynamic Instability and Its Modulation by EB Proteins. *Cell*, *162*(4), 849-859. https://doi.org/10.1016/j.cell.2015.07.012

Zhang, R., LaFrance, B., & Nogales, E. (2018). Separating the effects of nucleotide and EB binding on microtubule structure. *Proc Natl Acad Sci U S A*, *115*(27), E6191-E6200. https://doi.org/10.1073/pnas.1802637115